NTNU – Trondheim
Norwegian University of
Science and Technology

# Earthquake Response of Suspension Bridge Crossing the Sognefjord

Håkon Olav Skogmo

Civil and Environmental Engineering
Submission date: June 2013
Supervisor: Svein N Remseth, KT
Co-supervisor: Ragnar Sigbjørnsson, KT

Norwegian University of Science and Technology
Department of Structural Engineering

**Department of Structural Engineering**
Faculty of Engineering Science and Technology
**NTNU- Norwegian University of Science and Technology**

ACCESSIBILITY

# MASTER THESIS 2012

| SUBJECT AREA: Bridge Dynamics, Earthquake | DATE: 10.6.2013 | NO. OF PAGES: 112 |
|---|---|---|

TITLE:

**Earthquake Response of Suspension Bridge Crossing the Sognefjord**

Jordskjelv respons på hengebro over Sognefjorden

BY:

Håkon Olav Skogmo

SUMMARY:
This thesis assesses the proposed construction of a single span suspension bridge crossing the Sognefjord in light of earthquake response. There has been conducted a literature survey to investigate the theory developed to handle long-span suspension bridges. A method found was the Pseudo Excitation Method developed to assess response of long-span suspension bridges using random vibrations.
The modelling of the Sognefjord Bridge was conducted using SAP2000. Analysis showed that the first mode had a period of 36 seconds and that over 2000 different modes were identified for the system.
Before conducting the analyses for the system, two damping models were assessed, Rayleigh and hysteretic damping. When frequency response was calculated for the 300 first frequencies and the Rayleigh damping were controlled by the first and hundred natural frequencies the results proved that Rayleigh damping gave a response twice what found using hysteretic damping for several of frequencies in range between mode 1 and mode 100.
The Sognefjord Bridge is a very slender structure therefore were the damping effects from wind assessed. This was done using quasi-static theory. Using the aerodynamic derivatives from the Hardanger Bridge, a rough estimate the aerodynamic damping was obtained. This showed a reduction in frequency response of 25%.
The earthquake response calculation where conducted in MATLAB, using random vibration theory in the frequency domain. Three analyses were conducted assuming stationary conditions; one with wave–passage and incoherence effects, one with only the wave-passage effect and one with no spatial effects. There were considerable differences in the respond from the three analyses in both size and shape. The maximum response occurred in the analysis where both wave-passage and incoherence effects were included and was 0.81 meters.
As a result of the high period of the first mode of the system, the assumption of stationary conditions is not valid. A simplified method to assess the non-stationary condition were used, this showed that the maximum response for stationary conditions should be reduced substantially.

RESPONSIBLE TEACHER: Ragnar Sigbjörsson

SUPERVISOR(S) Svein Remseth (NTNU), Bjørn Isaksen (SVV)

CARRIED OUT AT: Department of Structural Engineering

# SEISMIC BEHAVIOUR OF LONG SPAN SUSPENSION BRIDGES

**Problem:**
Long span suspension bridges are currently under planning in Norway, the length of which is in the range 2 to 4 km, which implies tower heights up to 400 m

**Objective:**
To develop and test a computational model

**Main steps:**

- Literature survey
- Structural modelling of the combined system: towers, cables and deck
- Damping properties
- Description of the seismic wave field
- Response analysis
- Comparative analysis and comparison with current design provisions
- Reporting

**Potential outcome:**
Recommendations regarding structural design provisions

**Potential special outcome**:
Published paper in an ISI scientific journal

**Special requirements:**
Theory of random fields and random vibrations

# Preface

This thesis is the final part to fulfil the requirement for the degree Master of Science at the Norwegian University of Science and Technology (NTNU). The work has been carried out at the Faculty of Engineering Science and Technology, Department of Structural Engineering and has been done in collaboration with the Norwegian Public Road Administration (NPRA). Supervisors of this thesis have been Professor Ragnar Sigbjörnsson, Professor Svein N. Remseth and Dr. Bjørn Isaksen (NPRA).

I would like express my greet gratitude to my main supervisors Professor Ragnar Sigbjörsson. He has been a great motivator and given good guidance when problems have occurred. Also my co-supervisor Professor Svein N. Remseth has been good support in the writing.

I am also very grateful to the Norwegian Public Road Administration and Dr. Bjørn I. Isaksen for providing me with this case and supporting me with all the necessary technical details.

Trondheim, June 10, 2013

Håkon Olav Skogmo

# Abstract

This thesis assesses the proposed construction of a single span suspension bridge crossing the Sognefjord in light of earthquake response. The proposed bridge has a span of 3700 meter and its pylon has a height of 455 meters. If build this will be by far the longest suspension bridge ever build. The current regulations are not developed to handle constructions as this. There has therefore been conducted a literature survey to investigate the theory developed to handle long-span suspension bridges. A method found was the Pseudo Excitation Method developed to assess response of long-span suspension bridges using random vibrations. This method has in China been used in the seismic design of several long–span bridges and in the Chinese guidelines for seismic design of long-span bridges the preferred method. This method is presented in this thesis.

The modelling of the Sognefjord Bridge was conducted using SAP2000. Analysis showed that the first mode had a period of 36 seconds and that over 2000 different modes were identified for the system. An investigation of the modal participation factors proved that there are high modes contributing significant to the response.

Before conducting the analyses for the system two damping models were assessed; Rayleigh and hysteretic damping. When frequency response was calculated for the 300 first frequencies and the Rayleigh damping were controlled by the first and hundred natural frequencies the results proved that Rayleigh damping gave a response twice what found using hysteretic damping for several of frequencies in range between mode 1 and mode 100. Thus, was the hysteretic damping used in the analyses of the bridge.

In the Eurocode, NS-EN 1998-2 there is seen that wind is not required to be accounted for in seismic analyses. However, since the Sognefjord Bridge is a very slender structure the damping effects from wind were assessed. This was done using quasi-static theory. As the aerodynamic derivatives for this bridge not yet are examined, the values for the Hardanger Bridge were used. This gave a rough estimate of effects of the aerodynamic damping, which sowed a reduction in frequency response of 25% for the first natural frequency for displacement in y-direction at the mid-span. The reduction become less for higher modes, but was still significant.

The earthquake response calculation where conducted in MATLAB, using random vibration theory in the frequency domain. Three analysis were conducted assuming stationary conditions; seismic wave traveling along bridge accounting for both wave–passage and incoherence effects, seismic wave traveling along bridge accounting for only the wave-passage effect and seismic wave traveling perpendicular to the bridge where no spatial effects are present. The results showed that there were considerable differences in the respond from the three analyses in both size and shape. The maximum response occurred in z- direction in the analysis where both wave-passage and incoherence effects were accounted for and was 0.81 meters.

As a result of the high the period of the first mode of the system, the assumption of stationary conditions is not valid. To assess the effects of non-stationary condition a simplified method assuming the response in each DOF as single degree of freedom systems were used. The power spectral densities curves for the responses investigated showed this to be a good estimate as they

were fairly narrow-banded. Using this there was shown that the standard deviation of the maximum response for stationary conditions should be reduced substantially. For the maximum response the reduction was approximately 50%.

# Sammendrag

Denne avhandlingen vurderer den foreslåtte byggingen av en hengebru i et spenn over Sognefjorden i lys av jordskjelv. Den foreslåtte broen har et spenn på 3700 meter og tårnene har en høyde på 455 meter. Om broen blir bygd vil den være den lengste hengebro noensinne bygd med god margin. Dagens regelverk er ikke utviklet for å håndtere konstruksjoner som dette. Det har derfor blitt gjennomført en litteraturstudie for å undersøke teorier utviklet for å beregne jordskjelv respons på lange hengebruer. En metode som ble funnet er «the Pseudo Excitation Method» utviklet for å vurdere seismiske påvirker på hengebroer med lange spenn ved å bruke teori om stokastiske svingninger. Denne metoden har i Kina vært brukt i seismisk utforming av flere lange hengebroer og er i den kinesiske retningslinjen for seismisk utforming av lange broer den foretrukne metoden. Denne metoden er presentert i denne avhandlingen.

Modellering av den foreslåtte hengebroen over Sognefjorden ble utført ved bruk av SAP2000. Analyse viste at den første eigenmoden hadde en periode på 36 sekunder og at over 2000 forskjellige moder ble identifisert i systemet. De modale deltagelses faktorer avslører at det er moder så høye som mode 1200 som bidrar vesentlig til responsen i systemet.

Før respons analysene for systemet ble utført ble to dempings modeller for systemet vurdert, Rayleigh og hysterese demping. Når frekvens responsen ble beregnet for de 300 første frekvensene og Rayleigh-dempingen ble kontrollert ved den første og hundre naturlige frekvensene viste resultatene at Rayleigh demping ga en respons dobbelt så stor som ved bruk av hysterese demping for flere av frekvenser i området mellom mode 1 og mode 100. Dermed ble hysterese demping brukt i analysene av broen.

I Eurocoden, NS-EN 1998-2 er det satt at vind ikke skal tas hensyn til i jordskjelv analyser. Men siden den foreslåtte broen over Sognefjorden er en veldig slank struktur ble demping effekter fra vinden vurdert. Dette ble gjort ved hjelp av kvasi-statiske teori. Siden de aerodynamiske konstantene for denne broen ennå ikke er undersøkt, ble verdiene for Hardangerbrua brukt. Dette ga et grovt estimat av virkningene av den aerodynamiske dempingen, som ga en reduksjon for frekvens responsen på 25 % for den første naturlige frekvens for forskyvning i y-retningen i midt-spennet. Reduksjonen ble mindre for høyere moder, men var fortsatt betydelig.

Respons beregning for jordskjelv ble gjennomført i MATLAB, ved å bruke stokastisk vibrasjons teori i frekvensdomenet. Tre analyser ble gjennomført hvor det ble forutsatt stasjonære forhold; seismisk bølge i lengderetningen av broen hvor både «Wave-passage» og «Incoherence» effekter ble tatt hensyn til, seismisk bølge in lengderetning av broen hvor bare «Wave-passage» effekter er tatt hensyn til og seismisk bølge som kommer vinkelrett på broen hvor det derfor ikke er romlige effekter til stede. Resultatene viste at det var betydelige forskjeller responsen fra de tre analysene både i størrelse og form. Maksimal respons ble funnet i z-retning i analysen hvor både «Wave-passage» og «Incoherence» effektene ble vurdert og var 0,81 meter.

Som følge av den høye perioden i den første eigenmoden i systemet, er antagelsen om stasjonære forhold ikke gyldig. For å vurdere effekten av ikke-stasjonær forhold er en forenklet metode hvor responsen i hver frihetsgrad er beregnet som for et system av en frihetsgrad. Responsspekter kurvene for de undersøkte punktene viser at dette er et godt estimat siden de er smalbåndet. Ved

hjelp av dette ble det vist at standardavviket av responsen for stasjonære forhold bør reduseres betydelig. For den maksimale respons ble reduksjonen omkring 50%.

# Table of Content

# List of Figures

# List of Tables

# 1 Introduction

The Norwegian west coast is connected together through the road, E39, which stretches from Kristiansand in south to Trondheim in north. E39 connects the four most populated cities in Norway after Oslo (Bergen, Trondheim, Stavanger and Kristiansand) and is therefore of great importance. Today eight fjords have to be crossed with ferries on this distance. In 2010 the Norwegian Ministry of Transport and Communication ordered a report from the Norwegian Public Road Administration of the possibility of crossing these fjords without using ferries. One part of the report was looking at the technological aspect of these crossing. Therefore one of the crossings was chosen to develop concepts for crossing of wide and deep fjords. The crossing selected was Sognefjorden, which on the proposed stretch between Lavik and Oppedal has a width of 3700 meters and a depth of 1300 meters. Four concepts have been developed: suspension bridge with one span, suspension bridge/cable stayed bridge with several spans and floating foundations, floating bridge, pipe bridge and the combination of the two latter. In this thesis the concept of suspension bridge with one span (from now on called "the Sognefjord Bridge") is evaluated further in terms of earthquake response. A suspension bridge with a span of 3700 meters has never been built. Today the longest suspension bridge span in the world is the Akashi Kaikyō Bridge in Japan with a main span of 1991 meters (3), but a bridge over the Messina Strait in Italia with a span of 3300 meters is under planning (4).

The main challenge with long span bridges in the context of earthquake is the spatial effects, i.e. effects produced by the large extent of the structure. Three types of effects are recognized. The first is called the "wave passage effect" and is caused by different arrival times for the seismic waves at the various supports. The distance between the supports also causes loss of coherence because of reflections and refractions of seismic waves in inhomogeneous material, or by different in manner of superposition of wave travelling from an extended fault. This is called the "incoherence effect" (2, 5, 6). The third spatial effect is called "site response effect", this is the effect caused by the local soil conditions at the supports.

The response spectrum method which is the most common method for seismic calculations cannot account for these effects. Traditionally the time-history method has therefore been used in computation of long span structures. Since no earthquakes are alike, numerous time-histories must be used to give statistical average. This makes this method computationally expensive. As a result of this, much research has been invested in creating more efficient computational methods in the last decades. The common opinion is that the random vibration approach is the way to go. The main advantage of this method is that it provides a statically measure without requiring any arbitrary selected input variables as with the time-history method (2). Several experts have made great effort in developing the random vibration method. Lee and Penzien (7) developed a stochastic method for seismic analyses of structures subjected to multiple support excitations in both time and frequency domain, where cross-correlation of the multiple-support excitations where accounted for. Berra and Kausel (8) proposed an extension to the response spectrum method, where each spectral value for the given response spectrum was adjusted by mean of a correlation factor. Der Kiureghian and Neuenhofer (2) developed the response spectrum method, which included the effects of wave passage, incoherence and local soil conditions.

Ernesto and Vanmarcke (9) proposed a method where the multiple support system was reduced to a series of linear one-degree of freedom systems in a way that fully accounts for the multi-support input. Common for all these methods are that they requires a large computational power to solve high degree random differential equations. Nevertheless, Der Kiureghian and Neuenhofer's response spectrum method has been included as one of the proposed methods in the European seismic bridge code, NS-EN 1998-2 (10).

Another approach to random vibration analysis is the Pseudoexcitation method (PEM), this method was developed by Lin (11) and first published in 1991. Further development has been conducted since (12-18). PEM is a method for stationary and non-stationary random vibration analyses for long-span structures (18). There have been several engineering analysis conducted where PEM successfully have been applied and since 2008 the PEM method has the been recommended method in the Chinese guidelines for seismic analysis for long span bridges (16).

A challenge when using random vibration theory on long-span bridges is that they will have long natural periods. Normally using random vibration there is assumed stationary condition, i.e. the probability does not change with time. For structures where the natural periods are small compared to the duration of the load this is a fair assumption, but for long span bridges the natural periods can be expected to be in the same range as the duration of the earthquake. The stationary assumption can therefore not be justified and the structure should therefore be analysed using non-stationary conditions.

## 1.1 Objects and Limitations

- Much research has been conducted on the problem with dynamic analyses of structures of large extend. One of the research objective are therefore to do a literature survey on what research have been done and if there have been any new development the last years.

- A bridge with the span of the Sognefjord Bridge has never been built. There is therefore unknown what the natural frequencies will be. One of the research questions is therefore to develop an analysis model of the Sognefjord Bridge using SAP2000 and study these parameters. The drawings and the information provided by the Norwegian Public Road Administration will be used and no further calculation of dimensions or reinforcement will be conducted. Soil-structure interaction will not be accounted for.

- A complex and large structure as the Sognefjord Bridge will have hundreds of natural frequencies. The traditional Rayleigh damping which often is used in structural analysis controls the damping using two defined natural frequencies. Deciding these natural frequencies is not easy when there are so many. On research question is therefore to investigate an alternative damping model, hysteretic damping, and compare the result with the result using Rayleigh damping.

- In Norway earthquake is not a large problem, nevertheless does the Eurocode require that structures are checked against earthquake. The pylons of the Sognefjord Bridge will be the highest structure ever built on the mainland of Norway and a bridge with this span has never been. There is therefore difficult to know what response to expect. One research question is therefore to calculate the response of the bridge. The structure will be analyses assuming stationary conditions and the spatial effects will be incorporated. If there is enough time non-stationarities will be investigated. Traffic loads will not be regarded.

# 2 Theory

## 2.1 Random Vibrations

Earthquakes are highly unpredictable events. Time of occurrence, frequency content, magnitude and duration are all variables that not can be predicted in advance. Earthquakes can therefore be characterizes as a random vibration. The best way of characterizing an earthquake in advance is therefore using probability.

### 2.1.1 Stationary Random Process in General

A normal assumption when dealing with random vibration in engineering purposes is to assume stationary condition. By stationary condition, there is meant that the probability conditions for the random process are independent of absolute time. To decide if the random process is stationary, a rule of thumb is that if the process last for a long time compared to the period of the systems lowest natural frequency, the process is time independent and stationary conditions can be assumed. However, if the system has a beginning and an end the process is non-stationary. Earthquakes have definitely a start and an end, and are therefore non-stationary processes. In most cases the structures period is low compared to duration of the earthquake. Therefore, often a weakly stationary process is defined to simplify the analyses. A weakly stationary process is a process where only the mean value and autocorrelation function is not allowed to vary with time.

For seismic ground motions a Gaussian probability distribution is usually assumed. This distribution is given by Eq. (3.1.1), where $\bar{x}$ is the mean value and $\sigma^2$ is the variance expressed by Eq. (3.1.2).

$$p(x) = \frac{1}{\sqrt{2\pi}} \exp(-\frac{(x-\bar{x})^2}{2\sigma^2} \tag{3.1.1}$$

$$\sigma^2 = \int_{-\infty}^{\infty} (x-\bar{x})^2 \, p(x) dx \tag{3.1.2}$$

A random process can be thought of as an infinite collection of sample functions x(t) occurring simultaneously, in this case n numbers of Gaussian distributions at an arbitrary time instants. This joint probability density function, $p(x,t)$, is also called a Gaussian random process. The joint probability density function (19) is only dependent of the mean values and the covariance, therefore the Gaussian random process is strictly stationary.

In addition to the assumed Gaussian distribution, seismic ground motion record is also assumed to be ergodic. A stationary process is ergodic if the average of all the individual samples is equal the joint distribution average, i.e. each individual sample can represent the random process.

An important function when investigating different values in a random process is the autocorrelation function. The autocorrelation function is defined by Eq. (3.1.3), where T is the duration and $\tau$ is the separation time between the sample functions.

$$R_{xx} = E\left[x(t)x(t+\tau)\right] = \lim_{T\to\infty} \frac{1}{T} \int_{-T/2}^{T/2} x(t)x(t+\tau)dt \tag{3.1.3}$$

The Wiener –Khintchine theorem states that for an arbitrary stationary random process x(t), the auto-power spectral density (auto-PSD) is the Fourier transformed of the autocorrelation function as expressed in Eq(3.1.4).

$$S_{xx} = \frac{1}{2\pi} \int_{-\infty}^{\infty} R_{xx}(\tau)\exp(-i\omega\tau)d\tau \tag{3.1.4}$$

As a result, if an auto-PSD exists, the autocorrelation can be found by the inverse Fourier transform, Eq. (3.1.5).

$$R_{xx}(\tau) = \int_{-\infty}^{\infty} S_{xx}(\tau)\exp(iw\tau)d\omega \tag{3.1.5}$$

Three important properties for the auto-PSD can be obtained.

1. From Eq.(3.1.4) , it can be shown by introducing the Euler formula that $S_{xx}$ is an even function.

$$S_{xx}(\omega) = S_{xx}(-\omega) \tag{3.1.6}$$

2. $S_{xx}$ is a non-negative real number (19)

$$S_{xx}(\omega) \geq 0 \tag{3.1.7}$$

3. The auto-PSD for the deviates of the random process x(t) can be calculated on the following matter (20).

$$S_{\dot{x}\dot{x}}(\omega) = \omega^2 S_{xx}(\omega) \tag{3.1.8}$$

$$S_{\ddot{x}\ddot{x}}(\omega) = \omega^4 S_{xx}(\omega) \tag{3.1.9}$$

The cross-correlation functions between to stationary random functions of time x(t) and y(t) is defined by Eq. (3.1.10) and (3.1.11).

$$R_{xy} = E\left[x(t)y(t+\tau)\right] = \lim_{T\to\infty} \frac{1}{T} \int_{-T/2}^{T/2} x(t)y(t+\tau)dt \tag{3.1.10}$$

$$R_{yx} = E\left[y(t)x(t+\tau)\right] = \lim_{T\to\infty}\frac{1}{T}\int_{-T/2}^{T/2} y(t)x(t+\tau)dt \tag{3.1.11}$$

As for the auto-PSD, the cross-power spectral density (cross-PSD) can be calculated by matter of Fourier transformation of the cross-correlation functions

$$S_{xy} = \frac{1}{2\pi}\int_{-\infty}^{\infty} R_{xy}(\tau)\exp(-i\omega\tau)d\tau \tag{3.1.12}$$

$$S_{yx} = \frac{1}{2\pi}\int_{-\infty}^{\infty} R_{yx}(\tau)\exp(-i\omega\tau)d\tau \tag{3.1.13}$$

### 2.1.2 Non-Stationary Random Vibrations in General

Earthquakes are as earlier stated non-stationary random processes, but are in most cases simplified by using a stationary random process. For long-span bridges the first natural period is often higher than 15 seconds. In comparison, the duration of a strong near-fault earthquake is about 30 seconds (21). This means that the first period of the system is in the same range as the duration of the earthquake. Stationary condition can therefore not be justified for these types of constructions.

Non-stationary condition can be introduced using the evolutionary power spectra method developed by Priestly (22), Eq. (3.1.14).

$$f(t) = \int_{-\infty}^{\infty} A(\omega,t)\exp(i\omega t)d\alpha(\omega) \tag{3.1.14}$$

Here $A(\omega,t)$ is a non-uniform amplitude modulation function, also called an envelope. $\alpha(\omega)$ is an orthogonal process that satisfies the relations in Eq. (3.1.15) and Eq. (3.1.16).

$$x(t) = \int_{-\infty}^{\infty} \exp(i\omega t)d\alpha(\omega) \tag{3.1.15}$$

$$E\left[d\alpha^*(\omega_1)d\alpha(\omega_2)\right] = S_{xx}(\omega_1)\delta(\omega_2-\omega_1)d\omega_1 d\omega_2 \tag{3.1.16}$$

Here $\delta$ is the Dirac function, which is zero for all values except when $\omega_1 = \omega_2$.

This method is difficult to compute and the non-uniform modulation assumption is therefore often replaced by a uniform modulation assumption (18), which leads to Eq. (3.1.17)

$$f(t) = \int_{-\infty}^{\infty} g(t)\exp(i\omega t)dZ(\omega) = g(t)x(t) \tag{3.1.17}$$

Here is the non-uniformly modulated function, $A(\omega,t)$, replaced by an uniformly modulated function g(t). This simplifies the equation substantially.

### 2.1.3

### 2.1.4 Parametric Model Used to Describe the Spectral Density

The most common method used to describe the spectral density of the random field with a parametric model, is using the Kanai-Tajimi spectrum (23) and its extension proposes by Clough and Penzien (24). Parameters in these models can be modified to account for different soil conditions. The Kanai model is presented in in Eq. (3.1.18).

$$S_{\ddot{x}g} = \frac{1+4\xi_g^2\left(\frac{\omega}{\omega_g}\right)^2}{\left(1-\left(\frac{\omega}{\omega_g}\right)^2\right)^2+4\xi_g^2\left(\frac{\omega}{\omega_g}\right)^2}S_0 \tag{3.1.18}$$

Here, $\omega_g$ and $\xi_g$ is the characteristic frequency and damping ratio for a given soil condition. $S_0$ is the amplitude of a Gaussian white process that should be adapted the expected magnitude of the earthquake. This is done using the prediction for the most probable peak factor for a stationary random Gaussian process, Eq. (3.1.19). In which $a_{\max}$ is the maximum acceleration amplitude, also known as the PGA, $\sigma_0$ is the unknown standard deviation and r is the peak factor. Vanmarcke and Lai (25) found that 2.74 was a reasonable value for the peak factor.

$$r = \frac{a_{\max}}{\sigma_0} \tag{3.1.19}$$

The magnitude adapted $S_0$ is then found by Eq. (3.1.20).

$$S_0 = \frac{{\sigma_0}^2}{\int_0^{\infty} S_{\ddot{x}_g}(\omega, S_0 = 1)d\omega} \tag{3.1.20}$$

The Kanai-Tajimi filter passes low frequencies that are not typical for earthquake records. Therefore a high pass filter that attenuates the low frequencies is necessary. Clough and Penzien (24) proposed an extension to the Kanai filter, Eq. (3.1.21).

$$S_{\ddot{x}_g}(\omega) = \frac{1+4\xi_g^2\left(\frac{\omega}{\omega_g}\right)^2}{\left(1-\left(\frac{\omega}{\omega_g}\right)^2\right)^2+4\xi_g^2\left(\frac{\omega}{\omega_g}\right)^2}\frac{\left(\frac{\omega}{\omega_h}\right)^4}{\left(1-\left(\frac{\omega}{\omega_h}\right)^2\right)^2+4\xi_h^2\left(\frac{\omega}{\omega_h}\right)^2}S_0 \tag{3.1.21}$$

Here, $\omega_h$ and $\xi_h$ are the frequency and damping parameter for specific soil conditions.

Much research has been conducted in finding parameter for these spectra and several parameters have been proposed. Kiuregihan and Neuenhofer (2) proposed the values presented in Table 2.1.

**Table 2.1 Parameters for the Kanai-Tajimi filter and Clough and Penzien filter proposed by Kiureghian and Neuenhofer (2)**

| $\omega_g$ [rad/s] | $\xi_g$ | $\omega_g$ [rad/s] | $\xi_h$ |
|---|---|---|---|
| 15 | 0.6 | 1.5 | 0.6 |

### 2.1.5 Power Spectral Density for Spatial Varying Ground Accelerations

Seismic ground motions are varying over distances and the effects this causes for structures of large extent has been a concern for a long period. Research has shown that these effects can have major significance for the response of the structures (26). In most cases will these effects reduce the response, but for some cases the response will increase. Therefore, when dealing with structures of large extent and multiple-supports, multiple excitations should be applied. The PSD matrix for multiple excitation of N supports are shown in Eq. (3.1.22).

$$S_{xx}(i\omega) = \begin{bmatrix} S_{\ddot{x}_1\ddot{x}_1} & S_{\ddot{x}_1\ddot{x}_2} & \cdots & S_{\ddot{x}_1\ddot{x}_N} \\ S_{\ddot{x}_2\ddot{x}_1} & S_{\ddot{x}_2\ddot{x}_2} & \cdots & S_{\ddot{x}_2\ddot{x}_N} \\ \vdots & \vdots & \ddots & \vdots \\ S_{\ddot{x}_N\ddot{x}_1} & S_{\ddot{x}_N\ddot{x}_2} & \cdots & S_{\ddot{x}_N\ddot{x}_N} \end{bmatrix} \tag{3.1.22}$$

Here, $S_{\ddot{x}_k\ddot{x}_l}$ is the spectral density corrected for spatial effects, Eq. (3.1.23).

$$S_{\ddot{x}_k\ddot{x}_l} = \rho_{kl}(i\omega)\sqrt{S_{\ddot{x}_k}(\omega)S_{\ddot{x}_l}(\omega)} \tag{3.1.23}$$

Research on local effects has shown that they have little effect on the structural response(18), therefore differences between $S_{\ddot{x}_k}$ and $S_{\ddot{x}_l}$ are of low significance and can therefore be assumed equal. The acceleration coherence function, $\rho_{kl}(i\omega)$ is found by Eq. (3.1.24).

$$\rho_{kl}(i\omega) = |\rho_{kl}(i\omega)| \exp(-i\omega \frac{d_{kl}^L}{v_{app}}) \tag{3.1.24}$$

The last term in this equation expresses the wave passage effect. Here $d_{kl}^L$ are the projected distances between two supports and $v_{app}$ is the wave propagation velocity. Since $d_{kl}^L$ is distance relative to the coordinate system, the wave passage term becomes a Hermitian matrix.
The first term in Eq. (3.1.24) is characterizing the incoherence effect (2). Several coherence models have been developed and can be uses to describe the incoherence (27-30). One of the

most common models is the Harichandran –Vanmarcke model (27). The model is presented in Eq.(3.1.25),

$$\left|\rho_{kl}(\omega, d_{kl})\right| = A\exp\left[-\frac{2d_{kl}}{\alpha\theta(\omega)}(1-A+\alpha A)\right]+(1-A)\exp\left[-\frac{2d_{kl}}{\alpha\theta(\omega)}(1-A+\alpha A)\right] \quad (3.1.25)$$

where $\theta(\omega)$ is determined from Eq. (3.1.26).

$$\theta(\omega) = K\left[1+\left(\frac{\omega}{\omega_0}\right)^b\right]^{-0.5} \quad (3.1.26)$$

The constants in Eq.(3.1.25) and Eq.(3.1.26) are obtained through studies of the Smart-1 array (information about the Smart-1 array can found in (5)): A=0.736, $\alpha = 0.147$, K=5210, $\omega_0 = 6.85\,\text{rad/s}$, b=2.78. The distance term $d_{kl}$ is not relative to the coordinate system, i.e. only positive numbers, thus is the incoherence term a symmetric matrix.

### 2.1.6 Extreme Values

In a design calculation an important value is the extreme value of the response. Davenport (31) approximated this values by using a Poisson model which considered the independence of the crossing of a positive and negative symmetric threshold by the random process(5). The mean value of the expected extreme value is given by Eq. (3.1.27).

$$E(y_{\max}) \approx \left((2\ln(\upsilon T))^{1/2} + \frac{\gamma}{(2\ln(\upsilon T))^{1/2}}\right)\sigma_y \quad (3.1.27)$$

Where T is the time interval, i.e. the duration of the earthquake, the Euler constant $\gamma$ =0.5772, $\sigma_y$ is the standard deviation of the response and $\upsilon$ is given by Eq. (3.1.28).

$$\upsilon = \frac{1}{\pi}\frac{\int_0^\infty \omega_i S_{yy}(\omega)dw}{\int_0^\infty S_{yy}(\omega)dw} \quad (3.1.28)$$

The term between the brackets in Eq. (3.1.27) is known as the peak factor, $k_p$. This extreme value model is developed for wind engineering. An extreme value model for earthquake was developed by A.D. Kiureghian based on the work of E.H. Vanmarcke (18), but this model is not presented in this thesis.

## 2.2 Pseudo Excitation Method (PEM)

The pseudo excitation method is a method for solving high-degree of freedom stochastic differential equation with multiple excitations developed by Lin and Zhang (15).

### 2.2.1 Stationary Conditions

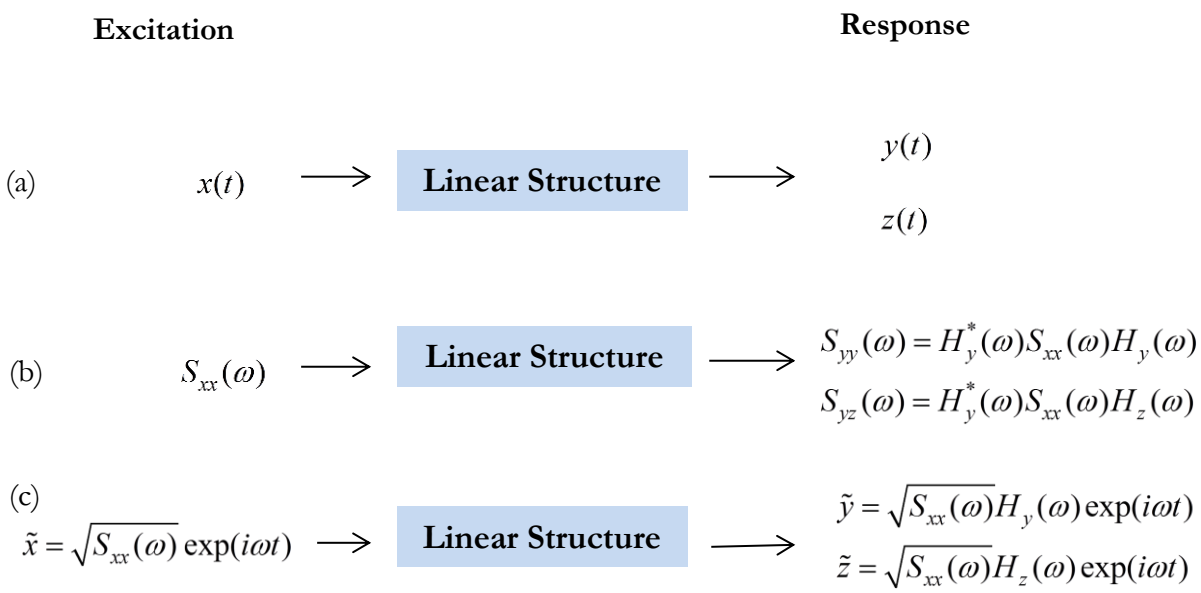


**Figure 2.1 Diagram showing the basic principle of PEM for stationary conditions**

If a linear system is subjected to a zero-mean single stationary random excitation x(t) with a given spectra density $S_{xx}$, and two arbitrary selected responses, y(t) and z(t) are selected. Using the conventional method, the auto -PSD can be calculated as shown in Figure 2.1(b). Where $H_y(\omega)$ and $H_z(\omega)$ are the complex frequency response function for the two responses and where * denotes the complex conjugated. The general expression for the frequency response function for a coupled system with conventional damping is shown in Eq. (3.2.1).

$$H(\omega) = (-\omega^2 M + i\omega C + K)^{-1} \tag{3.2.1}$$

By replacing the random excitation, x(t) by an assumed sinusoidal excitation(11), Eq.(3.2.2), the responses, y(t) and z(t) can be written as harmonic responses.

$$\tilde{x} = \sqrt{S_{xx}(\omega)}\exp(i\omega t) \tag{3.2.2}$$

This can be shown by using the frequency response method(20). Assuming the amplitude equal one, the excitation x(t) can be written as an harmonic input, Eq. (3.2.3).

$$x(t) = \exp(i\omega t) \tag{3.2.3}$$

As a result can the response functions also be written as a harmonic outputs when the system is linear, Eq. (3.2.4) and Eq. (3.2.5).

$$y(t) = H_y(\omega)\exp(i\omega t) \tag{3.2.4}$$

$$z(t) = H_z(\omega)\exp(i\omega t) \tag{3.2.5}$$

When assuming Eq. (3.2.2), the harmonic responses for y(t) and z(t) is written respectively as Eq. (3.2.6) and Eq. (3.2.7).

$$\tilde{y} = \sqrt{S_{xx}(\omega)}H_y(\omega)\exp(i\omega t) \tag{3.2.6}$$

$$\tilde{z} = \sqrt{S_{xx}(\omega)}H_z(\omega)\exp(i\omega t) \tag{3.2.7}$$

By taking the product of the response and its complex conjugate, Eq. (3.2.8) and Eq. (3.2.9) are obtained.

$$\tilde{y}^*\tilde{y} = \sqrt{S_{xx}}H_y^*(\omega)\exp(-i\omega t)\sqrt{S_{xx}}H_y(\omega)\exp(i\omega t) = H_y^*(\omega)S_{xx}H_y(\omega) \tag{3.2.8}$$

$$\tilde{y}^*\tilde{z} = \sqrt{S_{xx}}H_y^*(\omega)\exp(-i\omega t)\sqrt{S_{xx}}H_z(\omega)\exp(i\omega t) = H_y^*(\omega)S_{xx}H_z(\omega) \tag{3.2.9}$$

The last term in these equation are the same as the conventional expressions, Figure 2.1(b), hence Eq. (3.2.10) and Eq. (3.2.11).

$$S_{yy}(\omega) = \left|H_y(\omega)\right|^2 S_{xx} = \tilde{y}^*\tilde{y} \tag{3.2.10}$$

$$S_{yy}(\omega) = H_y^*(\omega)S_{xx}H_z(\omega) = \tilde{y}^*\tilde{z} \tag{3.2.11}$$

There can also be noted that the sinuous part of Eq. (3.2.10) and Eq. (3.2.11) disappears when its multiplied with their complex conjugates, therefore can expression for the auto-PSD and the cross-PSD be written as Eq. (3.2.12) and Eq. (3.2.13).

$$S_{yy}(\omega) = \tilde{y}^*\tilde{y} = a_y^* a_y^T \tag{3.2.12}$$

$$S_{yz}(\omega) = \tilde{y}^*\tilde{z} = a_y^* a_z^T \tag{3.2.13}$$

In which $a_y$ is given by Eq. (3.2.14)

$$a_y = H_y(\omega)\sqrt{S_x} \tag{3.2.14}$$

For systems subjected to multiple stationary excitations the PSD matrix has to be decomposed to obtain an expression for the pseudo excitation vector, Eq. (3.2.15).

$$\tilde{\mathbf{x}} = \sqrt{d_j}\mathbf{l}_j\exp(i\omega t) = a_{yj}\exp(i\omega t) \tag{3.2.15}$$

This decomposition can be done using Cholesky's method, Eq.(3.2.16), since the PSD is a Hermitian matrix (18, 32).

$$\mathbf{S}_{xx}(\omega) = \mathbf{L}^{*}\mathbf{D}\mathbf{L}^{T}\sum_{j=1}^{r} d_j \mathbf{l}_j^{*}\mathbf{l}_j^{T} \tag{3.2.16}$$

Here **L** is the lower triangular with a diagonal with values of unity, **D** is a nonzero diagonal matrix with values $d_j$ (18).

Using Eq.(3.2.15) the displacement vector can then be calculated in the same way as for a single excitation, hence Eq. (3.2.17) and Eq. (3.2.18).

$$\tilde{\mathbf{y}}_j = \mathbf{a}_{yj}\exp(i\omega t) \tag{3.2.17}$$

$$\tilde{\mathbf{z}}_j = \mathbf{a}_{zj}\exp(i\omega t) \tag{3.2.18}$$

The corresponding auto-PSD and cross-PSD can be calculated by Eq. (3.2.19) and Eq. (3.2.20).

$$S_{yy}(\omega) = \sum_{j=1}^{r} \tilde{y}_j^{*}\tilde{y}_j^{T} = \sum_{j=1}^{r} a_{yj}^{*}a_{yj}^{T} \tag{3.2.19}$$

$$S_{yz}(\omega) = \sum_{j=1}^{r} \tilde{y}_j^{*}\tilde{z}_j^{T} = \sum_{j=1}^{r} a_{yj}^{*}a_{zj}^{T} \tag{3.2.20}$$

### 2.2.2 Non-Stationary Random Vibrations Using Uniformly Modulated Evolutionary Random Excitations

As shown in Chapter 2.1.2 can the expression for non-stationary condition be reduced to Eq. (3.2.21) when a uniform modulation function is used.

$$f(t) = g(t)x(t) \tag{3.2.21}$$

Here g(t) is a uniform slowly varying modulating function. Two typical definitions of the uniform modulating functions are shown in Eq. (3.2.22) and Eq. (3.2.23).

$$g(t) = \begin{cases} I_0\left(\frac{t}{t_1}\right)^2 & 0 \le t \le t_1 \\ I_0 & t_1 \le t \le t_2 \\ I_0\exp(c(t-t_2)) & t \ge t_2 \end{cases} \tag{3.2.22}$$

$$g(t) = \begin{cases} 1 & t \ge 0 \\ 0 & t < 0 \end{cases} \tag{3.2.23}$$

Another way to describe the envelop function g(t) is using a function as Eq.(3.2.24). If this function is integrated with respect to time, the function will adopt a shape similar to the Arias intensity plot if the constants $\alpha$ and $\beta$ are calibrated properly. This is shown in Figure 2.2, there is notable that this plot is done for a near-fault earthquake with low magnitude and therefore becomes the time duration of the uniform modulation function short.

$$g(t) = t^{\alpha} \exp(-\beta t^{\alpha}) \tag{3.2.24}$$

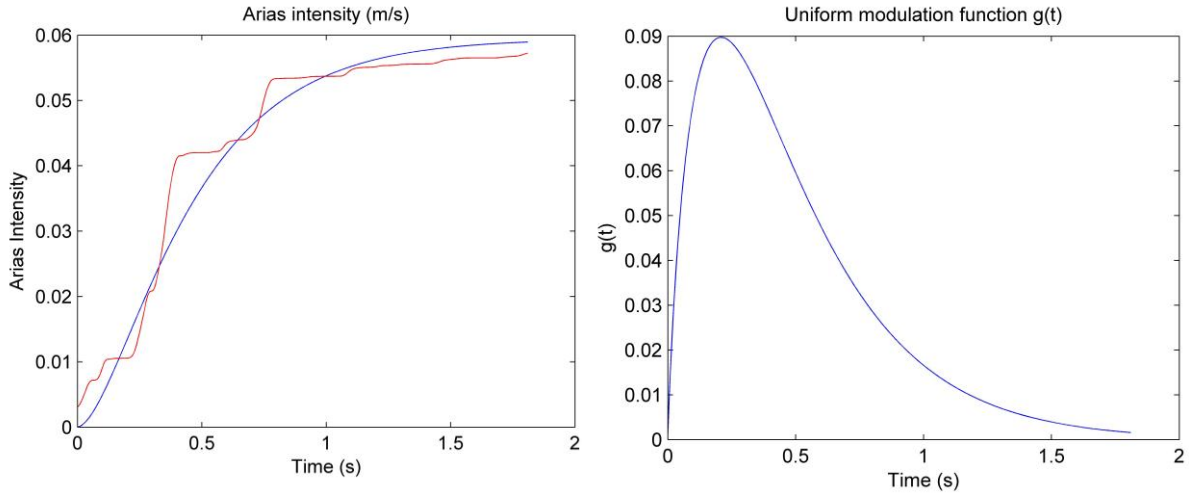


**Figure 2.2 To the left: Plot of arias intensity (red) and the integrated uniform modulation function (blue). To the right: Uniform fodulation function g(t)**

The basic principle when using PEM for a single excitation is illustrated by Figure 2.3. Using the pseudo excitation method, excitation for a single degree system can be written as shown in Figure 2.3(b). The arbitrarily pseudo response quantities $\tilde{y}(t)$ and $\tilde{z}(t)$ are not as easily obtained as for the stationary random excitation. This is because the frequency response function $H(\omega,t)$ is now time dependent. The response can be calculated either by a numerical integration scheme as Newmark (24) or precise integration method (33), by solving the differential equation in traditional manner for a decoupled system or using the convolution integral. Using a convolution integral the response vector can be written as Eq. (3.2.25). Here $h(t_j - \tau_j)$ is the impulse response function (19).

$$\tilde{\mathbf{y}}(\omega, t_j) = \int_0^{t_j} h_j(t_j - \tau_j) g(\tau_j) \exp(i\omega t) d\tau_j \sqrt{S_{xx}} \tag{3.2.25}$$

The auto-PSD and cross-PSD for the response can be calculated in the same manner as for the stationary random excitation, this is shown in Figure 2.3(c).

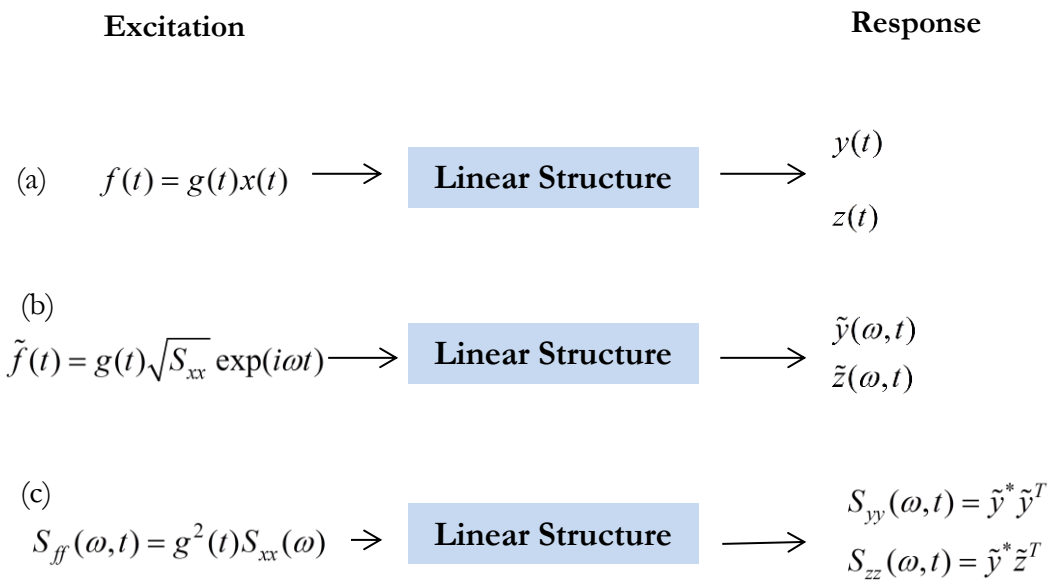


**Figure 2.3 Basic principle for the pseudoexcitation method for a single excitation**

For multiple excitations the evolutionary random excitation vector can be written as Eq. (3.2.26). Where **G**(t) is a diagonal matrix containing the uniform modulation functions and $\mathbf{x}(t)$ is a vector containing the stationary random excitations.

$$\mathbf{f}(t) = \mathbf{G}(t)\mathbf{x}(t) \tag{3.2.26}$$

The stationary random excitation can be replaced by a pseudo-excitation, $\tilde{f}(t)$, given by Eq. (3.2.27).

$$\tilde{\mathbf{f}} = \mathbf{G}(t)\mathbf{B}\mathbf{Q}\sqrt{S_{\ddot{x}_g}(\omega)}\exp(i\omega t) \tag{3.2.27}$$

Here **B** is a decomposition of the term expressing the wave passage effect, Eq. (3.2.28) , Q is a decomposition of expression of the incoherence effect. The latter can be decomposed using Cholesky's method in the same manner as in Chapter 2.2.1 or if the system is assumed fully coherent Q can be expresses as vector of unity. There can also be noted that if the local effects are neglected the stationary random excitation, $S_{xx}$ is the same for all the supports.

$$\mathbf{B} = diag(\exp(-i\omega t_1), \exp(-i\omega t_2), ...., \exp(-i\omega t_n)) \tag{3.2.28}$$

The auto-PSD for the non-stationary pseudo-excitation is given by Eq. (3.2.29).

$$S_{ff}(\omega,t)=\tilde{f}^{*}(t)\tilde{f}^{T}(t)=$$

$$S_{\ddot{x}_g}(\omega)\begin{bmatrix} g^2(t-t_1) & g(t-t_1)g(t-t_1)\times \exp(i\omega(t_1-t_2))\rho_{12} & \cdots & g(t-t_1)g(t-t_n)\times \exp(i\omega(t_1-t_n))\rho_{1n} \\ g(t-t_2)g(t-t_1)\times \exp(i\omega(t_2-t_1))\rho_{21} & g^2(t-t_2) & \cdots & g(t-t_2)g(t-t_n)\times \exp(i\omega(t_2-t_n))\rho_{2n} \\ \vdots & \vdots & \ddots & \vdots \\ g(t-t_n)g(t-t_1)\times \exp(i\omega(t_n-t_1))\rho_{n1} & g(t-t_n)g(t-t_1)\times \exp(i\omega(t_n-t_2))\rho_{n2} & \cdots & g^2(t-t_2) \end{bmatrix} \tag{3.2.29}$$

The same methods as for non-stationary single excitation can be used to obtain output for an arbitrarily selected response. Using the convolution integral the response can be found by Eq. (3.2.30). In which $\sqrt{\alpha_j}$ and $l_k$ are variable coming from decomposition of the coherence matrix by using such as Cholesky's method.

$$\tilde{\mathbf{y}}_k(\omega,t_k)=\sqrt{\alpha_j S_{\ddot{x}_g}}\,l_j\mathbf{B}\int_0^t \mathbf{H}(t_k-\tau_k)\mathbf{G}(\tau_k)\exp(i\omega\tau_k)d\tau_k \tag{3.2.30}$$

For two arbitrarily responses $\tilde{y}_{kj}(t)$ and $\tilde{y}_{lj}(t)$, the corresponding spectral densities can be computed by means of Eq. (3.2.31).

$$S_{y_k y_l}(\omega,t)=\sum_{j=1}^{r}\tilde{y}_{kj}(t)\tilde{y}_{lj}(t) \tag{3.2.31}$$

## 2.3 Simplified Method Two Assess Non- Stationarities

In section 2.2.2 there was shown that a convolution integral has to be solved to find the non-stationary response. As this is very computational demanding an alternative method to approximate the effect of non-stationarities is proposed.

Langen and Sigbjörnsson (19) calculated an example for a single-degree system excited by an evolutionary non-stationary random vibration, Eq. (3.2.23)

$$\ddot{y} = 2\xi\omega_0\dot{y} + \omega_0^2 y = \frac{Q(t)}{m} \tag{3.3.1}$$

The spectral density input for the system was defined by Eq.(3.3.2).

$$S_{xx} = \begin{cases} I & t \geq 0 \\ 0 & t < 0 \end{cases} \tag{3.3.2}$$

As the envelop function the uniform modulated function in Eq. (3.2.23) was used. The variance of the non-stationary solution of the system was shown be the result of Eq. (3.3.3).

$$\sigma_{yy}^2(t) = \begin{cases} \sigma_{yy}^2(\infty)\left(1-\exp(-\zeta\omega_0 t)\left(1+2\left(\frac{\zeta\omega_0}{\omega_d}\right)^2\sin^2(\omega_d t)+\frac{\zeta\omega_0}{\omega_d}\sin(2\omega_d t)\right)\right) & t \geq 0 \\ 0 & t < 0 \end{cases} \tag{3.3.3}$$

Here $\xi$ is the damping of the system, $\omega_0$ is the natural frequency of system, $\omega_d$ is the damped natural frequency given by Eq. (3.3.4) and $\sigma_{yy}^2$ is the variance of the stationary solution.

$$\omega_d = \omega_0\sqrt{(1-\zeta^2)} \tag{3.3.4}$$

This can be used to approximate the non-stationary solution from the stationary solution of a multi-degree of freedom system. Using the response spectrum curve for the displacement of a given DOF, the dominating frequency for this DOF can be found. By setting the natural frequency $\omega_0$, equal this dominating frequency the function can be plotted. The time when a steady stated is reached is found, i.e. the point where function is closing on its asymptote. If the duration of the earthquake is known, the time dependent variance at the end of the earthquake is found from the plot. The ratio between the variance at steady state and the variance at end of the earthquake is obtained and can be used to estimate the reduction of variance due to non-stationary conditions. If the response spectrum for the DOF is narrow banded this should produce a fair estimate.

## 2.4 Damping

In a construction there are many mechanism contributing to damping. Examples of this are; micro cracks, friction in connections and thermal effects as straining and frictions in the materials. The most common way to account for these effects is using viscous damping. This is a simple way to introduce damping in the system, but has its limitations. Therefore also other types of damping will be discussed.

### 2.4.1 Viscous Damping

Viscous damping is a simple way to introduce damping idealizes as a viscous dashpot. Here the damping force is proportional to the velocity in the system as shown in Eq. (3.4.1), where $f_D$ is the damping force, c is the viscous damping coefficient and $\dot{u}$ is the velocity.

$$f_D = c\dot{u} \tag{3.4.1}$$

For a multi degree of freedom (MDOF) system a damping matrix of viscous damping coefficients are made. Several methods can be used to construct this matrix, but the most common method is Rayleigh-damping. In Rayleigh-damping both the mass and stiffness matrix are used to construct the damping matrix, this is shown in Eq. (3.4.2).

$$\boldsymbol{c} = a_0\boldsymbol{m} + a_1\boldsymbol{k} \tag{3.4.2}$$

Here $a_0$ and $a_1$ is the proportionality constants which can be obtained by solving the system in Eq. (3.2.12).

$$\frac{1}{2}\begin{bmatrix} 1/\omega_i & \omega_i \\ 1/\omega_j & \omega_j \end{bmatrix}\begin{Bmatrix} a_0 \\ a_1 \end{Bmatrix} = \begin{Bmatrix} \xi_i \\ \xi_j \end{Bmatrix} \tag{3.4.3}$$

To solve this system the damping ratios $\xi_i$ and $\xi_j$, corresponding to the natural frequencies $\omega_i$ and $\omega_j$ must be set. Damping ratios for different frequencies are rarely available, therefore are often the same damping ratios set for both frequencies, i.e. $\xi_i = \xi_j = \xi$ (24). Using this assumption, a simplified equation for the proportionality constants can be expressed, Eq. (3.4.4).

$$\begin{Bmatrix} a_0 \\ a_1 \end{Bmatrix} = 2\frac{\zeta}{\omega_m + \omega_n}\begin{Bmatrix} \omega_m\omega_n \\ 1 \end{Bmatrix} \tag{3.4.4}$$

With Rayleigh damping the damping in the system is controlled by what natural frequencies, $\omega_i$ and $\omega_j$ that are selected. Typically the first natural frequency and a higher natural frequency that contributes significantly to the dynamic response are chosen. The modes between the two frequencies will be damped less than $\xi$, while the other modes will be damped greater than $\xi$ as illustrated in Figure 2.4.

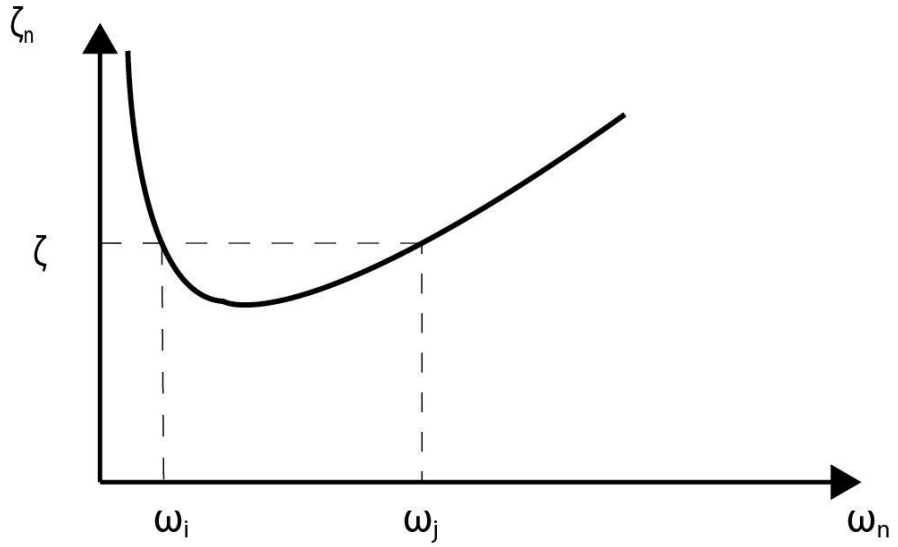


**Figure 2.4 Rayleigh damping - relation between damping ratios and frequencies**

For a construction with many natural frequencies and higher order modes with large modal participation factors there are some difficulties in applying the Rayleigh-damping. The challenge is choosing the second natural frequency needed to calculate the damping coefficients. One solution is to choose the highest mode as the second natural frequency, but this will give a very conservative damping for the intermediate modes. Another solution is to find the highest mode which contributes significant to the response of the system, but this can be difficult to decide.

There is also possible to use an extended Rayleigh damping. When using an extended Rayleigh damping, damping at multiple natural frequencies are set. This gives a system with more than two proportionality constants. However, as for the traditional Rayleigh damping there can be difficult to choose what natural frequencies to use.

### 2.4.2 Hysteretic Damping

An alternative to viscous damping is using hysteretic damping, also called rate-independent damping, structural damping and material damping. In viscous damping the energy dissipation is dependent on the excitation frequency, this is seen in Eq.(3.4.5). This equation expresses the energy dissipation per cycle.

$$E_D = \pi c \omega u_0^2 = 2\pi\zeta \frac{\omega}{\omega_n} u_0^2 \tag{3.4.5}$$

A great deal of research indicates that the energy loss is independent of the response frequency (24). This is a disadvantage with viscous damping as the Rayleigh damping.

The hysteretic damping force is expressed in Eq.(3.4.6), where $\eta$ is the damping coefficient.

$$f_D = \frac{\eta k}{\omega}\dot{u} \tag{3.4.6}$$

By replacing the damping term, c in Eq.(3.4.5), the equation for energy dissipation in a hysteretic damped system is obtained, Eq. (3.4.7). As seen is the energy dissipation independent of the excitation frequency.

$$E_D = \pi \eta k u_0^2 \tag{3.4.7}$$

An equivalent viscous damping coefficient $\eta$, can be obtained by equating the energy dissipation for viscous damping with the energy dissipation for hysteretic damping. The equation obtained from this procedure will be frequency dependent. This dependency can be removed by setting the natural frequency equal to the excitation frequency, Eq. (3.4.8) is then obtained.

$$\eta = 2\zeta_{eq} \tag{3.4.8}$$

The hysteretic damping can be rewritten to a complex form, the damping force is then written as Eq. (3.4.9).

$$f_D = i\eta k u \tag{3.4.9}$$

### 2.4.3 Non-Classical Damping

Different materials has different damping properties. In a structure consisting of two or more parts made by material with significant different damping properties, these properties should be accounted for. An example of this is a suspension bridge where the pylons are made by concrete and the cables and bridge deck are made by steel. Concrete have a considerable higher damping ratio than steel and therefore should the damping in the pylons be higher than in the cables and bridge deck. The different damping properties can be accounted for using a non-classical

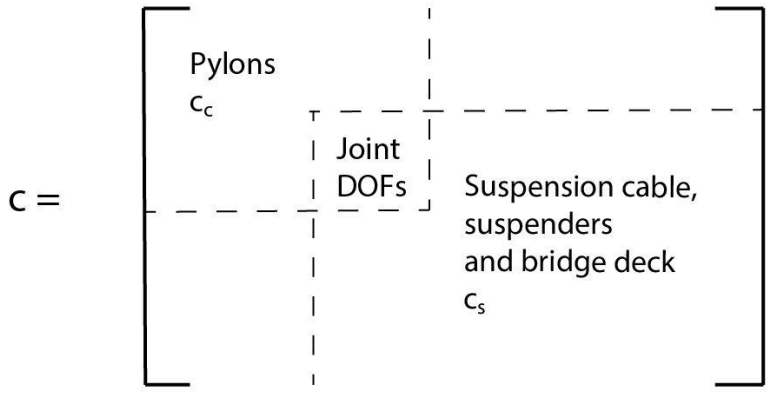


**Figure 2.5 Assembling of a non-classical damping matrix (Principle drawing)**

damping matrix. In the case of Rayleigh damping this matrix can be created by dividing the mass and stiffness matrix into two parts; one containing elements corresponding to DOFs in the pylons and one with elements corresponding to DOFs in cables and bridge deck. Using these two matrixes, a damping matrix for each of the structural parts is made. These can be combined using direct assembly to obtain the complete damping matrix for the structure. The basic principle is shown in Figure 2.5.

### 2.4.4 Aerodynamic Damping

According to the book *Wind loads on structures* by Claës Dyrbye and Svend O. Hansen (34) can the aerodynamic damping be of same magnitude as the structural damping. For a slender structure as a long suspension bridge there is therefore likely that the aerodynamic damping can have a significant impact.

The aerodynamic damping can be introduced as a quasi-static load using the buffeting theory. As presented, the theory is given for a line-like structure, i.e. constant height is assumed. Furthermore, there is assumed that structural displacements and cross-sectional rotations are small. Most of this theory is not relevant for this thesis and are therefore not explained in detail. For further reading is Theory of Bridge Aerodynamics by Einar Strømmen (35) recommended.

The buffeting load can be expressed as in Eq.(3.4.10), where $\bar{\boldsymbol{q}}$ is a static part, $\boldsymbol{B_q v}$ is the dynamic loading from turbulence, $\boldsymbol{C_{ae}\dot{u}}$ is the aerodynamic damping induced by velocity and $\boldsymbol{K_{ae}u}$ is the aerodynamic stiffness induced by the displacement.

$$\boldsymbol{q_{tot}}(x,t) = \bar{\boldsymbol{q}} + \boldsymbol{B_q v} + \boldsymbol{C_{ae}\dot{u}} + \boldsymbol{K_{ae}u} \tag{3.4.10}$$

Only the aerodynamic damping part of this expression is used. The velocity vector is given by Eq.(3.4.11), where the definition of direction is shown in Figure 2.6.

$$\dot{u}(x,t) = [\dot{u}_y \quad \dot{u}_z \quad \dot{u}_\theta] \tag{3.4.11}$$

The aerodynamic damping matrix is given by Eq. (3.4.12). Here $\rho$ is the density of air, V is the mean wind velocity, B are the width of the cross-section, D is the height of the cross-section, $\bar{C}_D$, $\bar{C}_L$, $\bar{C}_M$, $C'_D$, $C'_L$ and $C'_M$ are load coefficients.

$$\boldsymbol{C}_{ae} = \frac{-\rho V B}{2}\begin{bmatrix} 2(D/B)\bar{C}_D & (D/B)(C'_D - \bar{C}_L) & 0 \\ 2\bar{C}_L & C'_L + (D/B)\bar{C}_L & 0 \\ 2B\bar{C}_M & BC'_M & 0 \end{bmatrix} \tag{3.4.12}$$

The load coefficients are determined using wind tunnel experiments. They will vary with the angle of incidence $\alpha$, but are often assumed to be constant.

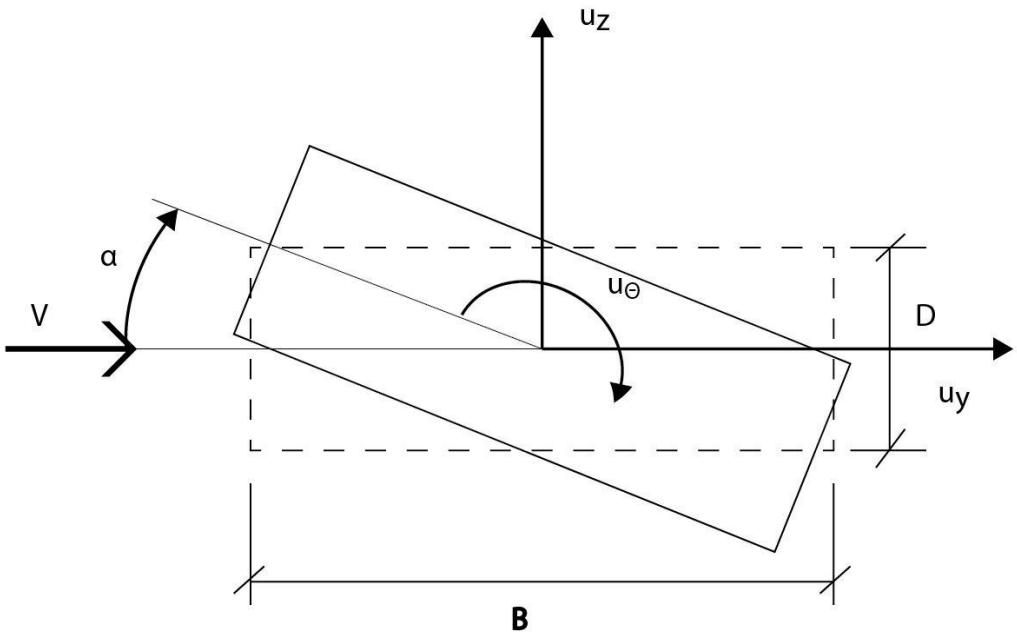


**Figure 2.6 Definition of directions and cross-section data for aerodynamic damping**

## 2.5 Equation of Motion for Multiple Excitations

When dealing with multiple-support problems, the equation of motion is extended with the degrees of freedom (DOF) of the supports. In portioned form with all the DOFs the equation of motion is written as Eq. (3.5.1).

$$\begin{bmatrix} \mathbf{m}_s & \mathbf{m}_{sb} \\ \mathbf{m}_{sb}^T & \mathbf{m}_b \end{bmatrix} \begin{Bmatrix} \ddot{\mathbf{x}}_t \\ \ddot{\mathbf{x}}_b \end{Bmatrix} + \begin{bmatrix} \mathbf{c}_s & \mathbf{c}_{sb} \\ \mathbf{c}_{sb}^T & \mathbf{c}_b \end{bmatrix} \begin{Bmatrix} \dot{\mathbf{x}}_t \\ \dot{\mathbf{x}}_b \end{Bmatrix} + \begin{bmatrix} \mathbf{k}_s & \mathbf{k}_{sb} \\ \mathbf{k}_{sb}^T & \mathbf{k}_b \end{bmatrix} \begin{Bmatrix} \mathbf{x}_t \\ \mathbf{x}_b \end{Bmatrix} \begin{Bmatrix} \mathbf{0} \\ \mathbf{p}_g(t) \end{Bmatrix} \tag{3.5.1}$$

In which subscript s denotes structural DOFs, subscript b denotes the base DOFs, subscript t denotes the total displacements and the force vector $\mathbf{p}_g(t)$ is the support forces. The total displacement vector $\mathbf{x}_t$ can be decomposed into two parts, Eq. (3.5.2).

$$\mathbf{x}_t = \mathbf{x} + \mathbf{x}_s \tag{3.5.2}$$

In this equation **x** is the dynamic displacement vector and $\mathbf{x}_s$ is the quasi-static displacement vector (2). An expression for the quasi-static displacement can be found by solving the static part of Eq. (3.5.1) . The following equation is obtained, Eq(3.5.3).

$$\mathbf{x}_s = -\mathbf{k}_s^{-1}\mathbf{k}_{sb}\mathbf{x}_b = \mathbf{R}\mathbf{x}_b \tag{3.5.3}$$

Here **R** is the influence matric. Substituting Eq. (3.5.2) and Eq. (3.5.3) into Eq. (3.5.1), the first of the two portioned equations can be written as Eq.(3.5.4).

$$\mathbf{m}_s\ddot{\mathbf{x}} + \mathbf{c}_s\dot{\mathbf{x}} + \mathbf{k}_s\mathbf{x} = (\mathbf{m}_s\mathbf{k}_s^{-1}\mathbf{k}_{sb} - \mathbf{m}_{sb})\ddot{\mathbf{x}}_b + (\mathbf{c}_s\mathbf{k}_s^{-1}\mathbf{k}_{sb} - \mathbf{c}_{sb})\dot{\mathbf{x}}_b + (\mathbf{k}_s\mathbf{k}_s^{-1}\mathbf{k}_{sb} - \mathbf{k}_{sb})\mathbf{x}_b \tag{3.5.4}$$

As can be seen, the last term of the equation is zero and therefore disappears. If lumped mass is assumed, the $\mathbf{m}_{sb}$ terms also disappears and the equation is reduced to Eq. (3.5.5).

$$\mathbf{m}_s\ddot{\mathbf{x}} + \mathbf{c}_s\dot{\mathbf{x}} + \mathbf{k}_s\mathbf{x} = (\mathbf{m}_s\mathbf{R})\ddot{\mathbf{x}}_b + (\mathbf{c}_s\mathbf{R} - \mathbf{c}_{sb})\dot{\mathbf{x}}_b \tag{3.5.5}$$

When a hysteretic damping is applied, the damping is depending on the displacement instead of the velocity as shown in section 2.4.2. The portioned equation of motion with a hysteretic damping can be written as Eq. (3.5.6).

$$\begin{bmatrix} \mathbf{m}_s & \mathbf{m}_{sb} \\ \mathbf{m}_{sb}^T & \mathbf{m}_b \end{bmatrix} \begin{Bmatrix} \ddot{\mathbf{x}}_t \\ \ddot{\mathbf{x}}_b \end{Bmatrix} + (1+i\eta) \begin{bmatrix} \mathbf{k}_s & \mathbf{k}_{sb} \\ \mathbf{k}_{sb}^T & \mathbf{k}_b \end{bmatrix} \begin{Bmatrix} \mathbf{x}_t \\ \mathbf{x}_b \end{Bmatrix} = \begin{Bmatrix} \mathbf{0} \\ \mathbf{p}_g(t) \end{Bmatrix} \tag{3.5.6}$$

In which $\eta$ is the damping constant. Rewriting the first of the equations in the same manner as for conventional damping, Eq. (3.5.7) is obtained.

$$\mathbf{m}_s\ddot{\mathbf{x}} + (1+\eta)\mathbf{k}_s\mathbf{x} = (\mathbf{m}_s\mathbf{k}_s^{-1}\mathbf{k}_{sb})\ddot{\mathbf{x}}_b + i\eta(\mathbf{k}_s\mathbf{k}_s^{-1}\mathbf{k}_{sb} - \mathbf{k}_{sb})\mathbf{x}_b \tag{3.5.7}$$

Here the last term becomes zero, therefore the equation can be written as Eq. (3.5.8).

$$\mathbf{m}_s\ddot{\mathbf{x}} + (1+\eta)\mathbf{k}_s\mathbf{x} = (\mathbf{m}_s\mathbf{R})\ddot{\mathbf{x}}_b \tag{3.5.8}$$

The ground acceleration in each of the support DOF, $\ddot{\mathbf{x}}_b$ can be written as a ground acceleration along the wave traveling direction, $\ddot{\mathbf{u}}_b$. This is done using a transfer matrix $E_{mN}$ as shown in Eq. (3.5.9). Subscript N is the number of supports and m is the number of support DOFs.

$$\ddot{\mathbf{x}}_b = \mathbf{E}_{mN}\ddot{\mathbf{u}}_b \tag{3.5.9}$$

$E_{mN}$ can be made by setting elements of corresponding support and translation DOFs to unity. By setting translation matrix as this, there is assumed that the same spectral density is applied in all three translation directions. The equation of motion can then be written as Eq.(3.5.10).

$$\mathbf{m}_s\ddot{\mathbf{x}} + (1+\eta)\mathbf{k}_s\mathbf{x} = (\mathbf{m}_s\mathbf{R})\mathbf{E}_{mN}\ddot{\mathbf{u}}_b \tag{3.5.10}$$

### 2.5.1 Equation of Motion When Using PEM

The power spectral density can be decomposed into Eq. (3.5.11) when local soil conditions are disregarded.

$$\mathbf{S}_{xx}(i\omega) = \mathbf{B}^*\sqrt{S_{\ddot{x}_g}}\mathbf{Q}^*\mathbf{Q}^T\sqrt{S_{\ddot{x}_g}}\mathbf{B} = \mathbf{P}^*\mathbf{P}^T \tag{3.5.11}$$

Where **B** and **Q** are described in section 2.2.2 and P is given by Eq. (3.5.12)

$$\mathbf{P} = \mathbf{B}\sqrt{S_{\ddot{x}_g}}\mathbf{Q} \tag{3.5.12}$$

According to the PEM, the pseudo-excitation can be written as Eq. (3.5.13).

$$\ddot{\tilde{\mathbf{U}}}_b = \mathbf{P}\exp(i\omega t) \tag{3.5.13}$$

By replacing $\ddot{\mathbf{u}}_b$ in Eq. (3.5.10) with the pseudo-excitation, Eq. (3.5.14) is obtained (17).

$$\mathbf{m}_s\ddot{\mathbf{x}} + (1+\eta)\mathbf{k}_s\mathbf{x} = (\mathbf{m}_s\mathbf{R})\mathbf{E}_{mN}\mathbf{P}\exp(i\omega t) \tag{3.5.14}$$

This equation is solved as described in section 2.2.1 and the pseudo-relative displacement is found. To calculate the pseudo-absolute displacement, the pseudo-static displacement vector fist must be found, Eq. (3.5.15).

$$\tilde{\mathbf{X}}_s = \frac{1}{\omega^2}\mathbf{R}\mathbf{E}_{mN}\mathbf{P}\exp(i\omega t) \tag{3.5.15}$$

The pseudo-absolute displacement is then expressed by Eq. (3.5.16).

$$\tilde{\mathbf{X}}_t = \tilde{\mathbf{X}} + \tilde{\mathbf{X}}_s \tag{3.5.16}$$

Using this equation the auto-PSD matrix for the absolute displacement is Eq. (3.5.17) (17).

$$\mathbf{S}_{X_t X_t}(\omega) = ((\tilde{\mathbf{X}} + \tilde{\mathbf{X}}_s)^*(\tilde{\mathbf{X}} + \tilde{\mathbf{X}}_s)^T) = \mathbf{Z}\ \mathbf{Z}^{T*} \tag{3.5.17}$$

Where $\mathbf{Z}$ is expressed by Eq. (3.5.18).

$$\mathbf{Z} = ((\mathbf{H}(\omega)\mathbf{M}_s\mathbf{R} + \frac{1}{\omega^2}\mathbf{R})\mathbf{E}_{mN}\mathbf{P}\exp(i\omega t) \tag{3.5.18}$$

## 2.6 Regulations

In Norway the National public road administration (NPRA) is responsible for the planning, construction and operations of public Norwegian roads. The NPRA is responsible for developing the Norwegian handbooks for roads called "Håndbøker". These books are divided into two levels; the first levels consist of regulations, norm and guidelines, the second level consists of manuals, textbooks and road data. For bridge engineering is "Håndbok 185- Bruprosjektering " (36) the main regulation.

In 2010 was the Norwegian building code, "Norsk standard" replaced by the common European code, the Eurocode. This led to a revision of "Håndbok 185 Bruprosjektering" adapted the Eurocode regulations. The revision is named "Håndbok 185 Bruprosjektering -Eurokodeutgave" (37) and are not formally a regulation, but has preliminary status as a guideline. Therefore the old regulation is formally still current. However, the recommendation from NPRA is to use the new issue as basis for all bridge engineering (37).

### 2.6.1 Handbook - "Håndbok 185 Bruprosjektering -Eurokodeutgave"

"Håndbok 185 Bruprosjektering -Eurokodeutgave", from now on only called "the handbook" states the hierarchy of handbooks, standards and other documents. Here is the handbook listed in front of the Eurocode. This means that if the Eurocode (NS-EN) and the Handbook contradicts, the handbook must be followed.

The handbook states that for seismic loads, the loads are found using NS-EN 1998-1 (38) and NS-EN 1998-2(10). As for the analyses they can be conducted using response spectra, spectral density function or a time series. Of this method only the response spectra method are described further.

In the handbook combinations of seismic loads with other loads are not mentioned specific. But there is stated that loads that are time and location dependent or is occurring with their maximum value at the same time, should be applied as one load by combinations of loads. By this there is assumed that traffic load should be applied. In the old handbook, 'Håndbook 185 – Bruprosjektering" there is stated that seismic loads should not be combined with other forces of nature.

### 2.6.2 Eurocode – NS-EN 1998

NS-EN-1998 is the regulations for design of structures for earthquake resistance. It consists of six parts, where only two of them are relevant for this thesis; NS-EN 1998-1 is the general regulation and NS-EN 1998-2 is the specific regulation for bridges. In the introduction of NS-EN 1998-2 suspension bridges are not defined to be part of the scope of this standard. Regardless of this, the main features of NS-EN 1998-2 are summarized to get an indication of what should be accounted for.

For bridges with continuous decks NS-EN 1998-2 requires that spatial effects are accounted for if one of these two conditions is met.

- If the ground type at one or more of the supports differs with more than one ground type from the rest. Ground types are defined in NS-EN 1998-1(38).
- If the length of the continuous deck exceeds the length $L_{Lim}$ and the soil properties are approximately uniform. $L_{Lim}$ is set to $L_g/1.5$, where $L_g$ for soil type A is 600m .

When spatially effects should be accounted for, NS-EN 1998-2 states that even only in a simplified way the wave-passage, incoherence and site-response effects should be regarded. In annex D of NS-EN 1998-2 several method to account for the spatially effects are presented.

Load combination for constructions are listed in NS-EN 1990 (39), but are also rendered in the NS-EN 1998-2. The loads that should be combined and accounted for is permanent actions, characteristic value of prestressing after losses, design seismic action, traffic loads and quasi – permanent values of actions of long duration (earth pressure, buoyancy, currents etc.) (10). Wind is not required to be accounted for.

# 3 Modelling

## 3.1 The Sognefjord Bridge

Figure 3.2 shows the longitudinal section of the design of the Sognefjord Bridge. There can be seen from the figure that the span of this bridge is 3700 meter and that the pylons are 455 meters high. The clearance from the sea at the mid-span should be 70 meters in a width of 400 meters to secure passing of large ships. All the data presented is provided by the NPRA unless otherwise specified.

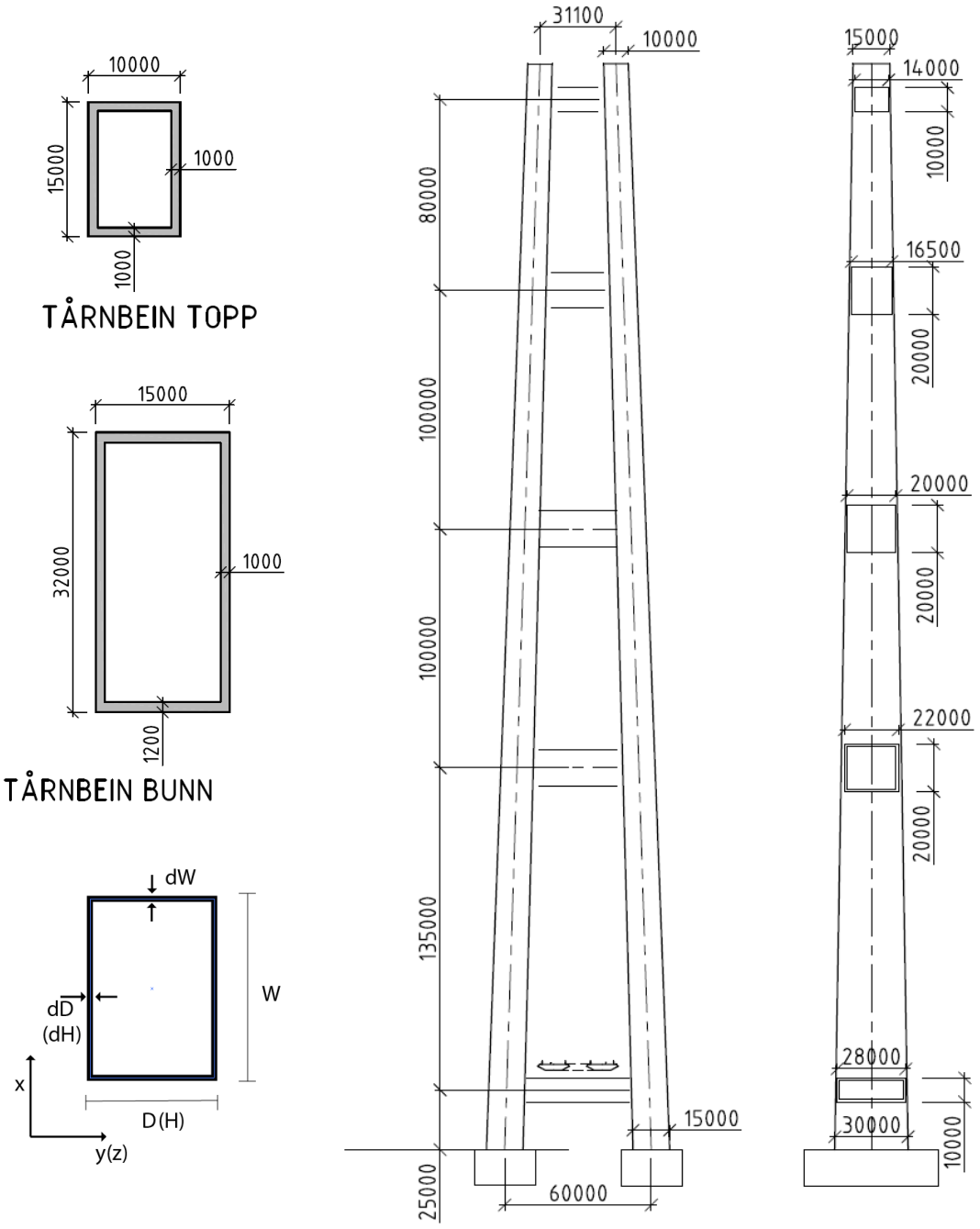


**Figure 3.1 Pylon, Left top: section view top leg. Left middle: section view bottom leg. Left bottom: section definition**

In Figure 3.1 is the drawing of the pylon displayed. There can be seen that the pylon consist of two legs, fixed together by five transverse girders. The legs are tapered, and the section view of the bottom and the top are displayed in the left of Figure 3.1. Sectional properties for the legs are calculated from the measures of the drawing and displayed in Table 3.1. The definition of W, D, dW and dD can be seen in Figure 3.1, A is the area and I is the moment of inertia.

**Table 3.1 Section properties of bottom and top cross section of pylon legs**

| | Bottom | Top |
|---|---|---|
| W (m) | 15.0 | 10.0 |
| D (m) | 32.0 | 15.0 |
| dW (m) | 1.2 | 1.0 |
| dD (m) | 1.0 | 1.0 |
| A ($m^2$) | 95.2 | 46.0 |
| $I_y$ ($m^4$) | 12864.47 | 1347.83 |
| $I_x$ ($m^4$) | 3580.73 | 695.33 |

From Figure 3.1 there are seen that the five transverse girders are located with different spacing and that they have different cross-sections. Only the outer dimensions of these girders are given by the drawing, they are therefore assumed to be box sections with wall thickness of 1 meter. In Table 3.2 the dimensions and the calculated cross-section data is displayed. Some of the notations are changed from Table 3.1 because of the different orientation of the sections, but these definitions are shown in the brackets in Figure 3.1.

**Table 3.2 Dimensions and section properties for transverse girders in the pylons**

| Transverse girders: | 1 | 2 | 3 | 4 | 5 |
|---|---|---|---|---|---|
| Distance from ground (m) | 25 | 160 | 260 | 360 | 440 |
| W (m) | 28 | 22 | 22 | 16.5 | 14 |
| H (m) | 10 | 20 | 20 | 20 | 10 |
| dW (m) | 1 | 1 | 1 | 1 | 1 |
| dH (m) | 1 | 1 | 1 | 1 | 1 |
| A ($m^2$) | 72 | 80 | 80 | 69 | 44 |
| $I_z$ ($m^4$) | 1224.00 | 4946.67 | 4946.67 | 3953.00 | 654.67 |
| $I_x$ ($m^4$) | 6576.00 | 5746.67 | 5746.67 | 2913.94 | 1134.67 |

Material properties for the pylons are not provide by the drawing, the pylon are therefore assumed made by C45 concrete as used for the Hardanger Bridge.

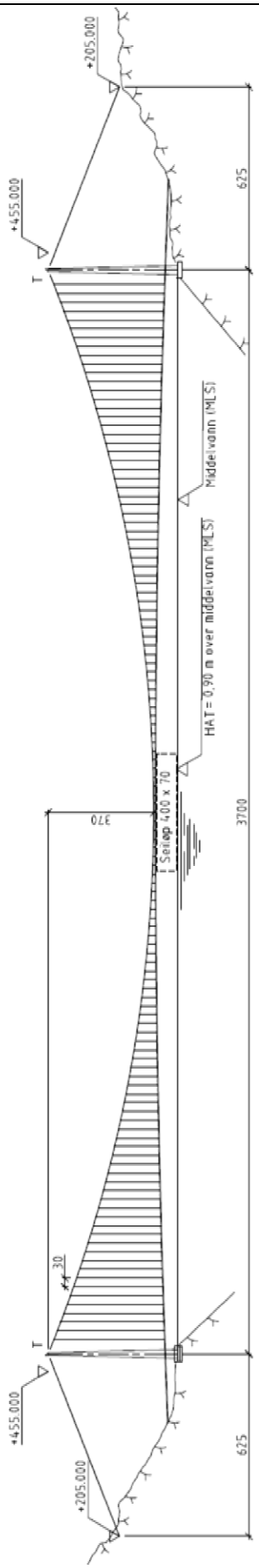


**Figure 3.2 Longitudinal section**

The data for the main cable and the suspenders are gien in Table 3.3 and Table 3.4. As shown by Figure 3.2, the suspenders are planned to have a spacing of 30 meters.

**Table 3.3 Data for main cable**

| | |
|---|---|
| Diameter (m) | 1.3 |
| Effective area $(m^2)$ | 1.15 |
| Mass (kg/m) | 9445 |
| E-modulus $(N/mm^2)$ | 200 000 |
| Tensile strength $(N/mm^2)$ | 1770 |

**Table 3.4 Data for suspenders**

| | |
|---|---|
| Type | Bridon LC100 |
| Diameter* (m) | 0.1 |
| Nominal metallic cross-section* $(m^2)$ | 0.699 |
| Mass* [kg/m] | 56.2 |
| E-modulus $(N/mm^2)$ | 160 000 |
| Tensile strength* $(N/mm^2)$ | 1445 |

*** Data acquired from Bridon product datasheet(1)**

The bridge deck is illustrated in Figure 3.3. It is planned built by using two steel box girders (from now on called bridge girders), each carrying two road lanes and one walkway. Data for the bridge girders are provided in Table 3.5.

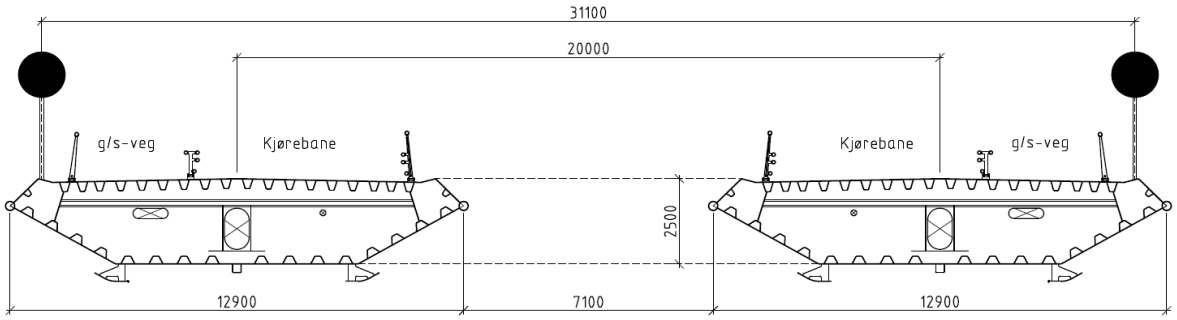


**Figure 3.3 Bridge deck**

The two box girders are connected together by transvers girders. These are spaced with equal interval as the suspenders. Two types of box sections are used, one for the five first transvers girders at each side of the bridge (box section 1) and another section for the rest (box section 2). The differences between these box sections are that box section 1 are larger than box section 2. Data for these two sections are given in Table 3.5 and Table 3.6. No material data are specified for these sections, they are therefore assumed made by the same steel as the bridge girders.

**Table 3.5 Data for bridge girders**

| | |
|---|---|
| Width (m) | 12.9 |
| Height (m) | 2.5 |
| A ($m^2$) | 0.4472 |
| $I_y$ ($m^4$) | 0.4398 |
| $I_z$ ($m^4$) | 6.2420 |
| $I_T$ ($m^4$) | 1.0780 |
| Mass* [kg/m] | 6542 |
| E- module [N/mm2] | 210 000 |
| G- module [N/mm2] | 80 000 |

* Mass per girder, included tarmac, railings etc.

**Table 3.6 Properties for the transverse girders**

| | Box section 1 | Box section 2 |
|---|---|---|
| A ($mm^2$) | 0.318 | 0.179 |
| $I_z$ ($mm^4$) | 0.3135 | 0.0662 |
| $I_x$($mm^4$) | 0.3135 | 0.1539 |
| $I_T$ ($mm^4$) | 0.3988 | 0.115 |

## 3.2 Bridge Model

To model the Sognefjord Bridge the analyses and design program SAP2000 have been used. This is a program developed by Computers and Structures which is recognised for their development of computer software for structure and earthquake engineering.

### 3.2.1 Pylons

The pylons are designed using general frame elements, i.e. the properties of the sections are explicitly specified instead of specifying the cross-section. Tapered legs are in SAP2000 made by defining a non-prismatic section. These are modelled by first defining the top and bottom cross-section. The legs are then made by setting the distance between the two cross-sections to 455 meters and setting the cross-section to vary linearly. As for the legs the transverse girders in the pylons are modelled using general frame elements.

A rough mesh is used for the pylons. The legs are meshed into lengths of about twenty meters and the transvers stiffeners are meshed as two elements.

There is assumed that the bridge foundation is on bedrock since solid soil conditions are needed to support a structure of this size. The natural period of bedrock is short compared with a structure as this and therefore is soil-structure interaction negligible. Due to this the supports are fixed, but since the DOFs in translation directions at the support are needed in the analyses, this is done using link element. Two different link elements are defined, one for the supports of the main cables and one for the supports of the pylons. The link element for the main cable supports is configured with stiffness of $10^{15}$ kN/m in transverse direction. The same configuration is also set for the link element for the pylon supports, but this link element is also fixed against rotations. The stiffness of $10^{15}$ kN/m is the highest stiffness that can be used before the natural frequencies found using SAP2000 and Matlab starts to deviate.

The drawings do not specify any reinforcement of the pylons and since design is not a part of this thesis, reinforcement is not accounted for.

### 3.2.2 Main Cables

SAP2000 gives the possibility of modelling cables using both catenary cable elements and straight frame elements. Since the cable planned to use in the Sognefjord Bridge has a diameter of 1.3 meter, the cable will behave similar to a beam. There is therefore chosen to use straight beam elements to model the cable.

122 elements are used to model the centre span. The projection of the elements down on the longitudinal axes of the bridge is 50 meters for the first elements on each side and 30 meter for the other elements, i.e. in accordance with the spacing of the suspenders. The shape of the cable is decided using the shape calculator feature in SAP2000. As for the side spans the cable is modelled as a single element straight beam.

The connection between the pylons and the main cables are plain bearing which allows displacement of the cable in the longitudinal direction. This bearing was failed to model, and the main cables were therefore also fixed to the pylons in longitudinal direction.

### 3.2.3 Suspenders

The suspenders are modelled using frame elements. Since the suspenders only will be subjected to a point load at the end and the stress gradients therefore will be zero, the suspenders are modelled as single frame elements. To apply cable properties to the frame element, the compression limit is set to zero. Also the moment of inertia, torsional constant and the shear area are all set to zero. The connection to the main cables and to the bridge deck is modelled by applying a moment release about the lateral direction.

### 3.2.4 Bridge Deck

Both bridge girders and transverse girders are modelled with general frame elements. To connect the bridge girders with the suspenders and the transvers girders, link elements are used. The link element is configured to fix the nodes connected by it. By connecting the suspenders, bridge girder and transvers girder with this element, the nodes will move together as a rigid body. When the link element is used to fix two joints together this is equivalent to assigning a joint constraint(40).

The bridge deck is only modelled between the towers. Since information on the stretch between the start of the bridge and the pylon not are available, the bridge deck at the pylons is fixed in all directions. The reason for this choice is that the bridge deck in reality continues beyond the pylons and therefore relatively fixed by the continuous deck. Pictures of the model is found in Appendix C.

### 3.2.5 Analyses of Model in SAP2000

Using SAP2000 a preliminary analysis is done to incorporate the geometrical stiffness due to the prestress of the main cables. This is done by doing a non-linear static analysis of the model where the P-delta/geometric stiffness effects are incorporated. A suspension bridge will undergo

large displacements when the gravity load is applied and this changes the geometry of the bridge significant. Therefore the use of a P-delta analysis with large displacements(40) is appropriate, i.e. the equilibrium of the deformed geometry is found. Since this type of analysis is more sensitive to convergence tolerances(40), the analysis is run both with the standard convergence tolerance in SAP2000, $10^{-4}$ and a lower tolerance of $10^{-6}$. The deviation in displacement for a node at the mid-span is 0.1 mm, convergence of the structure is therefore assumed.

Several attempts were needed to obtain the right height at the mid-span. The final model was modelled with headroom of 110.8 meters from the sea to the main cable. Running the analyses the displacement at mid-span was 25.5 meter, which corresponds to a headroom of 85.3 meters. The drawing specified this height to be 85 meter. To obtain zero deflection in the top of the pylon at this configuration a negative strain of 3.61E-3 is assigned to the main cables in the side spans.

# 4 Results and Discussion

The results presented in this chapter are found using SAP2000 and MATLAB. As earlier described is the Sognefjord Bridge modelled using SAP2000. SAP2000 do not have the functionality to handle spatial effects. There is therefore chosen to export the system matrixes from SAP2000 and use MATLAB to calculate the response of the bridge. MATLAB is also used to investigate the response with Rayleigh, hysteretic and aerodynamic damping. In all the MATLAB calculations the lumped mass matrix and the consistent stiffness matrix are used. All the formulas used in the calculations of response and damping are presented in Chapter 2.

There is in this chapter refereed to the coordinate system, this is defined as followed; x is the axis along the bridge, y is the axis perpendicular to the bridge and z is vertical axis.

## 4.1 Parameters Used in the Analyses

### 4.1.1 Damping

NS-EN 1998-2 (10) lists general values for equivalent viscous damping for bridge pylons. These values are in this thesis assumed valid for the rest of the construction, hence the damping ratios: $\zeta_{steel} = 0.02$ (welded steel) and $\zeta_{concrete} = 0.05$. Only the bridge deck is welded but for simplicity the same damping ratio is used for all steel components. For the nodes which connects the steel and concrete members an average damping ratio is set, $\zeta_{com} = 0.035$.

To calculate the aerodynamic damping forces, a wind velocity need to be assumed. There is not very likely that an earthquake will appear in combination with a very strong wind. Since the bridge is situated in a wide fjord not long from the coastal line a wind velocity of 15 $m/s^2$ at the mid-span is not seen as unlikely. The density of air is set to 1.25 $kg/m^3$ and the dimension of the sections provided by Table 3.5.

Since only a concept design is made for the Sognefjord Bridge, no research has been done on the aerodynamic load coefficients for the bridge girders. The load coefficient obtained by Sven Ole Hansen (41) and refereed by Ole Øiseth (42) for the Hardanger Bridge are therefore used, Table 4.1. Theses coefficients are assumed valid for both bridge girders, i.e. there will be now difference in aerodynamic damping loads, although one of the girders will be sheltered by the other. This is a very rough estimate, but will give an indication of the effects of aerodynamic damping.

**Table 4.1 Aerodynamic load coefficients**

| $\bar{C}_D$ | $\bar{C}_L$ | $\bar{C}_M$ | $C'_D$ | $C'_L$ | $C'_M$ |
|---|---|---|---|---|---|
| 0.7 | 0 | -0.25 | 2.4 | 0.01 | 0.74 |

In the quasi-static theory presented in section 2.4.4 there were assumed a line like structure, this is not the case for the bridge deck of the Sognefjord Bridge, but is seen as accurate enough for this thesis.

### 4.1.2 Spectral Density for the Ground Acceleration

The spectral density curve for the ground motion acceleration is made using the Kanai-Tajimi spectrum described in section 2.1.3. In this thesis Kiureghian and Neuenhofer's parameters for the spectrum are used as presented in the latter chapter. To adapt the spectrum to Norwegian conditions, a plausible PGA must be set. According to the national annex of the NS-EN 1998 1(39) the PGA for the area where Sognefjorden is situated is 0.72 $m/s^2$. This value is for an earthquake with a return period of 475 years. A bridge as the Sognefjord Bridge has a building cost of several billions kroners and would probably have a longer lifetime than ordinary buildings. The damage potential is high with the possibility of many cars driving over the bridge at once. A much more fair structure to compare this bridge with is large dams. Large dams are required to be checked for an earthquake with a return period of 10 000 years for ultimate limit state (43). A return period of 10 000 years are therefore used in these analyses. In accordance with the seismic zonation map of Norway (44), this corresponds to a PGA of 3 $m/s^2$. This PGA is equivalent with a standard deviation of the excitation spectrum of 1.1 $m/s^2$. The spectrum obtained is shown in Figure 4.1.

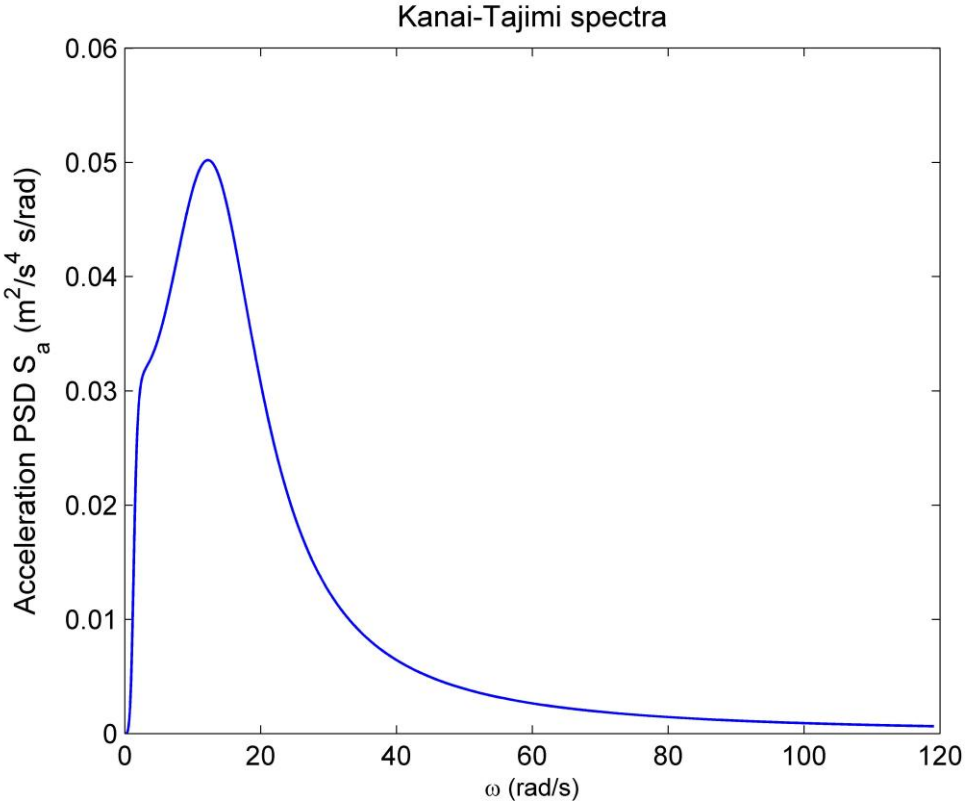


**Figure 4.1 Kanai-Tajimi spectre for PGA of 3 m/s with Kiureghian and Neuenhofer's parameters**

### 4.1.3 Spatial Effects

In the modelling of the structure, the structure where assumed standing on bedrock. Hence, the seismic wave velocity $v_{app}$ is assumed as high as 3000m/s. The distances between the supports are set in accordance with Figure 3.2 and the $d_{kl}^{L}$ matrix then becomes, Eq. (5.19).

$$\mathbf{d}^{L} = \begin{bmatrix} 0 & 625 & 4325 & 4960 \\ -625 & 0 & 3700 & 4325 \\ -4325 & -3700 & 0 & 625 \\ -4960 & -4325 & -625 & 0 \end{bmatrix} \tag{5.19}$$

The incoherence effects are in this thesis described using the Harichandran-Vanmarck model, described in section 2.1.5

## 4.2 System Matrixes

In Figure 4.2 the sparsity pattern of the mass and stiffness matrix of the system are shown. It can easily be seen that the masses are lumped. This is no surprise since SAP2000 uses a lumped mass formulation. The nz number at the bottom shows that there are 2272 non-zero elements in the matrix, which means that there are some zero elements on the diagonal as there are about 3500 DOFs in the system.

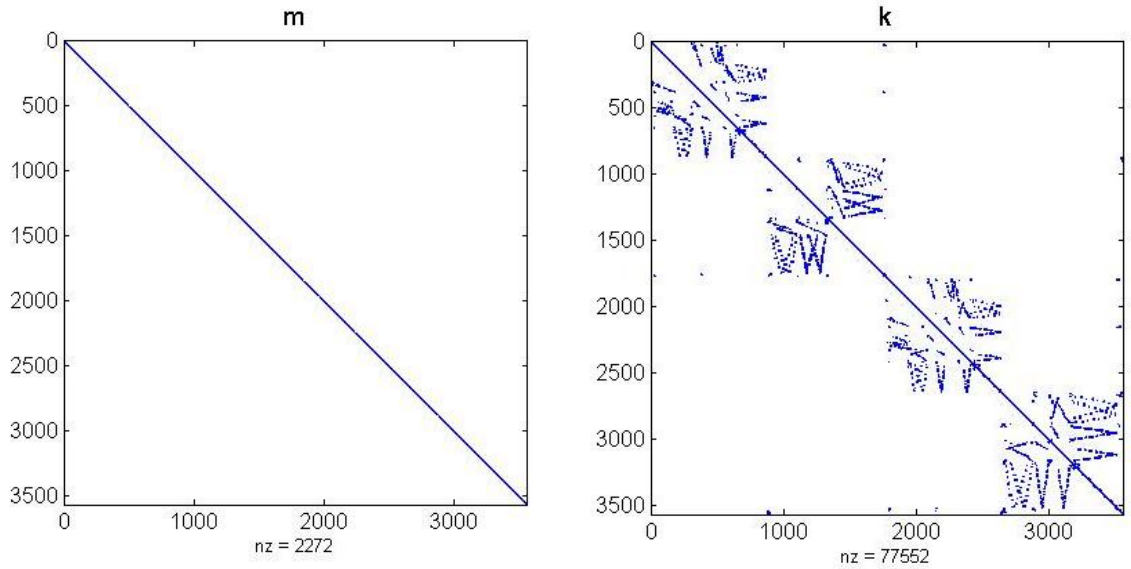


**Figure 4.2 Sparsity matrix of the mass matrix to the left and stiffness matrix to the right**

From the sparsity stiffness matrix there is seen that there are values outside the diagonal and that the matrix are symmetric, which is as expected. Since the bridge is symmetric about the mid-span one might expect the matrix to be bisymmetric, but since SAP2000 assign degrees of freedom as the construction is modelled, the matrix depends on the modelling order.

## 4.3 Modal Analyses

Although the modal technique will not be used calculating the response, natural frequencies and the modal shapes give important information and are therefore calculated using SAP2000.

### 4.3.1 Natural Frequencies

The natural frequencies extracted from the model are displayed in Table 4.2.

**Table 4.2 Selected natural frequencies for the Sognefjord Bridge (frequency given in rad/s)**

| Mode | 1 | 2 | 3 | 4 | 5 | 6 | 7 | 8 | 9 | 10 |
|---|---|---|---|---|---|---|---|---|---|---|
| Frequency | 0.174 | 0.297 | 0.379 | 0.395 | 0.476 | 0.520 | 0.533 | 0.544 | 0.564 | 0.611 |
| Mode | 11 | 12 | 13 | 14 | 15 | 16 | 17 | 18 | 19 | 20 |
| Frequency | 0.640 | 0.645 | 0.668 | 0.700 | 0.757 | 0.763 | 0.798 | 0.849 | 0.890 | 0.953 |
| Mode | 30 | 40 | 50 | 60 | 70 | 80 | 90 | 100 | 150 | 200 |
| Frequency | 1.171 | 1.561 | 2.015 | 2.409 | 2.701 | 3.103 | 3.525 | 3.835 | 5.670 | 7.355 |
| Mode | 250 | 300 | 350 | 400 | 450 | 500 | 600 | 700 | 800 | 900 |
| Frequency | 9.022 | 10.691 | 12.240 | 13.897 | 15.380 | 16.851 | 19.764 | 22.104 | 23.906 | 28.863 |
| Mode | 1000 | 1100 | 1200 | 1300 | 1400 | 1500 | 1600 | 1700 | 1800 | 1900 |
| Frequency | 41.851 | 75.892 | 119.022 | 158.191 | 190.117 | 222.516 | 233.151 | 249.234 | 305.617 | 554.317 |

As seen from the table the first frequency is as low as 0.17 rad/s, which equals a period of 36 seconds. As comparison is the elastic response spectra in the Eurocode only defined in the range from zero to four seconds, first at mode 40 are the periods within the defined range. Another important aspect is that the period of the first mode is longer than the typical duration of an earthquake.

**Table 4.3 Natural frequencies for one of the pylons standing alone (frequency given in rad/s)**

| Mode | 1 | 2 | 3 | 4 | 5 | 6 | 7 | 8 | 9 | 10 |
|---|---|---|---|---|---|---|---|---|---|---|
| Frequency | 0.335 | 0.340 | 0.760 | 1.454 | 1.539 | 2.058 | 3.162 | 3.322 | 3.902 | 4.995 |
| Mode | 11 | 12 | 13 | 14 | 15 | 16 | 17 | 18 | 19 | 20 |
| Frequency | 5.263 | 5.640 | 5.803 | 6.259 | 6.905 | 6.986 | 8.304 | 8.531 | 8.877 | 9.053 |
| Mode | 30 | 40 | 50 | 60 | 70 | 80 | 90 | 100 | 150 | 200 |
| Frequency | 12.566 | 16.032 | 18.741 | 22.707 | 24.539 | 26.249 | 29.362 | 36.446 | 363.968 | - |

Table 1.2 gives the natural frequencies of one of the pylons. As can be seen, the frequencies are still very low and the first natural frequency corresponds to a period of 18 seconds.

### 4.3.2 Mode Shapes

In Figure 4.3 and Figure 4.4 the mode shapes for the ten first natural frequencies are displayed for both one of the main cables and one of the bridge girders. The modes are normalized for the whole structure, and not for the local modes in the cable and the bridge deck. As seen from the figures the first five modes are clearly pure displacement modes for the bridge deck. The mode shapes in general locks very plausible, since the first, second and third order displacement in y direction and second and third order displacement in z direction are present in the first five mode shapes. Mode six is a rotational mode, but since the girders are offset the centre of the bridge deck, the mode also have displacement in x and y direction. Mode shape eight and nine is clearly displacements in the cables. In mode ten there is seen a modal displacement in the towers. In the Appendix D the mode shapes for the modes with the teen highest mass participation factors are plotted.

### 4.3.3 Modal Participation Factors

Table 4.4 displays the modes with the thirty highest modal participation factors in each direction. From the table there can be seen several modes higher than 2000 among the 30 most participating modes. If the mode shapes of these modes are checked in SAP2000 there is seen that they are translation displacements at the supports. The reason that they appears are the modelling of the supports with link elements that enables displacement at the supports. Since the supports are moving the whole structure follows and leads to significant modal participation factors. The high natural frequencies for these modes shows that the stiffness of the link elements is large compared to the rest of the structure, therefore these high modes can be ignored as they in practice can be regarded as fixed.

If the modes higher than 2000 are disregarded, it is seen from the table that the highest contributing modes are in the area between 1200 and 1300. From Table 4.2 there can be seen that mode 1300 corresponds to natural frequency of 160 seconds.

**Table 4.4 The thirty nodes with highest modal participation factor (MPF) in each direction (absolute values)**

| | UX | | UY | | UZ | | RX | | RY | | RZ | |
|---|---|---|---|---|---|---|---|---|---|---|---|---|
| | Mode | MPF | Mode | MPF | Mode | MPF | Mode | MPF | Mode | MPF | Mode | MPF |
| 1 | 21 | 569 | 16 | 363 | 356 | 368 | 10 | 117890 | 356 | 680341 | 15 | 727460 |
| 2 | 76 | 334 | 10 | 349 | 360 | 362 | 16 | 111196 | 360 | 669691 | 16 | 671288 |
| 3 | 111 | 150 | 1 | 337 | 13 | 291 | 1 | 52246 | 364 | 595923 | 10 | 646260 |
| 4 | 75 | 116 | 45 | 183 | 978 | 170 | 17 | 35968 | 354 | 592268 | 1 | 623547 |
| 5 | 194 | 103 | 17 | 166 | 19 | 121 | 18 | 14662 | 13 | 537722 | 11 | 606895 |
| 6 | 84 | 97 | 48 | 145 | 346 | 120 | 12 | 14510 | 342 | 365842 | 46 | 367058 |
| 7 | 147 | 93 | 139 | 117 | 1048 | 118 | 29 | 13471 | 978 | 314284 | 45 | 339191 |
| 8 | 2249 | 85 | 95 | 114 | 923 | 113 | 2250 | 11539 | 359 | 301065 | 2 | 312095 |
| 9 | 2266 | 72 | 90 | 95 | 5 | 110 | 2253 | 11313 | 3 | 295252 | 17 | 306668 |
| 10 | 261 | 66 | 29 | 78 | 1120 | 91 | 2249 | 10985 | 352 | 240599 | 48 | 267321 |
| 11 | 2261 | 65 | 238 | 77 | 2269 | 87 | 440 | 9297 | 974 | 236411 | 94 | 261246 |
| 12 | 3 | 65 | 179 | 74 | 419 | 85 | 2258 | 7822 | 19 | 223196 | 7 | 250319 |
| 13 | 221 | 56 | 2261 | 66 | 350 | 85 | 438 | 7554 | 346 | 222244 | 2253 | 217909 |
| 14 | 57 | 55 | 53 | 66 | 1170 | 79 | 2256 | 7550 | 1046 | 218944 | 139 | 216680 |
| 15 | 268 | 44 | 2250 | 59 | 732 | 77 | 969 | 5769 | 1048 | 218619 | 95 | 210606 |
| 16 | 14 | 42 | 34 | 59 | 2252 | 68 | 412 | 4864 | 981 | 209982 | 25 | 205359 |
| 17 | 453 | 39 | 39 | 58 | 31 | 62 | 95 | 4776 | 923 | 208955 | 140 | 203425 |
| 18 | 82 | 38 | 2253 | 56 | 390 | 62 | 90 | 3704 | 2259 | 204874 | 44 | 185961 |
| 19 | 2269 | 35 | 4 | 56 | 549 | 58 | 2255 | 3662 | 5 | 204296 | 2264 | 184547 |
| 20 | 2256 | 34 | 2249 | 53 | 1222 | 55 | 1047 | 3516 | 2272 | 196593 | 90 | 175948 |
| 21 | 2259 | 34 | 2266 | 52 | 2258 | 54 | 34 | 3464 | 925 | 185313 | 29 | 144949 |
| 22 | 185 | 31 | 2264 | 47 | 451 | 50 | 2252 | 3413 | 2269 | 173814 | 37 | 144237 |
| 23 | 89 | 31 | 145 | 39 | 384 | 49 | 1119 | 2732 | 1118 | 171667 | 238 | 142445 |
| 24 | 679 | 29 | 2256 | 36 | 2261 | 48 | 2270 | 2686 | 1120 | 168307 | 239 | 139543 |
| 25 | 2252 | 28 | 18 | 35 | 1274 | 48 | 2257 | 2608 | 2260 | 162479 | 177 | 138239 |
| 26 | 2260 | 26 | 83 | 35 | 40 | 42 | 32 | 2518 | 419 | 156944 | 179 | 136903 |
| 27 | 68 | 26 | 2269 | 35 | 2249 | 41 | 48 | 2476 | 350 | 156489 | 51 | 127518 |
| 28 | 2250 | 24 | 12 | 34 | 244 | 41 | 1171 | 2390 | 420 | 155130 | 2256 | 123878 |
| 29 | 154 | 23 | 2258 | 32 | 22 | 40 | 2254 | 2332 | 2251 | 155115 | 2254 | 122930 |
| 30 | 2264 | 23 | 69 | 31 | 2271 | 39 | 39 | 2142 | 14 | 148570 | 53 | 121633 |

### 4.3.4 Discussion

The results show that the first natural frequency of the Sognefjord Bridge is 36 seconds. As earlier mentioned, the earthquake duration for a strong near fault earthquake can be expected to be around 30 seconds. For a Norwegian earthquake with lower magnitude the duration is shorter, maybe around 10 seconds. The first natural frequency is therefore significantly longer than the duration for a strong Norwegian earthquake. This means that the assumption of stationary condition cannot be substantiated.

Using the modal participation factors the modes that contributes the most is detected. As shown in the result 1300 modes have to be used if the thirty most participating modes should be included. When comparing with Figure 4.1 the modes with natural frequencies above 120 seconds (mode 1200) will have very low significance to the response. As the modes higher than 1200 have low modal participation factor compared to the most participating modes, there is seen as sufficient to run analyses for frequencies up to 120 seconds. In the other end of the frequency spectre, there is seen from Figure 4.1 that the energy is low. This frequencies can however not be dismissed. As seen from Table 4.4 many of the lowest modes are among the most contributing, with substantially larger modal contributing factors than the rest.

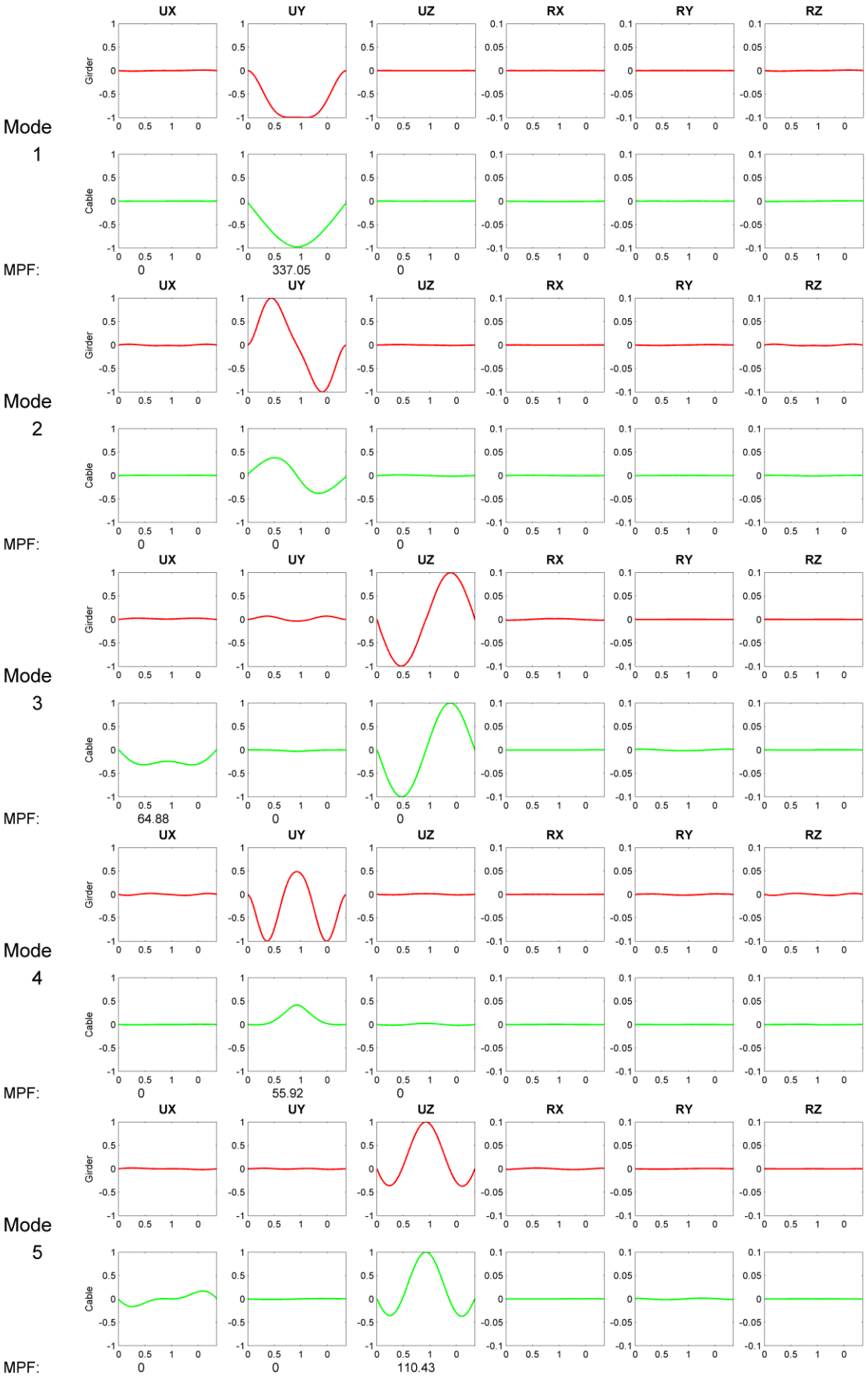


**Figure 4.3 Mode shape 1 to 5**

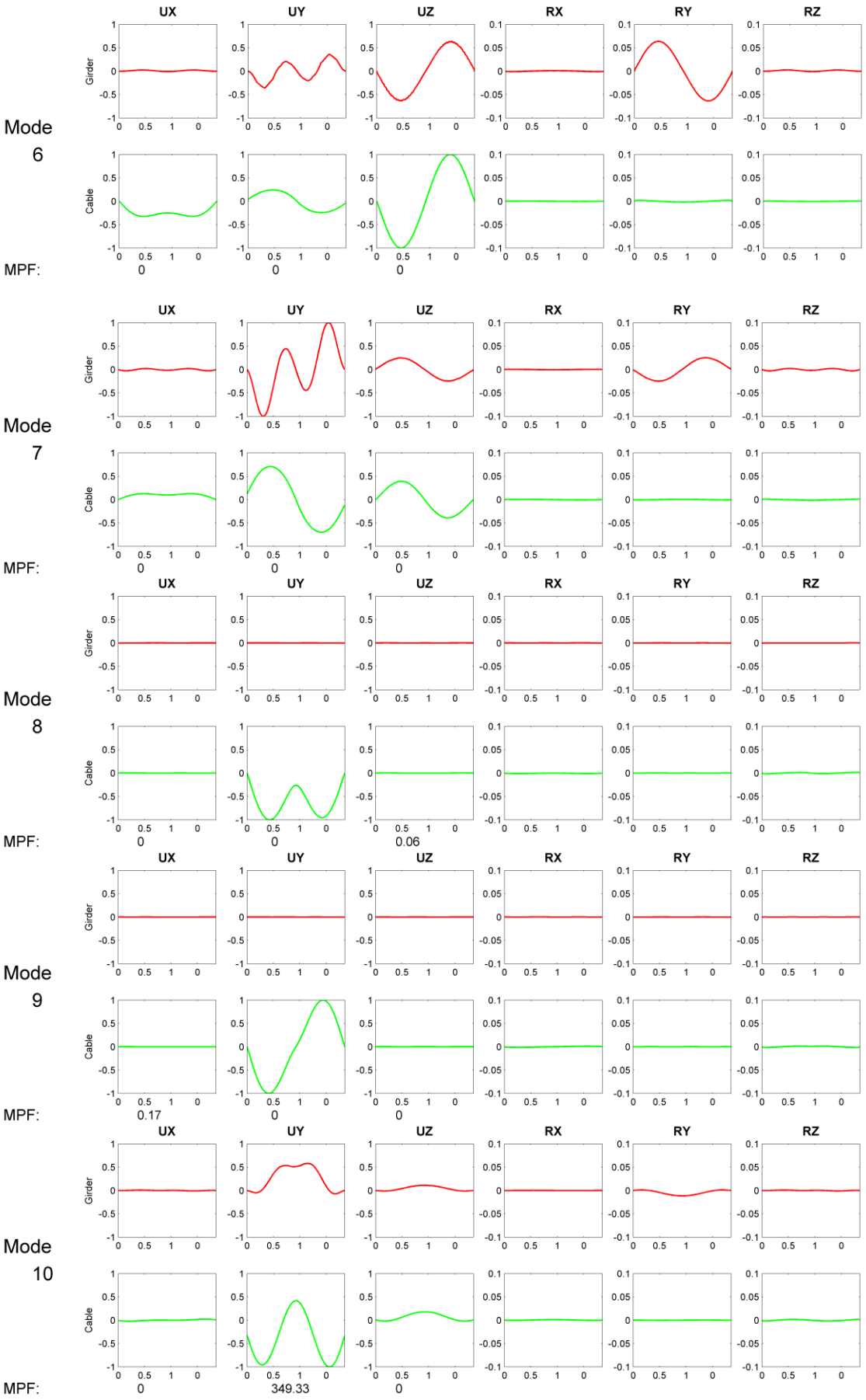


**Figure 4.4 Mode shape 6-10**

## 4.4 Results Damping

To investigate the differences in Rayleigh and hysteretic damping both sets of damping models were implemented in MATLAB. For both types non-classical damping where adopted, this was done as described in section 0.

An aerodynamic damping matrix was made by locating all the relevant DOFs, i.e. displacement in y and z direction and rotation about the x-axis for the bridge girders. The damping was then applied to both girders by assigning the elements in Eq. (3.4.12) to the rows and columns corresponding to the found degrees of freedoms.

A unit load vector with values at elements corresponding to DOFs in transverse direction was made. Using this load vector the frequency response function was found for following cases.

- System with Rayleigh damping
- System with hysteretic damping
- System with hysteretic damping and aerodynamic damping

These systems were solved for the 300 first natural frequencies. For the Rayleigh damping, the first and 100 natural frequencies (from now on called the first and second Rayleigh frequency) were used to determine the damping coefficients. The damping ratios used are described in the section 4.1.1.

Figure 4.5 shows the frequency response of a DOF in y-direction at the mid-span using Rayleigh and hysteretic damping. There is seen that for the first natural frequency the two different damping models give the same result. In the area from the first natural frequency to a frequency of about 4 rad/s the Rayleigh damping gives significant larger response than the hysteretic damping. The peak values are presented in Table 4.5. The second Rayleigh frequency was 3.82 rad/s and matches therefore the frequency found in the plot. As for frequencies higher than 4 rad/s there is seen that Rayleigh damping gives less response than the hysteretic damping.

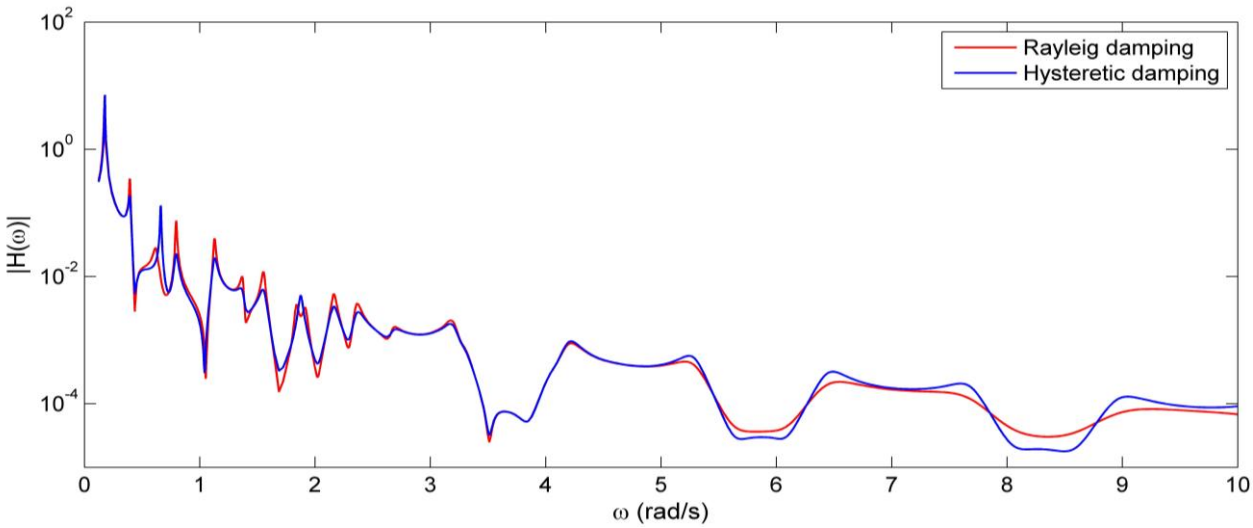


**Figure 4.5 Rayleigh and hysteretic damping**

**Table 4.5 Frequency response values at the peaks and the deviation of Rayleigh damping from hysteretic damping**

| $\omega$ (rad/s) | 0.3951 | 0.7979 | 1.1280 | 1.3670 | 1.5500 | 1.8390 |
|---|---|---|---|---|---|---|
| $\lvert H(\omega)\rvert$ -Rayleigh (kN/m) | 0.3459 | 0.0755 | 0.0394 | 0.0099 | 0.0118 | 0.0367 |
| $\lvert H(\omega)\rvert$-Hysteretic (kN/m) | 0.1873 | 0.0227 | 0.0192 | 0.0066 | 0.0061 | - |
| Deviation | 85 % | 232 % | 106 % | 51 % | 91 % | * |
| $\omega$ (rad/s) | 1.8750 | 1.9120 | 2.1630 | 0.2367 | 2.6900 | 3.1750 |
| $\lvert H(\omega)\rvert$ - Rayleigh (kN/m) | - | 0.0003 | 0.0053 | 0.0038 | 0.0016 | 0.0021 |
| $\lvert H(\omega)\rvert$ -Hysteretic (kN/m) | 0.0050 | - | 0.0038 | 0.0028 | 0.0015 | 0.0018 |
| Deviation | * | * | 41 % | 36 % | 9 % | 14 % |

* Hysteretic damping hit between two natural frequencies

The effects of the aerodynamic damping are shown in Figure 4.6. Here the frequency response for a DOF in y-direction at the mid-span is plotted for the hysteretic damping and the hysteretic damping in combination with aerodynamic damping. For the first natural frequency, the frequency response for the hysteretic damping is 7.15 kN/m and 5.3kN/m for the combination with aerodynamic damping. This means that the aerodynamic damping reduces the response with about 25%. The difference between the hysteretic damping with and without aerodynamic damping decreases for higher frequencies.

## 4.5 Discussion Damping

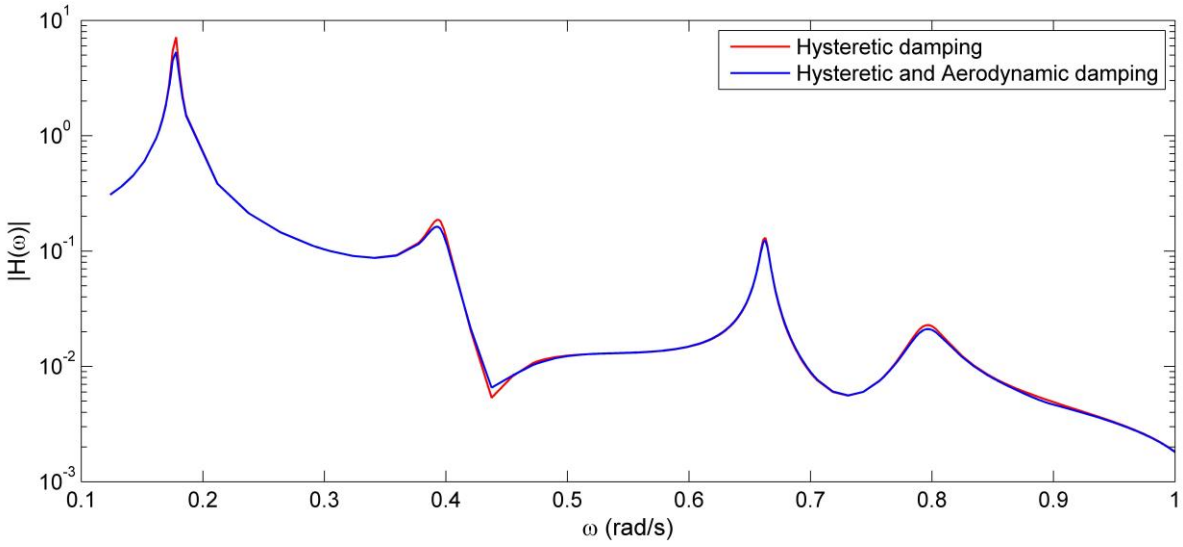


**Figure 4.6 Hysteretic and Aerodynamic damping**

The observations made from Figure 4.5 are consistent with the problem described in section 2.4.1 in using Rayleigh damping. The Rayleigh deviated with almost 100% for several of the natural frequencies, if an larger frequency range than been calculated the deviation would have

been even larger. Thus, if Rayleigh damping had been applied in the analysis of the Sognefjord Bridge and the second Rayleigh frequency had been set as the last natural frequency of the system, the response for the intermediate modes would have been largely conservative. Or in the other case, if the second Rayleigh frequency had been set to a lower natural frequency, damping had still been conservative at the intermediate modes and the damping for the higher natural frequencies would have been too high. Hence, hysteretic damping will be used for the rest of the analyses.

The aerodynamic damping was shown to have significant effect on the system. The influence becomes lower for higher modes, but as shown in section 4.3.3 have the lowest modes the largest contribution to the system. The aerodynamic derivatives used were those obtained for the Hardanger Bridge as have very different bridge deck, this make this calculation very rough. However, do the results show that aerodynamic damping is an important parameter for long-span structures as the Sognefjord Bridge and should therefore be applied also for earthquake analyses. Thus, aerodynamic damping will be applied to the analyses of the system.

## 4.6 Result Dynamic Analyses for Stationary Conditions

The dynamic response of the system for stationary conditions is calculated by using Eq. (3.5.17), with exception of the decomposition of the PSD matrix, i.e. **P** in Eq. (3.5.18) is not calculated explicit before applied to Eq. (3.5.18) Parameters used in the analyses are those discussed in section 4.1. The analysis is run in the frequency range from 0.1238 to 119.2 rad/s. This range is divided into 14895 elements; this is done by using a fine frequency mesh around the natural frequencies and a rougher mesh for the intermediate frequencies. The choice of frequency range is substantiated in section 4.3.4. The following three analyses are conducted.

**Analysis 1**
Seismic wave traveling along bridge/along x-axis and the wave-passage and the incoherence effects are accounted for.

**Analysis 2**
Seismic wave traveling along bridge/along x-axis and the wave-passage effect is accounted for.

**Analysis 3**
Seismic wave traveling perpendicular to bridge/along y-axis, where there is no spatial effects to account for since the seismic wave front will hit the supports at the same time. This will give the same result as if the wave was traveling in x direction and the spatial effect where not regarded.

Only the results for the translational DOF are presented and discussed as the inertia forces from the earthquake only acts in these. The auto-PSD of the response obtained from the calculations is presented through two figures for each analysis. One figure is containing plots of the response in all three directions for one of the main cables and one of the bridge girders in the distance between the pylons, while the other figure is containing plots of the response of both pylons in x- and y-direction

In the rest of the text is the pylon first hit by seismic wave front referred to as Pylon 1 and other pylon referred to as Pylon 2.

### 4.6.1 Analysis 1

In Figure 4.7 (a) is the response in the cable and the bridge girder displayed. From the plot there is seen that the response in this direction is small. The largest displacement is found in the cable 440 meters from Pylon 1 and is 0.18 meters.

Looking at Figure 4.7 (b) there is seen that the cable response is almost constant with a close to 0.4 meters almost the whole length. The bridge girder obtains the largest response at 1610 and 2090 meters from Pylon 1, where the response is 0.47 meters. As can be seen, the response of the bridge girder is symmetric about the mid-span.

The largest response of Analysis 1 is appearing in the z-direction. From the figure there is seen that the response of the cable and bridge girder almost is identical. There is also seen that there are three peaks with identical response. The three maxima are located at 1010, 1850 and 2780 meters from Pylon 1 with response of 0.81 meter.

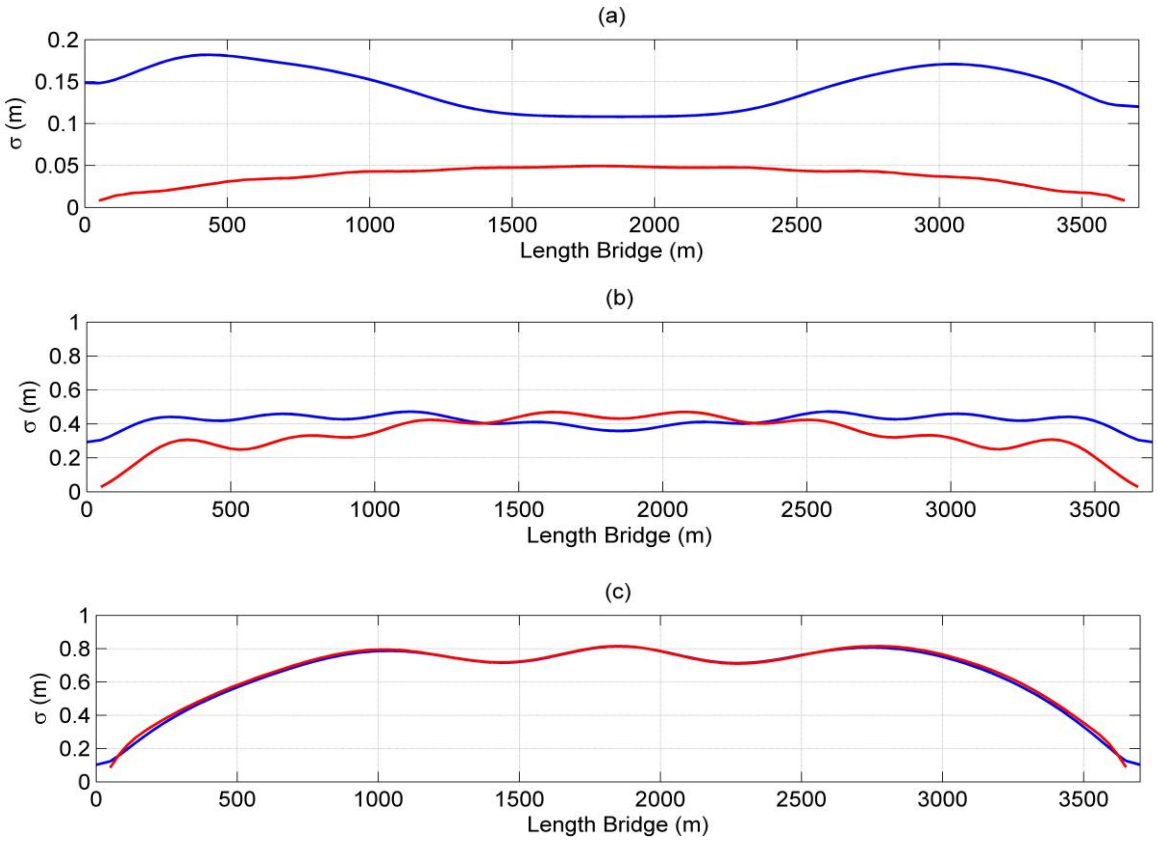


**Figure 4.7 Analysis 1, Cable (blue) and Bridge girder (red). (a) – x-direction, (b) – y-direction, (c) – z-direction**

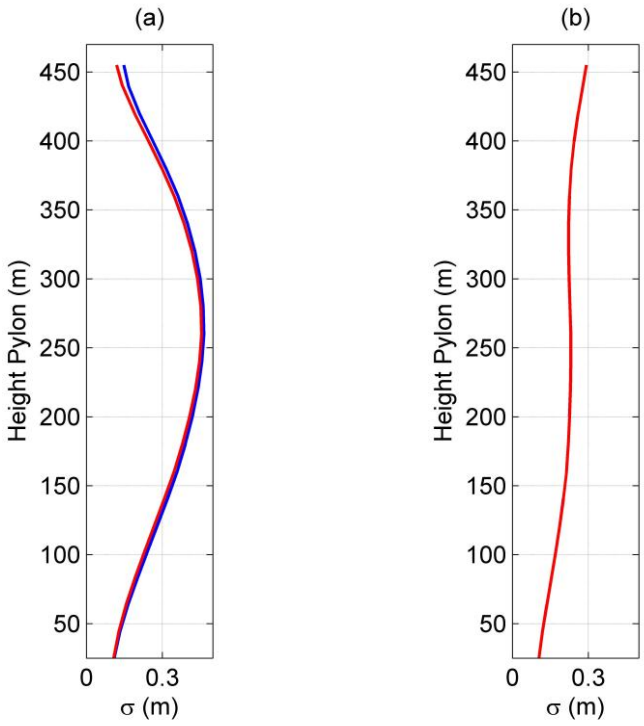


**Figure 4.8 Analysis 1. Pylon 1 (blue) and Pylon 2 (red). (a) - x-direction, (b) - y-direction**

In Figure 4.8 the response of the pylons are displayed for x- and y-direction. In x-direction there is seen that the pylon get a second order response curve with the maximum response of 0.46 meter at the height of 260 meters. There is seen that the response in the top of Pylon 1 and Pylon 2 in x-direction deviates, the deviation is 0.03 meter. The response in y-direction is a bit smaller, with maximum displacement at the top of 0.29 meter. At the bottom of the plot, at the height of 25 meter over the supports, the response is about 0.1 meter.

### 4.6.2 Analysis 2

In Figure 4.9 (a) the response in x-direction is displayed. There is seen that the response in both the cable and the bridge girder is a bit smaller than for Analysis 1. There are also notable that the response has become less symmetric.

The response in y-direction is seen in Figure 4.9 (b). Here the maximum response of the bridge girder has increased to 0.58 meters and appears at 2090 meters form Pylon 1. The symmetry seen in Analysis 1 is not seen anymore.

As for Analysis 1 is the response in z-direction the same for both the cable and the bridge girder. The maximum response has decreased to 0.75 meter at 2690 meters from Pylon 1. From the plot there is seen that the three peaks also seen in Analysis 1 are no longer identical and the response have lost its symmetry.

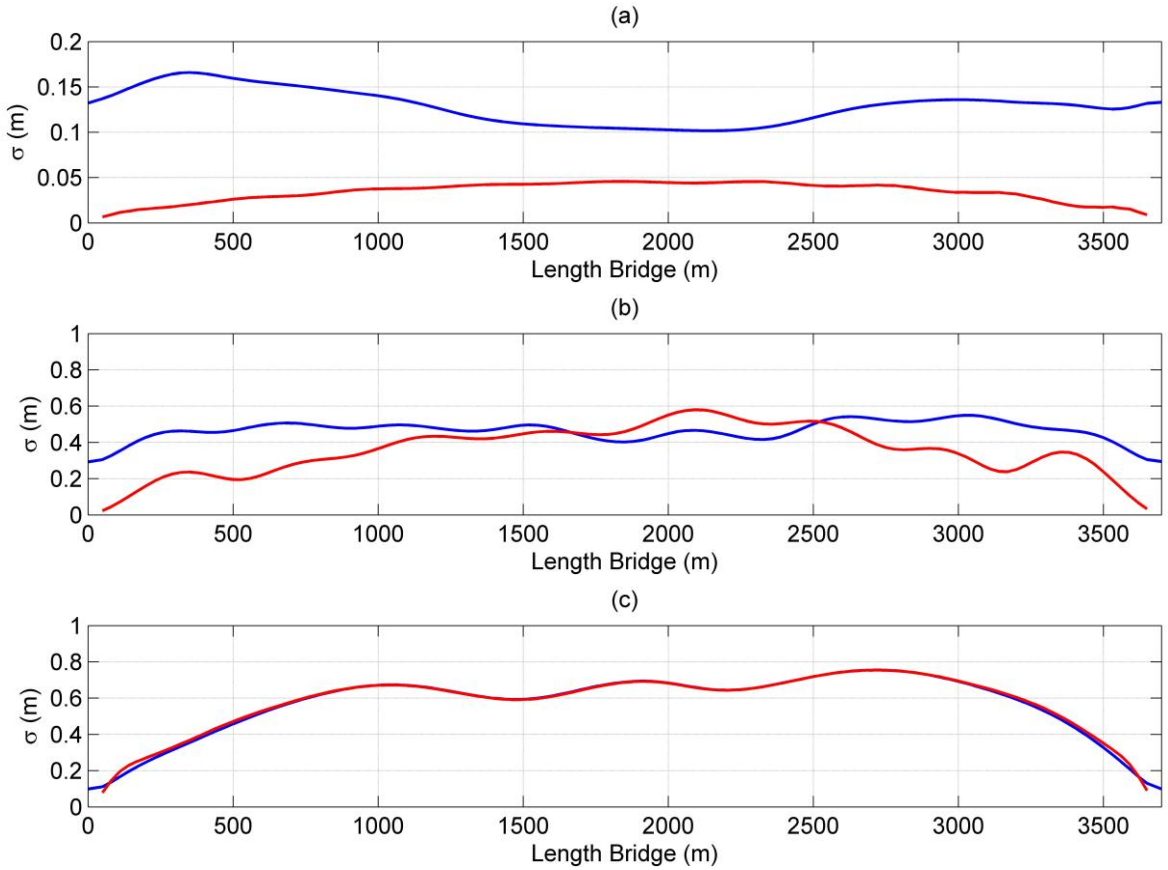


**Figure 4.9 Analysis 2, Cable (blue) and Bridge girder (red). (a) – x-direction, (b) – y-direction, (c) – z-direction**

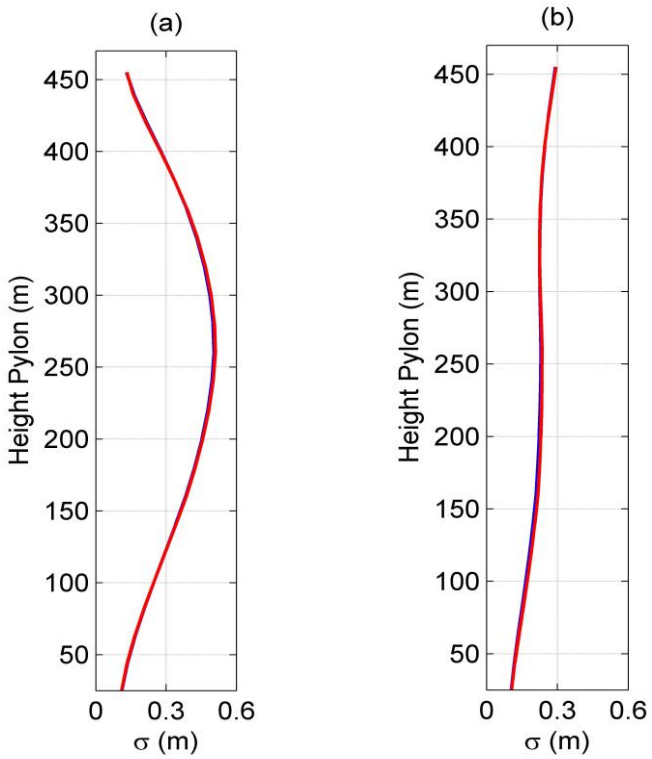


**Figure 4.10 Analysis 2. Pylon 1 (blue) and Pylon 2 (red). (a) - x-direction (b) - y-direction**

In Figure 4.10 there is seen that for Analysis 2 the response in both Pylon 1 and Pylon 2 are the same, which applies for both directions. The maximum value in x-direction is appearing at the same place as in Analysis 1, but has increased to 0.5 meters.

### 4.6.3 Analysis 3

Figure 4.12 (a) shows the response of the cable and bridge girder in x-direction. The maximum response of the cable is found 410 meter from Pylon 1 and is 0.16 meter. By looking at the figure there can be seen that the response of the cable is unsymmetrical.

The maximum response in y-direction for the bridge girder is found close to the mid-span at 1820 meter from Pylon 1 and is 0.61 meters. This is a little increase in response compared to Analysis 2. Both cable and bridge girder has a response that is almost symmetric about the mid-span.

In Figure 4.12 (c) there is seen that the response is unsymmetrical. The cable and the bridge girder have still almost the same response, but the maximum value has decreased further to 0.45 meter at 2660 meters from Pylon 1.

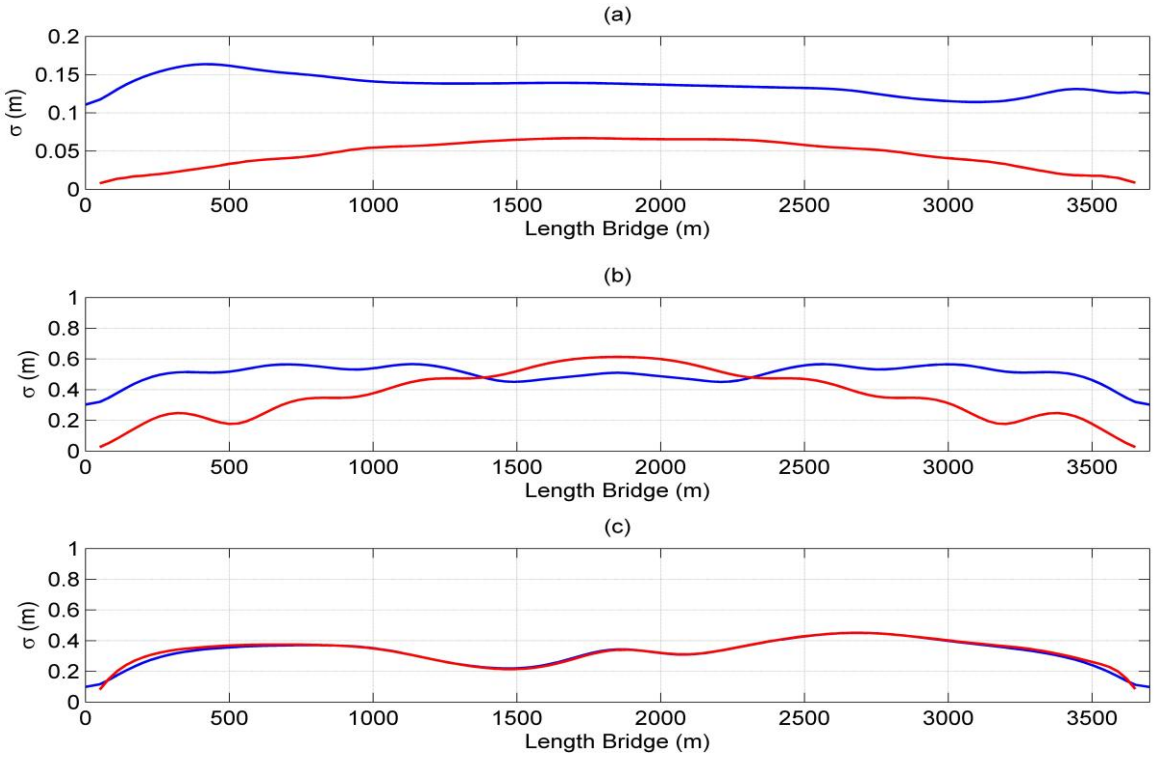


**Figure 4.12 Analysis 3, Cable (blue) and Bridge girder (red). (a) – x-direction, (b) – y-direction, (c) – z-direction**

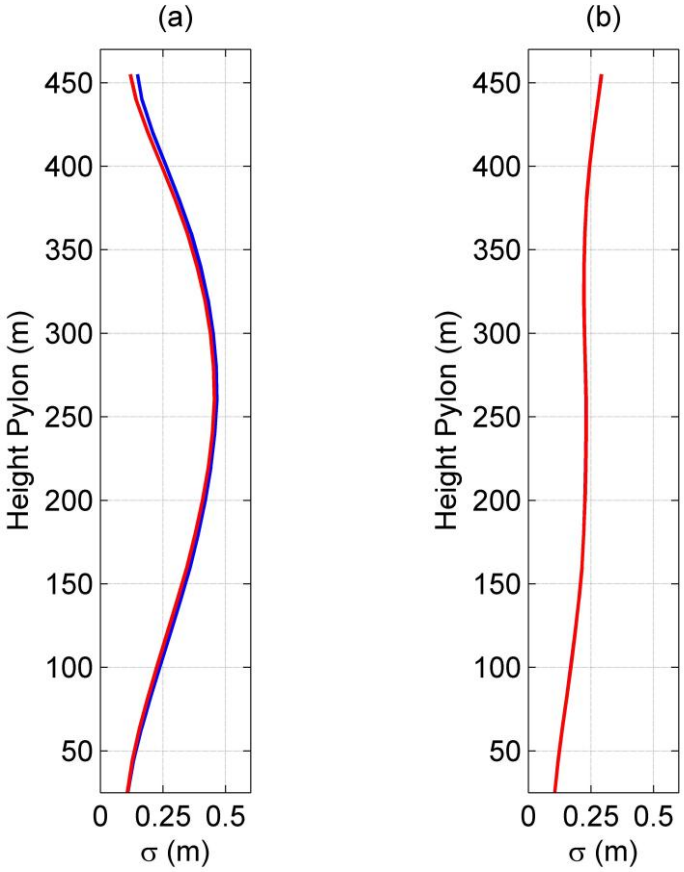


**Figure 4.11 Analysis 3. Pylon 1 (blue) and Pylon 2 (red). (a) - x-direction (b) - y-direction**

Figure 4.11 shows the response of the pylons in Analysis 3. The most remarkable with this figure is the difference in deflection in in x-direction. At the height of 260 meters Pylon 1 has a deflection of 0.57meter and Pylon 2 0.51 meters. For the top node of the pylons the difference in deflection between the two pylons are 0.01 meters in x-direction.

The maximum responses for the three analyses are summarized in Table 4.6 and in Table 4.7 the responses for the top of the pylons are summarized.

**Table 4.6 Maximum response and distance from Pylon 1**

| Maximum values | | Direction | Maximum σ (m) | Distance from Pylon 1 (m) |
|---|---|---|---|---|
| Analysis 1 | Bridge deck girder | x | 0.05 | 1820 |
| | | y | 0.47 | 1610 and 2090 |
| | | z | 0.81 | 1010, 1850 and 2780 |
| | Main cable | x | 0.18 | 440 |
| | | y | 0.47 | 1130 and 2570 |
| | | z | 0.81 | 1850 |
| Analysis 2 | Bridge deck girder | x | 0.05 | 1850 |
| | | y | 0.52 | 2480 |
| | | z | 0.75 | 2720 |
| | Main cable | x | 0.16 | 350 |
| | | y | 0.54 | 2630 |
| | | z | 0.74 | 2660 |
| Analysis 3 | Bridge deck girder | x | 0.07 | 1700 |
| | | y | 0.61 | 1820 |
| | | z | 0.45 | 2630 |
| | Main cable | x | 0.16 | 410 |
| | | y | 0.57 | 1130 and 2570 |
| | | z | 0.45 | 2690 |

**Table 4.7 Response in the top Pylons**

| | Direction | Pylon 1 σ (m) | Pylon 2 σ (m) |
|---|---|---|---|
| Analysis 1 | x | 0.15 | 0.12 |
| | y | 0.29 | 0.29 |
| | z | 0.1 | 0.1 |
| Analysis 2 | x | 0.13 | 0.13 |
| | y | 0.29 | 0.29 |
| | z | 0.1 | 0.1 |
| Analysis 3 | x | 0.11 | 0.12 |
| | y | 0.3 | 0.3 |
| | z | 0.1 | 0.1 |

## 4.7 Discussion of Dynamic Analyses in Frequency Domain

The maximum response of the structure was obtained in Analysis 3 in z-direction and was 0.81 meters. This is not large response for a structure as large and slender as the Sognefjord Bridge. A maximum response of this magnitude is in the lower range of what expected, but is a plausible result.

The maximum response in the top of the pylons was 0.3 meter in the y-direction. Also this is a small value of a pylon this high. The responses in the bottom of the plots are approximately 0.1 meters for both directions in all the analyses. If the excitation spectrum is converted to a displacement spectrum by using Eq. (3.1.9) and the standard deviation is calculated, this value is found to be 0.097 meter which corresponds with the plot.

In Analysis 3 the bridge was excited by a seismic wave traveling in the direction perpendicular to the bridge. There were therefore no spatial effects apparent as the seismic wave hit all the supports at once. When seismic load is applied to the whole bridge at once one would expect a symmetric response due to the symmetry of the bridge. In y-direction this symmetry is observed, but as for the x- and z-direction the response is not completely symmetric as stated in the results. A possible reason for the lack of symmetry in these directions is the modelling of the connection between the main cables and the pylons. As described in section 3.2.2, this connection was model by fixing the main cables to the pylon and archiving equilibrium for the static case by applying a negative strain to the side spans. But as the structure is exposed to an earthquake load the equilibrium vanishes and the main cable are not uniformly stressed anymore. This damages the symmetry of the bridge since there are different stresses along the main cable, and could cause an unsymmetrical response.

If this is the reason for the lack of symmetry, there is difficult to assess what effects this simplification of the cable-pylon connection has on the response. However, Figure 4.12 shows that the responses are close to symmetric and the simplification of the connections is therefore not thought to have much effect on the response.

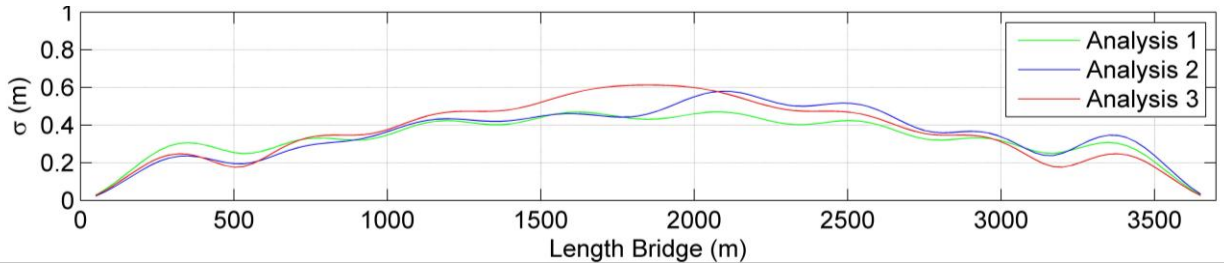


**Figure 4.13 Response in y-direction for all three analyses.**

In Figure 4.13 the distinction between the three analyses is seen. As stated in the results, there is seen that the result for Analysis 3 is symmetric. The reason for this is that when all supports moves uniformly, only the symmetric modes are excited as the structure is symmetrical. When the wave passage effect is included as in Analysis 2, the supports no longer moves uniformly. The anti-symmetric modes are then excited and a non-symmetric response is obtained as seen in Figure 4.13. In this analysis there where assumed full coherence. If the incoherence effects are included as in Analysis 1 there are seen that the response becomes symmetric. The large distance

between the pylons makes the support excitations uncorrelated. This is probably the reason the incoherence effects cancels out the wave passage effect.

The deviation between the different analyses is as seen in Figure 4.13 significant. In Table 4.8 the deviation between Analysis 3 and the two first analyses is presented. When accounting for the wave passage effect, i.e. Analysis 2, the smallest deviation is -16% in the y-direction. When also the incoherence effect is included, i.e. Analysis 1, the deviation increases to -23% in the latter direction.

**Table 4.8 Deviation in maximum response for the deflection of the bridge girder for Analysis 1 and Analysis 2 compared to Analysis 3**

| Direction | Analysis 1 | | Analyses 2 | |
|---|---|---|---|---|
| x | -0.02 | -26 % | -0.02 | -32 % |
| y | -0.14 | -23 % | -0.10 | -16 % |
| z | 0.36 | 81 % | 0.30 | 67 % |

Another notable observation from Table 4.8 is that the spatial effects increase the response in z-direction, and lower the response in x- and y-direction. The increases in z-direction are substantial, but the reason for these effects is unknown and therefore is further research needed to detect the cause.

This analysed were conducted using a lightly modified PEM method were the decomposition of the PSD matrix of the acceleration not conducted. The method used is therefore more like the traditional method since the three large matrix operations were carried out instead of the two vector operations as the proposed PEM method. As the consistent stiffness matrix where used in the calculations, the calculation of the frequency response function was the time demanding part of the analysis. This must have been carried out also if the PEM method had been implemented, and therefore is the choice of method not crucial for the computational time.

## 4.8 Result with Non-Stationary Conditions

In the latter section stationary condition were assumed. As discussed in section 4.3.1 is the periods of the bridge are two long to assume stationary conditions. Using the simplified method to assess non-stationary condition proposed in section 2.3 the effects of non-stationarity can be approximated. For these analyses the damping is set to be 5%, which is equal the damping in the concrete.

First looking at the quarter point where the maximum deviation of the system was found in Analysis 1. Figure 4.14 (a) shows the PSD of the displacement in z-direction at the quarter point of the bridge. As seen the response spectrum is narrow banded, i.e. almost all response depends on one frequency, $\omega = 0.67$ rad/s, which corresponds to mode 13. The simplified method should therefore give a good estimate of the effects of the non-stationarity when $\omega_0 = 0.67$ rad/s. In Figure 4.14 (b) the non-stationary response is shown, and the steady-stat is first reached after

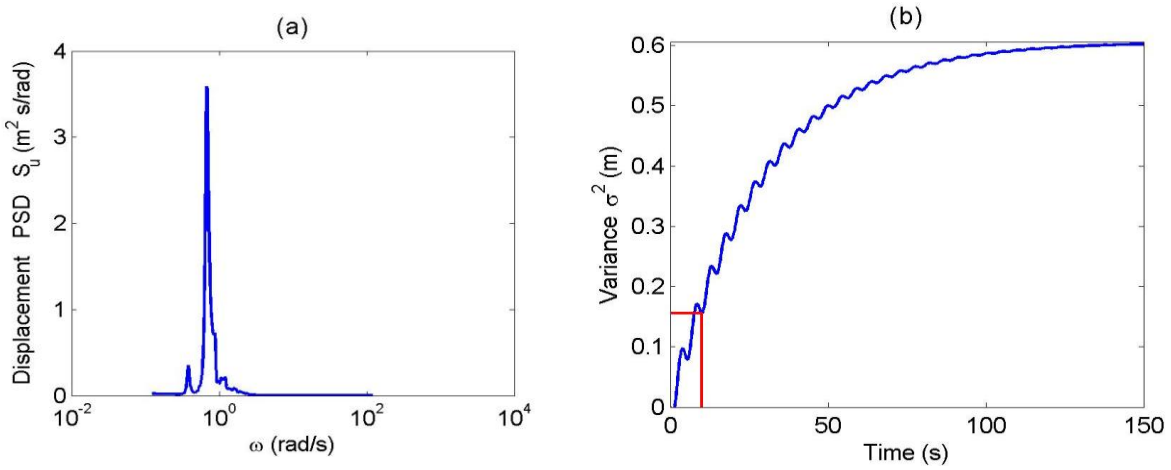


**Figure 4.14 (a) Displacement spectral density for DOF in z- direction in bridge deck girder at the quarter point. (b) Non-stationary response of DOF in (a)**

approximately 150 seconds, where the variance is about $0.6\,m^2$. If a strong Norwegian near-fault earthquake is assumed to have a duration of 10 seconds, there can be seen from the plot that the variance is 0.15 after 10 seconds. The variance of the stationary solution can therefore be reduced with a factor of four. Hence, the maximum response/standard deviation can be reduced to 0.405 meters.

Now looking on the maximum displacement for Analysis 3 as appears close to the mid-span in y-direction. The spectral density of the deflection is plotted in Figure 4.15 (a). From this figure there can be seen that there are three major contributing modes, mode 1, 10 and 45. Since there are several modes that contribute significantly to the displacement in this DOF, the result using the simplified method becomes more inaccurate. Setting the natural frequency of the single degree system to the average frequency of the two most contributing modes, $\omega_0 = 0.42$ rad/s, the non-stationary response can be plotted, Figure 4.15(b). The steady-state is first reached after about 200 seconds and the stationary variance can therefore be reduced with about 85%, hence the response in the discussed point becomes approximately 0.24 meters.

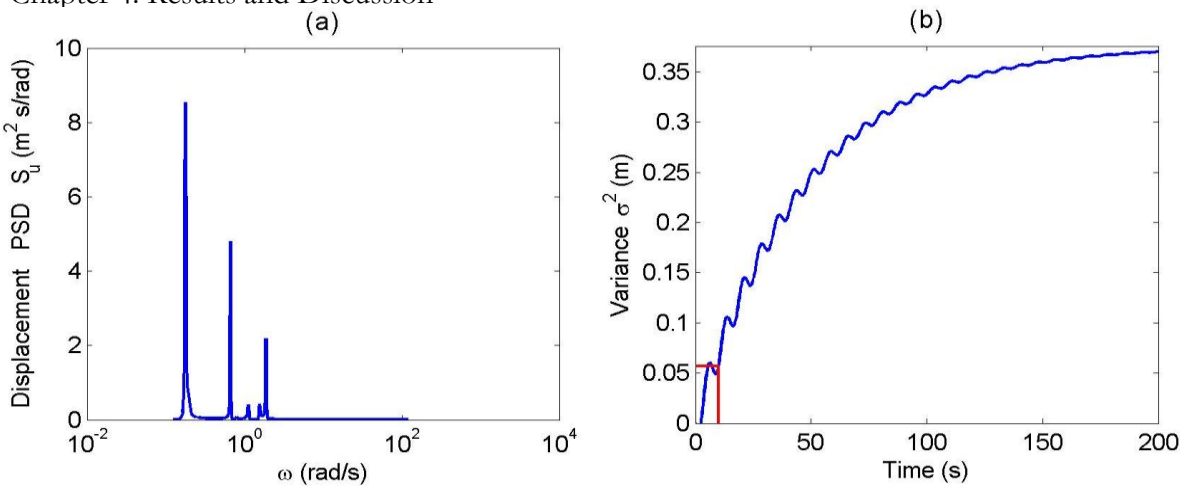


**Figure 4.15 (a) Displacement spectral density for DOF in x- direction in bridge deck girder at the quarter point. (b) Non-stationary response of DOF in (a)**

The third point investigated for the effects of non-stationarities is the top of Pylon 2 in y-direction for Analysis 3. In Figure 4.16 (a) the PSD of the displacement is plotted. There is seen that there is one significant maximum which correspond to mode 45, hence is the natural frequency of the single degree system set to, $\omega_0 = 1.875$ rad/s. By applying this to the simplified method, the non-stationary response in Figure 4.16(b) is obtained. The figure shows that this DOF reaches steady-state after about 50 seconds. After 10 seconds the variance is about 70 % of steady-state. The stationary response should therefore be reduced with approximately 15%, which give a non-stationary response of 0.25 meters.

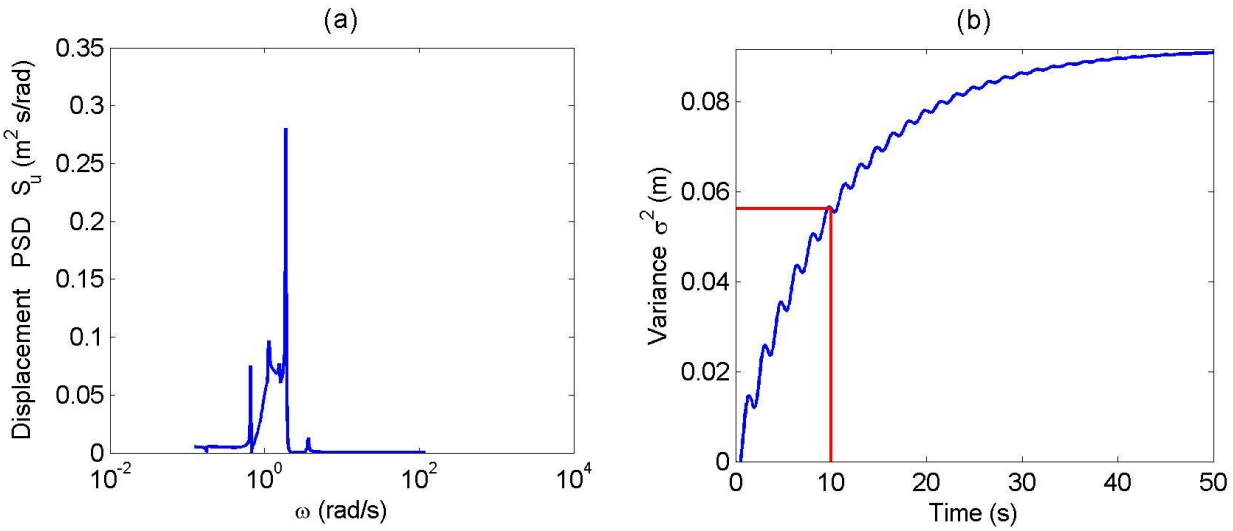


**Figure 4.16 (a) Spectral density of displacement for a DOF in y- direction on the top of Pylon 1. (b) Non-stationary response of DOF in (a)**

## 4.9 Discussion Non-Stationary Conditions

The result shows that the stationary response should for the three cases discussed be reduced with respectively 50%, 60% and 15%. These are large reductions which shows how important there is to apply non-stationary condition when calculating the responses of constructions as the Sognefjord Bridge. The method of assuming each DOF to be a single degree system is a major simplification. However, especially for the first case where the PSD of the response is very narrow banded and close to the PSD of a single degree system, this method should give a very good estimate of the effect of non-stationarities.

## 4.10 Extreme Values

Analysis 1 and Analysis 3 are the relevant analyses since they correspond to a seismic wave traveling along the bridge and perpendicular to the bridge. The extreme values are therefore found for the DOFs at three strategic points; the mid-span in one of the bridge girders, the quarter point of the span in the same bridge girder and at the top of Pylon 2. These values are presented in Table 4.9 for stationary conditions.

**Table 4.9 Peak factors and extreme values**

| | | Mid-span | | | Quarter point | | | Top Pylon 2 | | |
|---|---|---|---|---|---|---|---|---|---|---|
| | | x | y | z | x | y | z | x | y | z |
| Analysis 1 | $k_p$ | 2.40 | 2.05 | 2.02 | 2.35 | 1.89 | 1.97 | 2.24 | 2.17 | 2.32 |
| | E( $y_{max}$ ) | 0.12 | 0.88 | 1.65 | 0.10 | 0.61 | 1.53 | 0.27 | 0.63 | 0.24 |
| Analysis 3 | $k_p$ | 2.41 | 2.05 | 2.04 | 2.40 | 1.90 | 1.90 | 2.27 | 2.17 | 2.32 |
| | E( $y_{max}$ ) | 0.16 | 1.25 | 0.69 | 0.12 | 0.66 | 0.66 | 0.28 | 0.66 | 0.24 |

As can be seen from the table is the peak factors ( $k_p$ ) in the range between 1.69 and 2.41. In Analysis 1 the maximum value of the response where located in z- direction at the mid-span with a value of 0.81 meters. The peak factor for this point is 2.02 which lead to an extreme value of 1.65 meters. For Analysis 3 the maximum response were found in y-direction at the mid-span. Here is the peak factor 2.05 which give an extreme value of 1.25 meters.

## 4.11 Discussion of Extreme Values

As seen from the results of the extreme values, the peak factors are approximately two. The model that is used in this approximation of extreme values is a model made to consider the extreme values for wind. There are developed extreme values models more appropriate for earthquake engineering (18).

# 5 Conclusion

Suspension bridges are not a part of the scope of the Eurocode 8, nor is the particular Norwegian regulation adapted seismic analyses of long-span suspension bridges. Consequently, literature had to be used to find a method to calculate response of the Sognefjord Bridge. Much research has in the last decade been conducted on earthquake analysis on long-span bridges, in particular Kiureghian and Neuenhofer's work on including spatial effects in the analyses have been of great importance. Of work done the last years is the development of the pseudo excitation method developed by Lin and Zhang interesting.

The analysis model developed of the Sognefjord Bridge showed that the first period was 36 seconds. Investigating the natural frequencies and their associated modal participation factor showed that to include the thirty most participating modes in the calculations the first 1200 modes had to be included in the analysis. The conclusion is that due to the long period of the system the assumption of stationary conditions is not valid.

Before running the analyses two damping models, Rayleigh and hysteretic damping, were assessed. The frequency response plot showed that the Rayleigh damping gave a deviation from the hysteretic damping on almost 100% for several of the natural frequencies between the frequencies used to define the Rayleigh constants. There was consequently concluded that Rayleigh damping is not suitable to use in analyses of the Sognefjord Bridge. A rough estimate of the effect of aerodynamic damping was done using quasi-static theory and aerodynamic derivatives obtained from the Hardanger Bridge. The analysis shows that the aerodynamic damping was significant for an assumed wind velocity of 15m/s as the frequency response was reduced with about 25% for the first mode. There is concluded that the effects of aerodynamic damping should be considered also in earthquake analyses for the Sognefjord Bridge.

The response of the system was calculated using random vibration technique. In the analysis there were assumed stationary conditions and the magnitude of the input PSD corresponded to an earthquake return period of 10 000 years for the area where the bridge is situated. The maximum response appeared in z-direction at 1010, 1850 and 2090 meters from Pylon 1 when the earthquake was assumed traveling along the bridge and all spatial effects were included, the standard deviation of the response was here 0.81 meters. The spatial effects had significant effects on the system. The wave passage effect disturbed the symmetry of the response and gave a significant increase in response in z-direction. When the incoherence effect also was included, the symmetry of the system was restored. A possible explanation for this is the large distance between the pylons, which make the two excitations uncorrelated. In z-direction the maximum response increased when the incoherence effects were included. The conclusion is that spatial effects are shown to have large effects on the response, and hence, they must be included in analyses of long-span bridges as the Sognefjord Bridge. When analysing the system without any spatial effects there was discovered lack of symmetry in the system, this was not expected. The reason is thought to be a result of the modelling of the connection between the main cables and the pylons as fixed and should therefore be further investigated.

The effects of non-stationary conditions were approximated with a simplified method assuming each DOF as a single degree system. This was thought to be a good estimate since the response

spectra proved fairly narrow-banded. The result showed that the maximum response in the stationary analysis could be reduced with 50% to a response of about 0.4 meters. Hence, there is important to assess non-stationary condition when calculating earthquake response for the Sognefjord Bridge. The main conclusion of this thesis is that earthquake response of the Sognefjord Bridge not seems to be a problem even with an earthquake with a return period of 10 000 years.

# 6 Further Research

In this thesis the earthquake response of the Sognefjord Bridge has been assessed. The results showed that the responses were small and that an earthquake of Norwegian scale not likely would be a problem. Due to this, further research is mainly to validated the results obtained.

The connection between the main cables and the pylons were modelled as fixed. It is thought that this had a minor influence on the results. But the model should be further developed to include friction bearings at the top of the pylons, to confirm this assumption.

For the analyses the acceleration PSD used was adapted a PGA of $3\,m/s^2$ which corresponds to a Norwegian earthquake with a return period of 10 000 years. This might be a bit too high, thus there should be done a closer assessment on what magnitude extreme construction as the proposed Sognefjord Bridge should dimensioned for.

The aerodynamic damping of this bridge was assessed using aerodynamic derivatives from the Hardanger Bridge. There should therefore be conducted further research on the significance of aerodynamic damping when the aerodynamic derivatives for the bridge deck have been obtained.

When including spatial effects this reduced the response in x- and y- direction and increased the response in z-direction. Even if the responses were of low magnitude, there had been interesting to investigate these effects more closely to find a reason for them.

The effects of non-stationarities were in this thesis assessed using a simplified method, but the estimates showed that non-stationarities had large effect on the response. In further research this effects should be calculated as presented in the theory to validate the estimates and to obtain a more exact solution.

# Bibliography


1. Bridon. Products 2013.
2. Kiureghian AD, Neuenhofer A. RESPONSE SPECTRUM METHOD FOR MULTISUPPORT SEISMIC EXCITATIONS. Earthq Eng Struct Dyn. 1992 Aug;21(8):713-40. PubMed PMID: WOS:A1992JH03300005. English.
3. Akashi Kaikyō Bridge Wikipedia [cited 2013 24.05]. Available from: http://en.wikipedia.org/wiki/Akashi_Kaiky%C5%8D_Bridge.
4. Strait of Messina Bridge Wikipedia [cited 2013 24.05]. Available from: https://en.wikipedia.org/wiki/Strait_of_Messina_Bridge.
5. Zerva A. Spatial variation of seismic ground motions: modeling and engineering applications. Boca Raton, Fla.: CRC Press; 2008. 468 s. : ill p.
6. R. Sigbjörnsson RR, B. Halldorsson, J. T. Snæbjörnsson, & S. Ólafsson. The May 2008 Ölfus Earthquake in South Iceland: Modelling incoherence of strong ground motion. Proceedings of the International Conference on Earthquake Engineering (SE-50EEE). International Conference on Earthquake Engineering; Skopje, Republic of Macedonia.2013.
7. Lee M-C, Penzien J. Stochastic analysis of structures and piping systems subjected to stationary multiple support excitations. Earthq Eng Struct Dyn. 1983;11(1):91-110.
8. Berrah M, Kausel E. Response spectrum analysis of structures subjected to spatially varying motions. Earthq Eng Struct Dyn. 1992;21(6):461-70.
9. Heredia-Zavoni E, Vanmarcke E. Seismic Random-Vibration Analysis of Multisupport-Structural Systems. Journal of Engineering Mechanics. 1994;120(5):1107-28.
10. Standard N. Eurokode 8: Prosjektering av konstruksjoner for seismisk påvirkning, Del 2, Bruer. Lysaker: Standard Norge; 2005. 146, 11, 6 s. : ill. p.
11. Jiahao L. A fast CQC algorithm of psd matrices for random seismic responses. Computers & Structures. 1992 7/17/;44(3):683-7.
12. Lin J, Zhang W, Li J. Structural responses to arbitrarily coherent stationary random excitations. Computers & Structures. 1994 3/3/;50(5):629-33.
13. Lin J, Zhang W, Williams FW. Pseudo-excitation algorithm for nonstationary random seismic responses. Engineering Structures. 1994 5//;16(4):270-6.
14. Lin J, Zhao Y, Zhang Y. Accurate and highly efficient algorithms for structural stationary/non-stationary random responses. Computer Methods in Applied Mechanics and Engineering. 2001 11/9/;191(1–2):103-11.
15. Lin JH, Zhang YH, Li QS, Williams FW. Seismic spatial effects for long-span bridges, using the pseudo excitation method. Engineering Structures. 2004 7//;26(9):1207-16.
16. Lin JH, Zhang YH, Zhao Y. Pseudo Excitation Method and Some Recent Developments. Procedia Engineering. 2011 //;14(0):2453-8.
17. Zhang YH, Li QS, Lin JH, Williams FW. Random vibration analysis of long-span structures subjected to spatially varying ground motions. Soil Dynamics and Earthquake Engineering. 2009 4//;29(4):620-9.
18. Yahui Z, Jiahao L. Seismic Random Vibration of Long-Span Structures. Vibration and Shock Handbook. Mechanical Engineering Series: CRC Press; 2005. p. 30-1--41.
19. Langen I, Sigbjörnsson R. Dynamisk analyse av konstruksjoner. [Trondheim]: Tapir; 1979. XXI, 505 s. : ill. p.
20. Newland DE, Newland DE. An introduction to random vibrations, spectral and wavelet analysis. Harlow: Longman; 1993. xxix, 477 s. : ill. p.
21. Wang G-Q, Zhou X-Y, Zhang P-Z, Igel H. Characteristics of amplitude and duration for near fault strong ground motion from the 1999 Chi-Chi, Taiwan earthquake. Soil Dynamics and Earthquake Engineering. 2002;22(1):73-96.
22. Priestley MB. Power spectral analysis of non-stationary random processes. Journal of Sound and Vibration. 1967 7//;6(1):86-97.

23. Tajimi H, editor A statistical method of determining the maximum response of a building structure during an earthquake. Proceedings of the Second World Conference on Earthquake Engineering Tokyo and Kyoto, Japan, 1960.
24. Clough RW, Penzien J. Dynamics of Structures: Computers & Structures; 2003.
25. Vanmarcke EH, Lai SSP. STRONG-MOTION DURATION AND RMS AMPLITUDE OF EARTHQUAKE RECORDS. Bull Seismol Soc Amer. 1980;70(4):1293-307. PubMed PMID: WOS:A1980KE97100021. English.
26. Abdelghaffar AM, Rubin LI. SUSPENSION BRIDGE RESPONSE TO MULTIPLE-SUPPORT EXCITATIONS. Journal of the Engineering Mechanics Division-Asce. 1982;108(2):419-35. PubMed PMID: WOS:A1982NK77000014. English.
27. Harichandran R, Vanmarcke E. Stochastic Variation of Earthquake Ground Motion in Space and Time. Journal of Engineering Mechanics. 1986;112(2):154-74.
28. Loh C-H, Yeh Y-T. Spatial variation and stochastic modelling of seismic differential ground movement. Earthq Eng Struct Dyn. 1988;16(4):583-96.
29. Oliveira CS, Hao H, Penzien J. Ground motion modeling for multiple-input structural analysis. Structural Safety. 1991 5//;10(1–3):79-93.
30. Luco JE, Wong HL. Response of a rigid foundation to a spatially random ground motion. Earthq Eng Struct Dyn. 1986;14(6):891-908.
31. Davenport AG, editor Note on the distribution of the largest value of a random function with application to gust loading. ICE Proceedings; 1964: Ice Virtual Library.
32. Kreyszig E. Advanced engineering mathematics. Hoboken, NJ: John Wiley; 2006.
33. Zhong WX, Williams FW. A Precise Time Step Integration Method. Proceedings of the Institution of Mechanical Engineers, Part C: Journal of Mechanical Engineering Science. 1994 November 1, 1994;208(6):427-30.
34. Dyrbye C, Hansen SO. Wind loads on structures. Chichester: Wiley; 1997. XIV, 229 s. : ill. p.
35. Strømmen EN. Theory of bridge aerodynamics. Berlin: Springer; 2010. XXI, 302 s. : ill. p.
36. Håndbok 185 Bruprosjektering, (2009).
37. Håndbok 185 Bruprosjektering -Eurokodeutgave, (2011).
38. Standard N. Eurokode 8: Prosjektering av konstruksjoner for seismisk påvirkning, Del 1, Allmenne regler, seismiske laster og regler for bygninger. Lysaker: Standard Norge; 2008. 179, 12 s. : ill. p.
39. Standard N. Eurokode: grunnlag for prosjektering av konstruksjoner. Lysaker: Standard Norge; 2008. 72, 8 s. : ill. p.
40. CSi. CSi Analysis Reference Manual - For SAP2000, ETABS, SAFE, and CSiBridge2011.
41. Hansen SO, Lollesgaard, M., Rex, S., Jakobsen, J.B., Hansen, E.H. . The Hardanger Bridge: Static and Dynamic Wind Tunnel Test with a Section Model. Svend Ole Hansen ApS. 2006.
42. Øiseth OA. Dynamic behaviour of cable-supported bridges subjected to strong natural wind. Trondheim: Norges teknisk-naturvitenskapelige universitet; 2011. 1 b. (flere pag.) : ill. p.
43. NVE NV-oE-. 2003;Retningslinjer for laster and dimensjonering
44. Development of a seismic zonation for Norway: final report : prepared for Norwegian Council for Building Standardization (NBR). Oslo: NGI; 1998. 162, [28] s. : ill. p.

# A. Undamped Frequency Response

Figure A.1 Undamped frequency response shows the undamped frequency response for a DOF in y-direction at the mid-span.

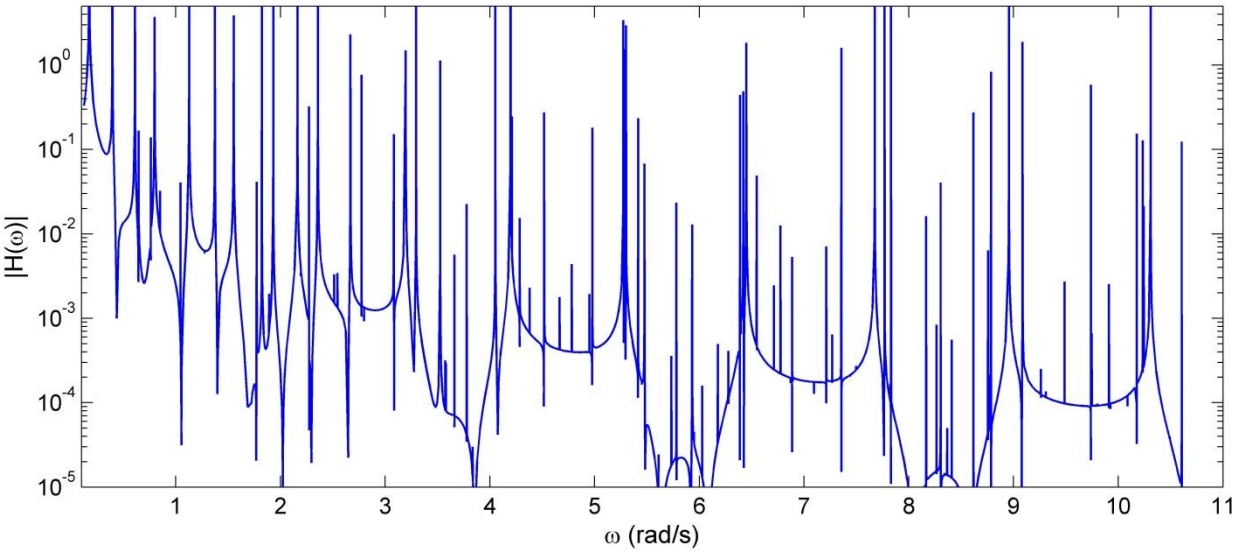


**Figure A.1 Undamped frequency response**

# B. Response Accelerations

Table B.1and Table B.2 contains the standard deviations of the response accelerations obtained from respectively Analysis 1 and Analysis 2.

**Table B.1 Response accelerations for Analysis 1**

| | UX | UY | UZ | RX | RY | RZ |
|---|---|---|---|---|---|---|
| Mid-span $(m/s^2)$ | 0.490 | 1.747 | 6.708 | 0.007 | 0.013 | 0.004 |
| Quarter-point $(m/s^2)$ | 0.380 | 1.405 | 5.736 | 0.014 | 0.008 | 0.006 |
| Top pylon $(m/s^2)$ | 1.764 | 2.179 | 3.877 | 0.019 | 0.018 | 0.007 |

**Table B.2 Response accelerations for Analysis 3**

| | UX | UY | UZ | RX | RY | RZ |
|---|---|---|---|---|---|---|
| Mid-span $(m/s^2)$ | 0.668 | 2.591 | 2.224 | 0.005 | 0.018 | 0.000 |
| Quarter-point $(m/s^2)$ | 0.476 | 1.892 | 1.269 | 0.014 | 0.009 | 0.005 |
| Top pylon $(m/s^2)$ | 2.129 | 2.340 | 3.887 | 0.019 | 0.017 | 0.007 |

# C. SAP2000 model

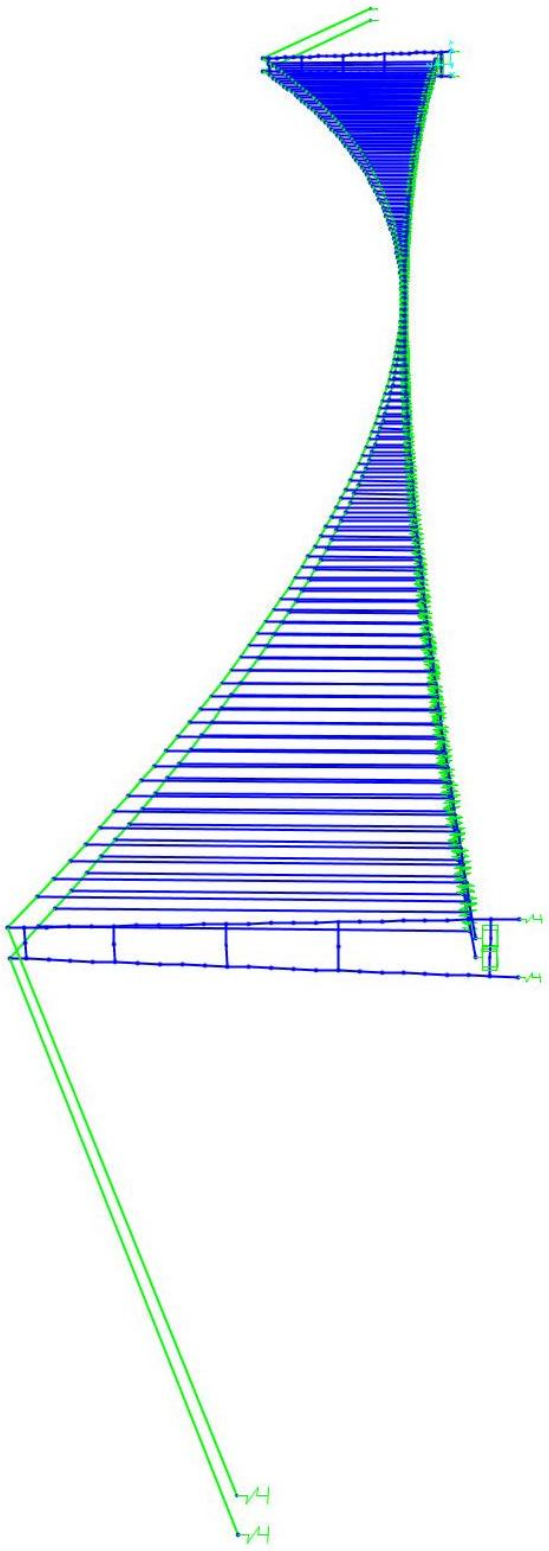

Figure C.1 Complete model

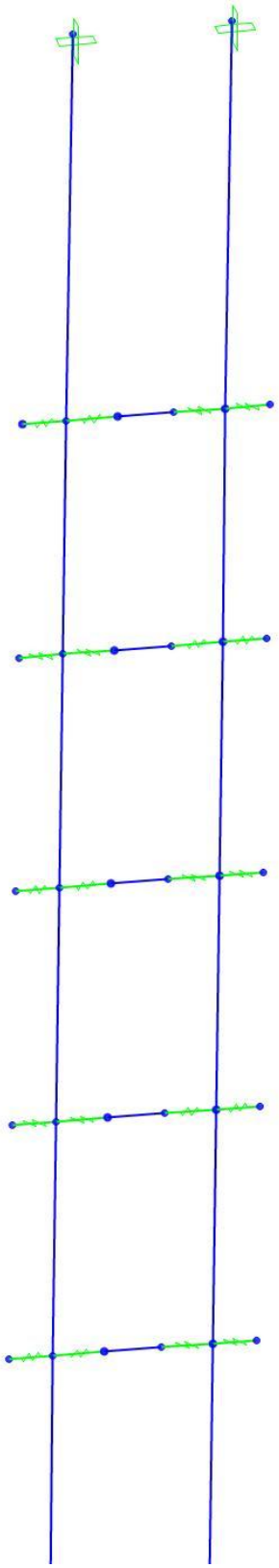

Figure C.2 Section of Bridge deck

# D. Modal Shaped Cable and Bridge Girder

Plot of the 10 most participation modes in the translation direction.

## D.1 UX

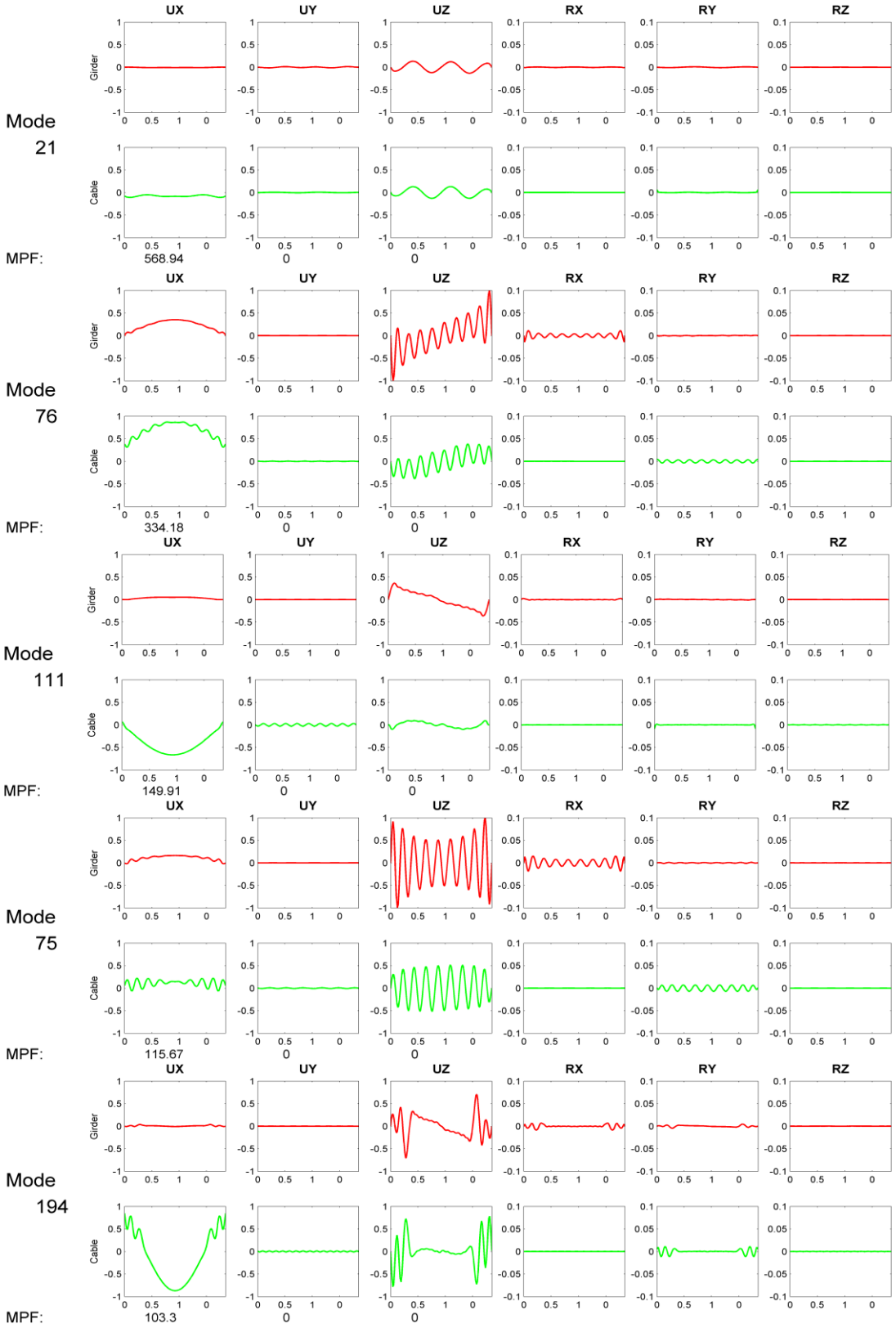


**Figure D.1 Ten most participating modes in x-direction Mode 1-5**

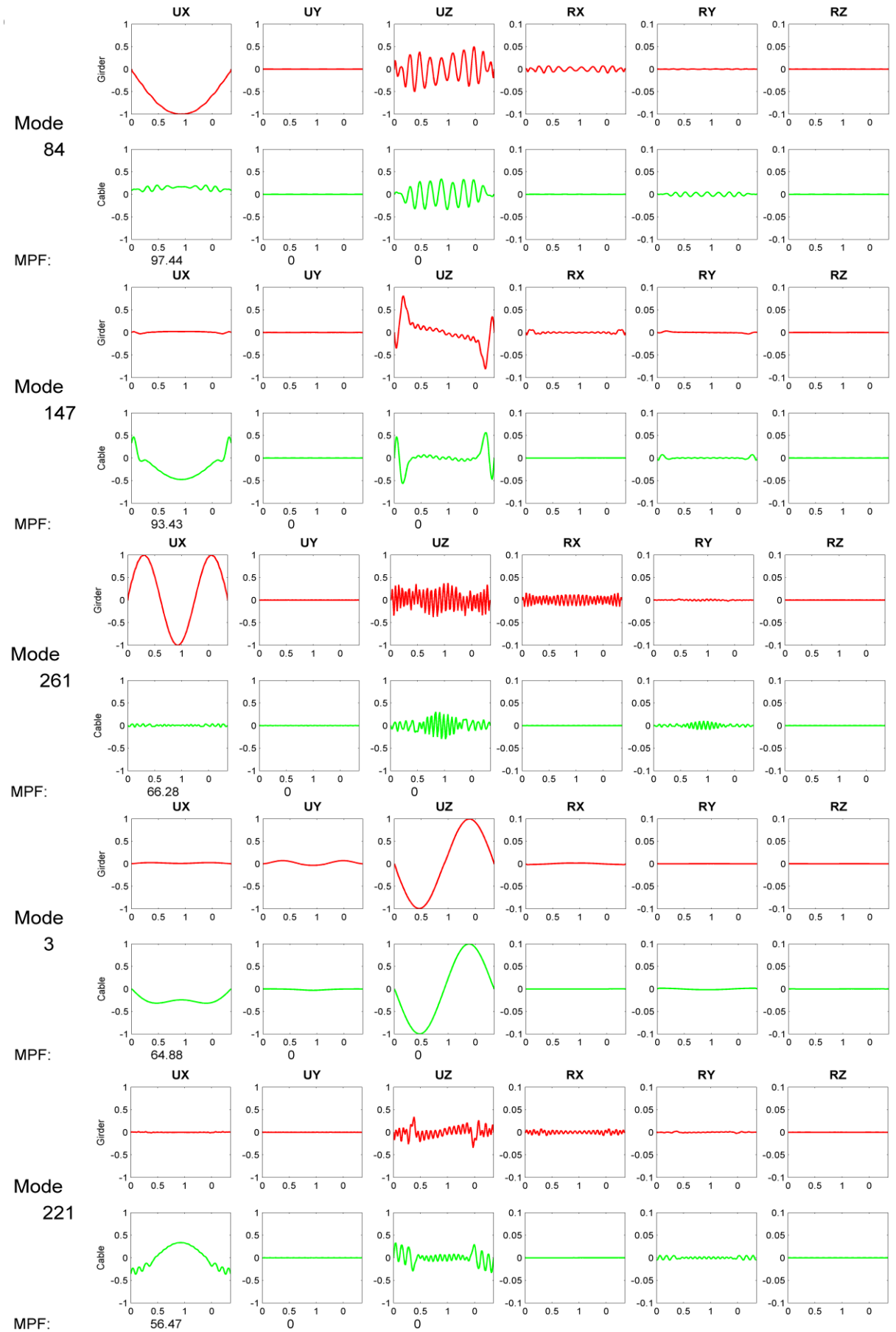


**Figure D.2 Ten most participating modes in x-direction Mode 6-10**

## D.2 UY

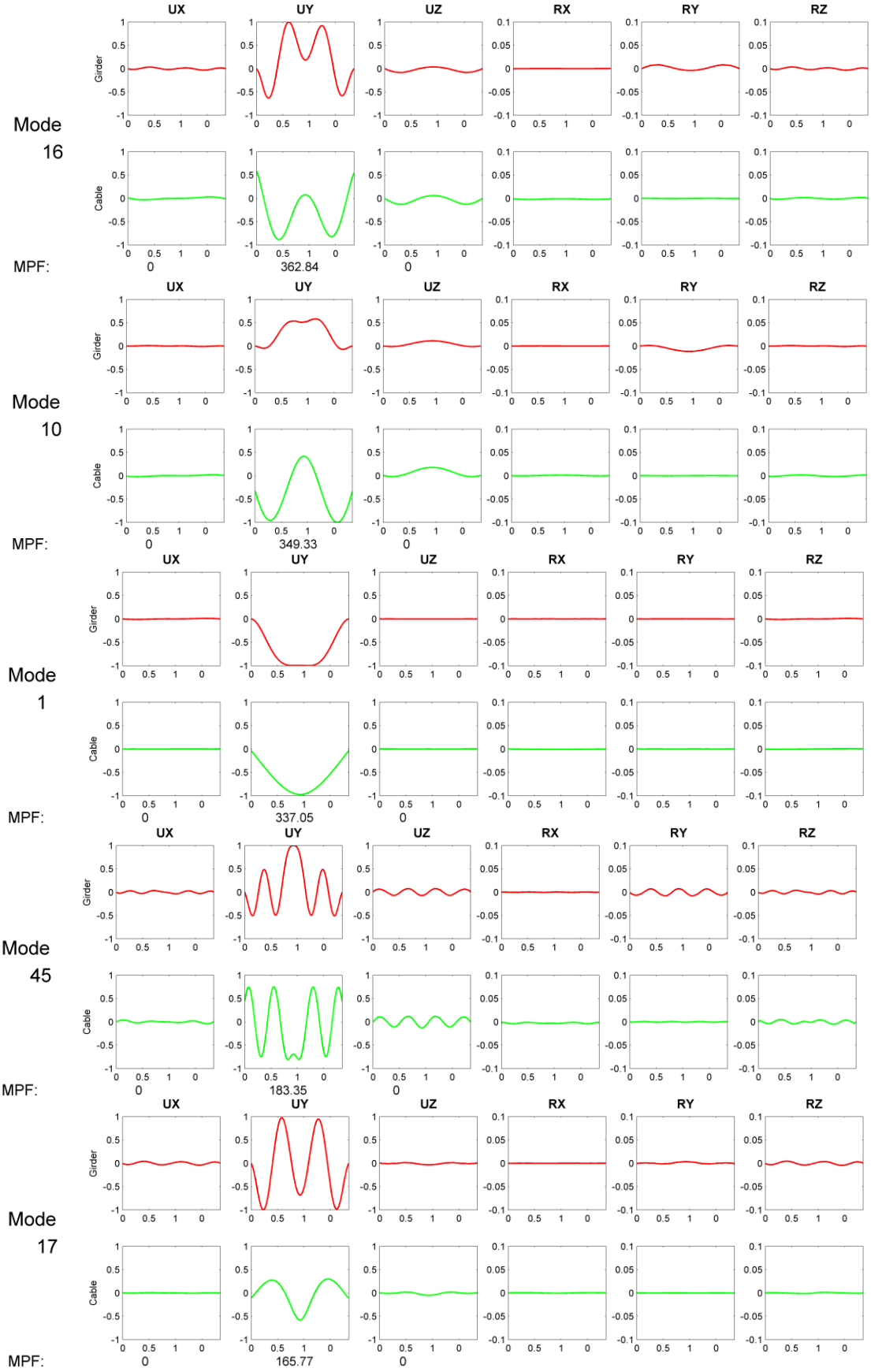


**Figure D.3 Ten most participating modes in y-direction Mode 1-5**

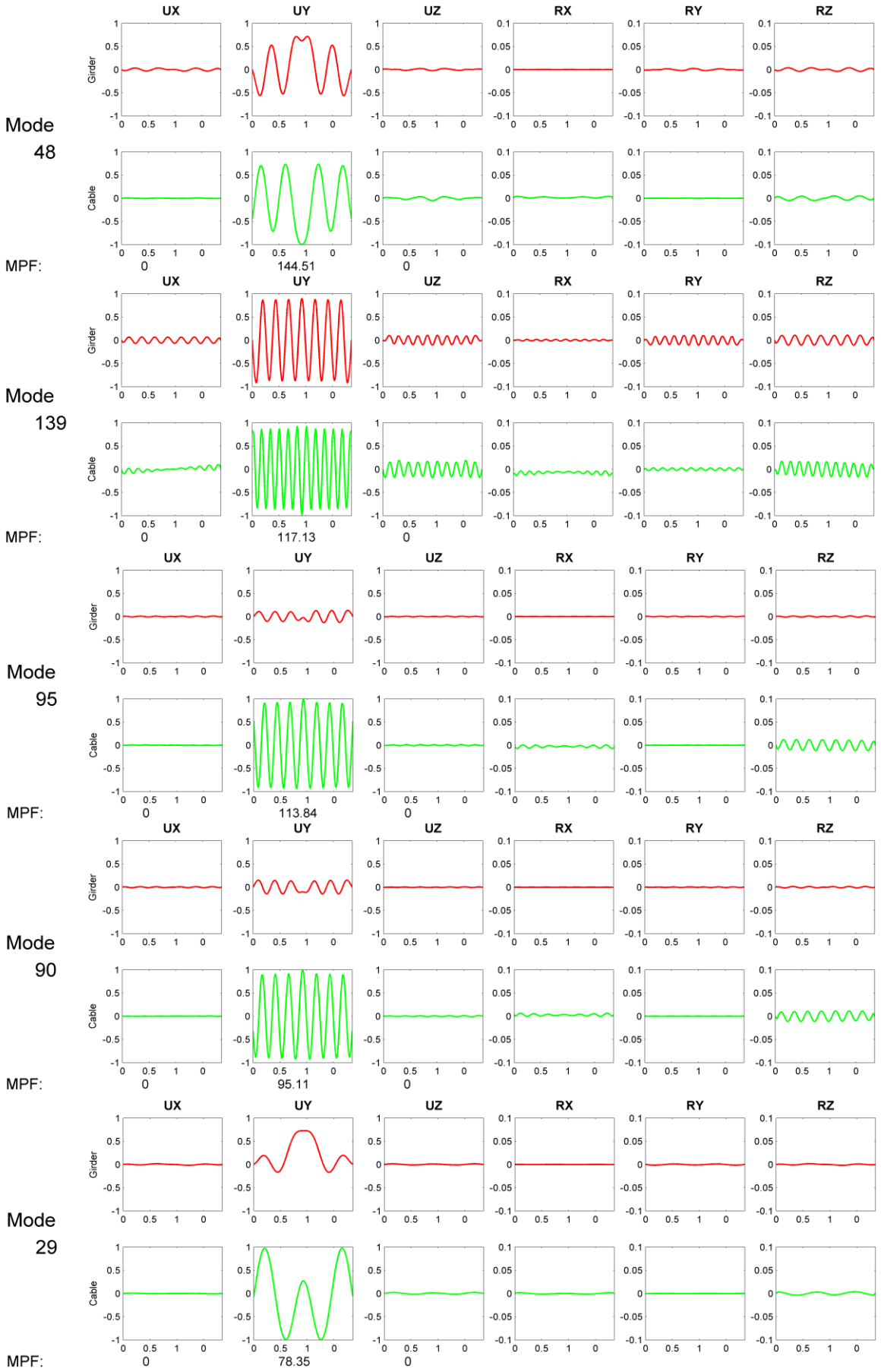


**Figure D.4 Ten most participating modes in y-direction Mode 6-10**

## D.3 UZ

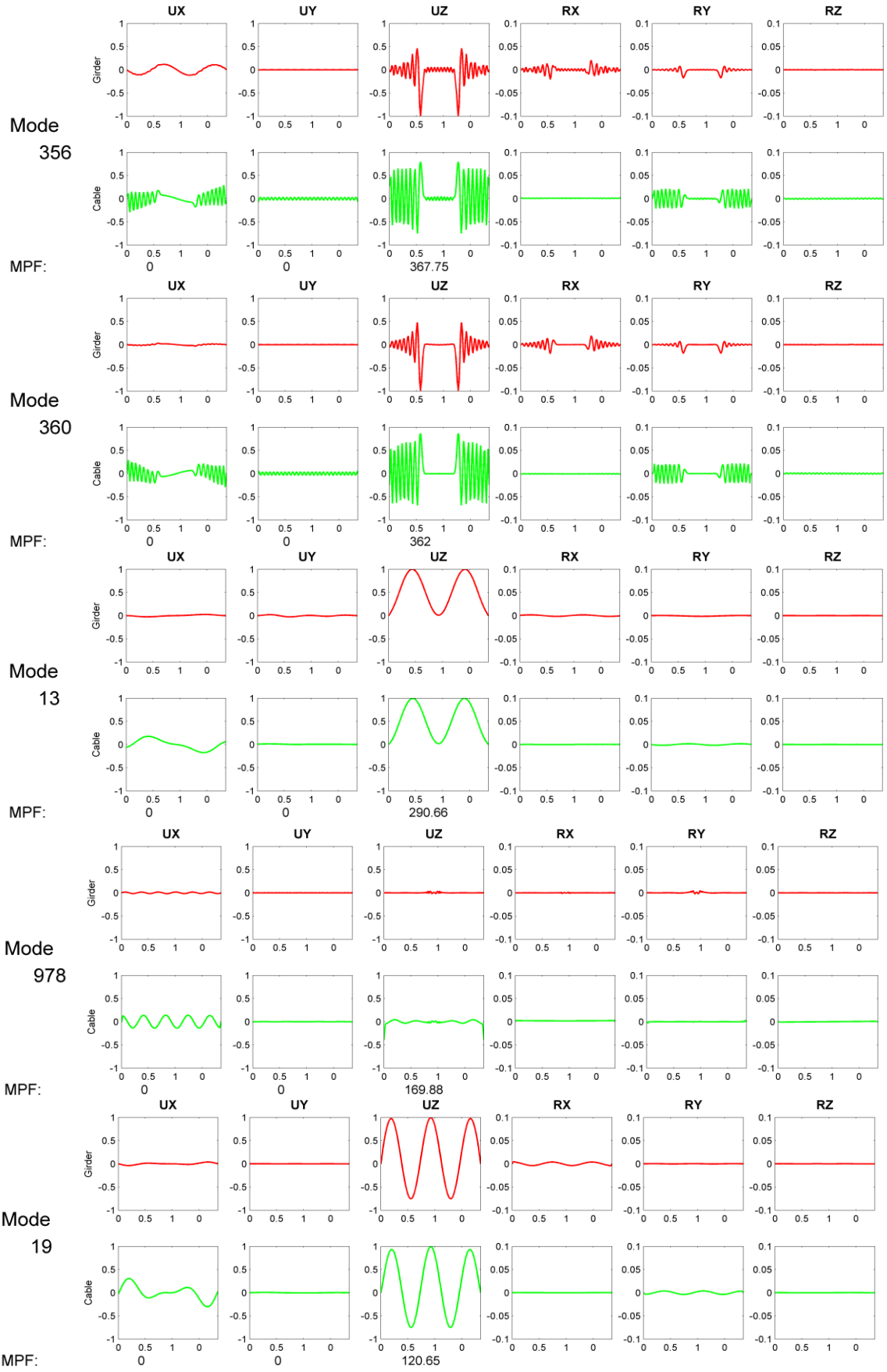


**Figure D.5 Ten most participating modes in z-direction Mode 1-5**

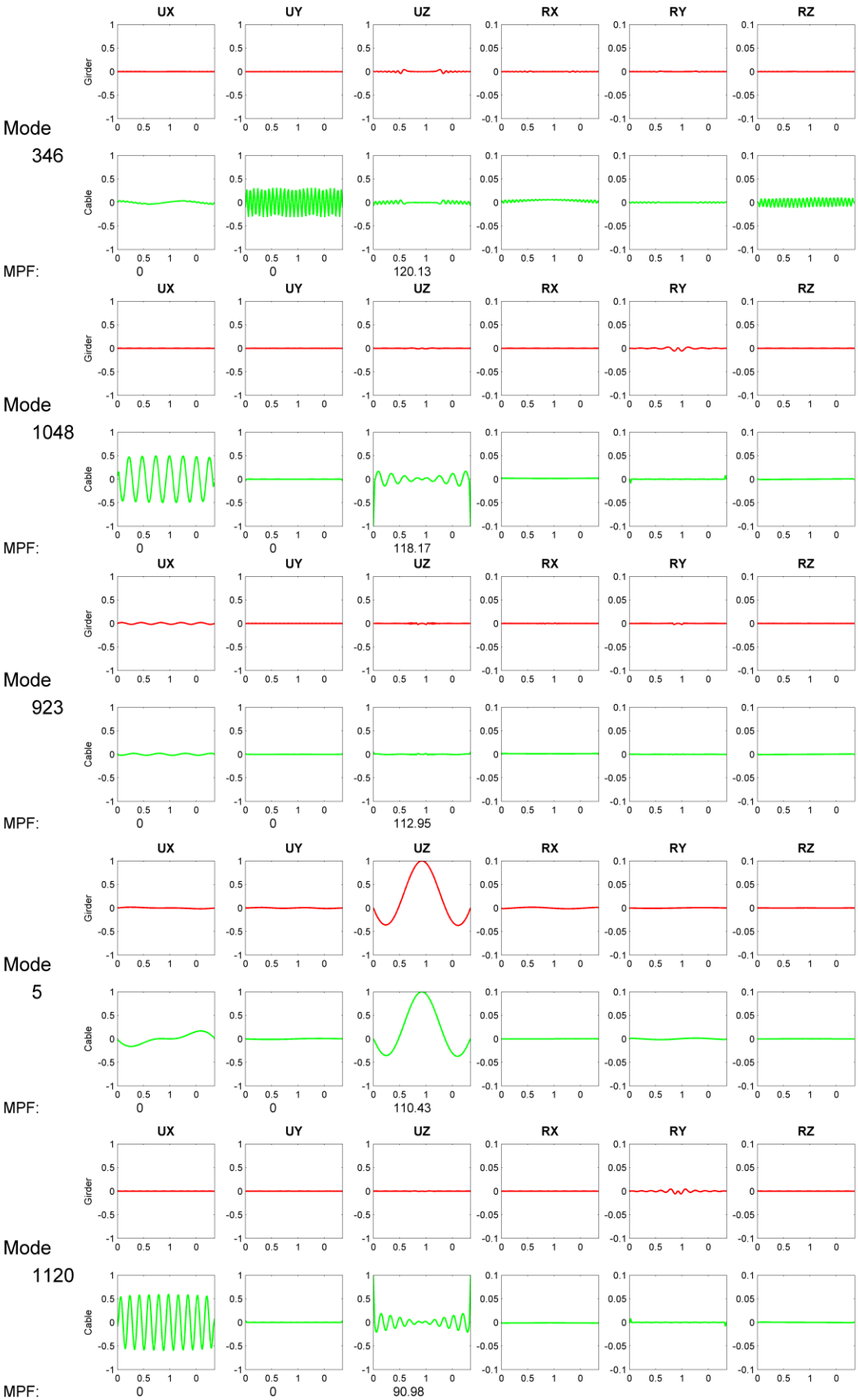


**Figure D.6 Ten most participating modes in z-direction Mode 6-10**

# E. Mode Shapes for Pylons

Single Pylon without the rest of the bridge, two line illustrate the two legs.

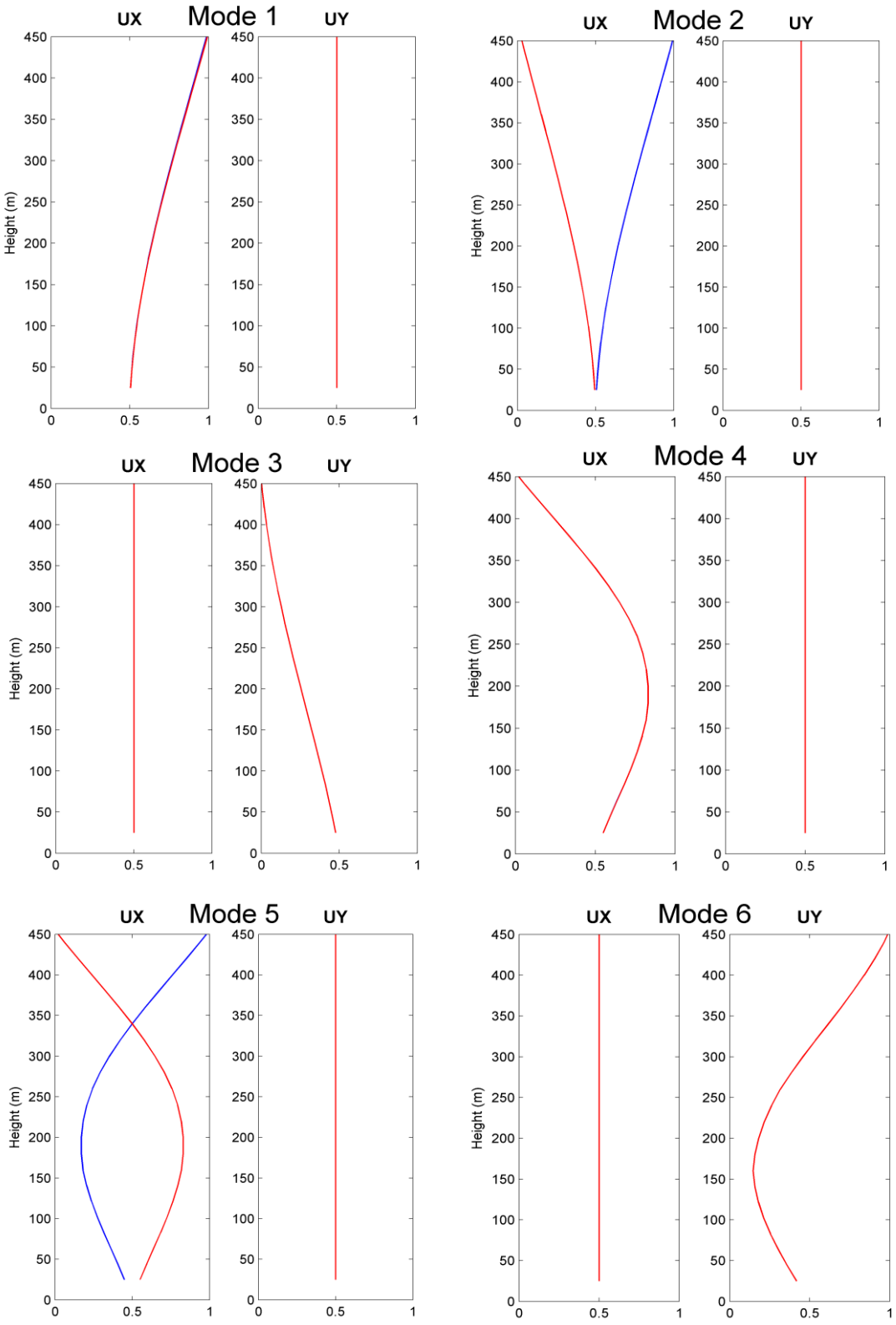


**Figure E.1 Tower mode shapes 1-6**

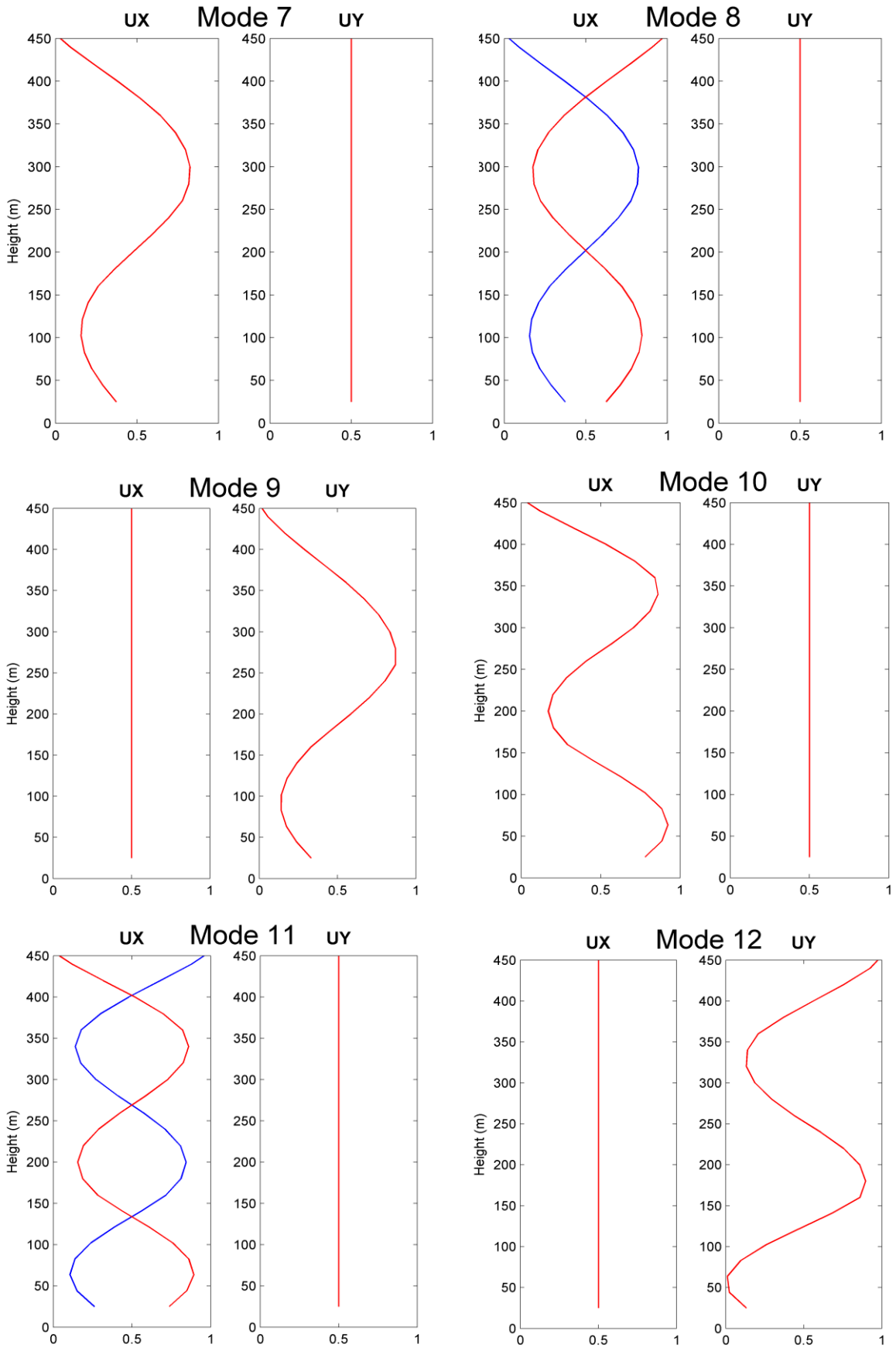


**Figure E.2 Tower mode shapes 7-12**

# F. MATLAB Calculations

In this appendix the MATLAB routines used in the response calculations are

## F.1 Import

This routine:

- Imports the output file from SAP2000 created by SAP2000 and created the mass and stiffness matrixes. Do to this the constrained DOF must be found by matching the constraint numbers.
- Import txt files were the nodes of concrete and steel are defined (made manually) and creates sum matrixes for the steel, concrete and common DOFs
- Solves the eigenvalue problem

```
function [kmodal,mmodal,T,m,k,mconcrete,msteel, mjoint, kconcrete,
ksteel,kjoint,fi]=Import(update)%
%%Descritin
%This script import the mass and stiffness matrix from the files in matlab,
%divided the matrixes into sub matrixes for steel, concrete and joint nodes
%The eigenfrequencies and eigenvecors are also found
%Created by Håkon Olav Skogmo

format long g
%Update stiffness and mass matrix and decouples system
%%Find numbers of equations
    fid=fopen('C:\Users\Hako\Dropbox\Skole\10. semester\Modell\Modell fra
scratch 3\Modell fra scratch 3.txa');
        n = textscan(fid,'%*s%*s%*s%*s%*s%*s%f', 'HeaderLines',
14,'collectoutput',1 );
    fclose(fid);
    n=n{1}(1,1);
    k=zeros(n);                     %Makes a matrix of zeros with n
elements
 %%Creates k matrix
    fid=fopen('C:\Users\Hako\Dropbox\Skole\10. semester\Modell\Modell fra
scratch 3\Modell fra scratch 3.txk');
        c = textscan(fid,'%d%d%f', 'HeaderLines', 1,'collectoutput',1 );
    fclose(fid);
    for j =1:length(c{1})
        k(c{1}(j,1),c{1}(j,2))=c{2}(j);     %Copies values from text file
to stiffness matrix
    end
    k=tril(k)+tril(k,-1)';          %Copies lower diag to upper diagonall
%%Creates mass matrix
    fid=fopen('C:\Users\Hako\Dropbox\Skole\10. semester\Modell\Modell fra
scratch 3\Modell fra scratch 3.txm');
        c1 = textscan(fid,'%d%d%f', 'HeaderLines', 1,'collectoutput',1 );
    fclose(fid);
    m=zeros(n);
    for j =1:length(c1{1})
        m(c1{1}(j,1),c1{1}(j,2))=c1{2}(j);     %Copies values from text
file to stiffness matrix
    end
    m=tril(m)+tril(m,-1)';          %Copies lower diag to upper diagonall
 %% Load tabel with nodes and DOF
    fid=fopen('C:\Users\Hako\Dropbox\Skole\10. semester\Modell\Modell fra
scratch 3\Modell fra scratch 3.txe');
```

```
        c = textscan(fid,'%f%f%f%f%f%f\r\n%f', 'HeaderLines',
1,'collectoutput',1 );
    fclose(fid);
    DOFlist=sortrows(c{1},1);
    %% Load concrete nodes and finds DOFS
    fid=fopen('C:\Users\Hako\Dropbox\Skole\10. semester\Matlab\Betong
noder.txt');
        c = textscan(fid,'%f', 'HeaderLines', 1,'collectoutput',1 );
    fclose(fid);
   concretenodes=c{1};
    ConcreteDOF =zeros(length(concretenodes),7);
        for j=1:length(concretenodes)
            a=find(DOFlist(:,1)==concretenodes(j));
            ConcreteDOF(j,:)=DOFlist(a,:);
        end
%% Load joint nodes/ nodes that are connected to both steel and concrete
   fid=fopen('C:\Users\Hako\Dropbox\Skole\10. semester\Matlab\Felles
noder.txt');
        c = textscan(fid,'%f', 'HeaderLines', 1,'collectoutput',1 );
    fclose(fid);
    jointnodes=c{1};
    JointDOF =zeros(length(jointnodes),7);
        for j=1:length(jointnodes)
            a=find(DOFlist(:,1)==jointnodes(j));
            JointDOF(j,:)=DOFlist(a,:);
        end
    ConcreteDOFtemp=ConcreteDOF;                % Copies the matrix with
Concrete DOF over in a temporary
    ConcreteDOFtemp(:,1)=[];                  %removes row with nodes number
    ConcreteDOFtemp=ConcreteDOFtemp(:);          % Put matrix into vector
    ConcreteDOFtemp(ConcreteDOFtemp==0)=[];      % Removes zeros elements
cause by fixed nodes
    JointDOFtemp=JointDOF;
    JointDOFtemp(:,1)=[];
    JointDOFtemp=JointDOFtemp(:);
    kconcrete=zeros(n);
    mconcrete=zeros(n);
    %Make concrete mass and stiffness matrix

kconcrete([ConcreteDOFtemp],[ConcreteDOFtemp])=k([ConcreteDOFtemp],[Concret
eDOFtemp]); % Copy stiffness terms in relation concrete elements

mconcrete([ConcreteDOFtemp],[ConcreteDOFtemp])=m([ConcreteDOFtemp],[Concret
eDOFtemp]); %Copy mass terms in relation concrete elements
    ksteel=k-kconcrete;
    msteel=m-mconcrete;
    kconcrete([JointDOFtemp],[JointDOFtemp])=0;
    mconcrete([JointDOFtemp],[JointDOFtemp])=0;
    % Make mass and stiffness matrix with joint steel and concrete elements
    kjoint=zeros(n);
    mjoint=zeros(n);
    kjoint([JointDOFtemp],[JointDOFtemp])=k([JointDOFtemp],[JointDOFtemp]);
    mjoint([JointDOFtemp],[JointDOFtemp])=m([JointDOFtemp],[JointDOFtemp]);
%%LOad lower part of DOF list, the constraint part
    fid=fopen('C:\Users\Hako\Dropbox\Skole\10. semester\Modell\Modell fra
scratch 3\Modell fra scratch 3.txe');
        c = textscan(fid,'%s%f%f%f%f%f\r\n%f', 'HeaderLines',
2171,'collectoutput',1 );
    fclose(fid);
    Constraints=c{2};
```

```
%% MAkes a list of DOF where the constraints equatiin are replaced with the
real DOF
   DOFwithCon=zeros(length(DOFlist),7);
 for j=1:length(DOFlist)
     if DOFlist(j,2)<0
        a= Constraints(:,2)==DOFlist(j,3);
        DOFwithCon(j,1)=DOFlist(j,1);
        DOFwithCon(j,2:7)=Constraints(a,:);
     elseif DOFlist(j,2)>0
         DOFwithCon(j,:)=DOFlist(j,1:7);
     else
         DOFwithCon(j,:)=DOFlist(j,:);
     end
 end
   save('C:\Users\Hako\Dropbox\Skole\10.
semester\Matlab\Variables\DOFwithCON.mat','DOFwithCon')
  if update==1
%% Find eigenvalues and eigenfrequencys
    [fi,lambda]=eig(k,m);
    w=sqrt(diag(lambda));
    T=linspace(1,n,n)';
    T(:,2)=2*pi./w;
%% Uncoupling mass and stiffness matrix
    kmodal=fi'*k*fi;
    mmodal=fi'*m*fi;
   kmodal=kmodal-tril(kmodal,-1)-triu(kmodal,1);
   mmodal=mmodal-tril(mmodal,-1)-triu(mmodal,1);
   %%Write data to files
    fid=fopen('C:\Users\Hako\Dropbox\Skole\10.
semester\Matlab\eigenperioder.txt', 'w');
        fprintf(fid,'%1.0d %18.12f\n', T');
    fclose(fid);
    fid=fopen('C:\Users\Hako\Dropbox\Skole\10.
semester\Matlab\eigenvector.txt', 'w');
        fprintf(fid,'%3s %d\r %3s %d\r', 'Number of DOF', n, 'Number of
eigenvectors', length(T));
        fprintf(fid,'%9.6f\n', fi' );
    fclose(fid);
    fid=fopen('C:\Users\Hako\Dropbox\Skole\10. semester\Matlab\kmodal.txt',
'w');
        fprintf(fid,'%4s %6d8\n', 'Number of eigenvectors',length(T));
        fprintf(fid,'%1.4f\n', diag(kmodal));
    fclose(fid);
     fid=fopen('C:\Users\Hako\Dropbox\Skole\10.
semester\Matlab\mmodal.txt', 'w');
        fprintf(fid,'%4s %6f\n', 'Number of eigenvectors',length(T));
        fprintf(fid,'%1.4f\n', diag(mmodal));
    fclose(fid);
 elseif update==0
   % Import eigenvalues from file
     fid=fopen('C:\Users\Hako\Dropbox\Skole\10.
semester\Matlab\eigenperioder.txt');
          c = textscan(fid,'%d%f', 'HeaderLines', 0,'collectoutput',1 );
    fclose(fid);
    T=zeros(length(c{1}(:)),2);
    T(:,1)=c{1}(:);
    T(:,2)=c{2}(:);

    %Import eigenvvectores from file
   fid=fopen('C:\Users\Hako\Dropbox\Skole\10.
semester\Matlab\eigenvector.txt');
```

```
        c = textscan(fid,'%*s%*s%*s%d\n', 'HeaderLines',
0,'collectoutput',1 );
        c1 = textscan(fid,'%*s%*s%*s%d\n', 'HeaderLines',
0,'collectoutput',1 );
        c2 = textscan(fid,'%f\n', 'HeaderLines', 0,'collectoutput',1 );
    fclose(fid);
    DOF=c{1}(1);
    Nreigvec=c1{1}(1);
    fi=reshape(c2{1},Nreigvec,DOF)';
    Nreigvec=length(T);
    %Import kmodal
    fid=fopen('C:\Users\Hako\Dropbox\Skole\10.
semester\Matlab\kmodal.txt');
        c = textscan(fid,'%f', 'HeaderLines', 1,'collectoutput',1 );
    fclose(fid);
    fid=fopen('C:\Users\Hako\Dropbox\Skole\10.
semester\Matlab\mmodal.txt');
        c = textscan(fid,'%f', 'HeaderLines', 1,'collectoutput',1 );
    fclose(fid)
    mmodal=zeros(Nreigvec);
    kmodal=zeros(Nreigvec);
    for j= 1:Nreigvec
        mmodal(j,j)=c{1}(j);
        kmodal(j,j)=c{1}(j);
    end
 end

end
```

## F.2 Frequency Response

The function calculated the frequency response for this cases

- Undamped system
- Rayleigh damping
- Hysteretic damping
- Hysteretic and aerodynamic damping

Functions used are cae, Import, Freq, Damping

```
%% Frequency response
% Calculate the frequency response for different damping models
% Uses the functions:
%   * cae
%   * freq
%   * Import
%   * damping
%    *Iforce
% (c) Håkon Olav Skogmo



clear all;
clc;
close all;
calc=0; % 0 plot old results. 1 recalculate result
```

```
if calc==1
update=0;
[~,~,T,m,k,mconcrete,msteel, mjoint, kconcrete,
ksteel,kjoint,~]=Import(update);
temp=sortrows(T,2);
Tsorted=sort(T(:,2),'descend');
wn=2*pi./Tsorted;
%%Import function
  [crayleigh, cmaterial,~]=damping(T, k,m, msteel, mconcrete,mjoint,ksteel,
kconcrete, kjoint);
%% Function that find aerodynamic damping
[Caedamp]=Cae(length(m));
%% Makes frequency vecor
[w,p]=Freq(wn);
  %Clear variable not need anymore
  clearvars msteel mconcrete mjoint ksteel  kconcrete  kjoint
%D
%D(1:6) DOF in midspan
%D(7:12) DOF in quarter-points
%D(13:18) DOF in top Pylon
D=[3546,3545,3544,3543,3542,3541,2986,2984,2988,2987,2985,2983,309,312,307,
310,308,311];
 nw=length(w)
 [IUx,IUy,IUz,~,~,~]=Iforce(length(m));
I=IUx+IUy+IUz;
Hwrayleigh=zeros(length(D),nw);
Hwmaterial=zeros(length(D),nw);
Hwcae=zeros(length(D),nw);
Hwundamped=zeros(length(D),nw);
for j=1:length(w)
    tic;
    Tempcae=abs((-w(j)^2*m+k+1i*cmaterial+1i*w(j)*Caedamp)\I);
    Temprayleigh=abs((-w(j)^2*m+k+1i*w(j)*crayleigh)\I);
    Tempmaterial=abs((-w(j)^2*m+k+1i*cmaterial)\I);
    Tempundamped=abs((-w(j)^2*m+k)\I);
    Hwcae(:,j)=Tempcae(D);
    Hwrayleigh(:,j)=Temprayleigh(D);
    Hwmaterial(:,j)=Tempmaterial(D);
    Hwundamped(:,j)=Tempundamped(D);
    toc
    j

end
elseif calc==0
    Hwundamped=importdata('C:\Users\Hako\Dropbox\Skole\10.
semester\Matlab\Datafiler\Damping\Hwundamped.mat');
    Hwrayleigh=importdata('C:\Users\Hako\Dropbox\Skole\10.
semester\Matlab\Datafiler\Damping\HwRayleigh.mat');
    Hwmaterial=importdata('C:\Users\Hako\Dropbox\Skole\10.
semester\Matlab\Datafiler\Damping\Hwmaterial.mat');
    Hwcae=importdata('C:\Users\Hako\Dropbox\Skole\10.
semester\Matlab\Datafiler\Damping\Hwcae.mat');
    w=importdata('C:\Users\Hako\Dropbox\Skole\10.
semester\Matlab\Datafiler\Damping\Omega.mat');
end
%% PLot material and rayleigh damping
h=figure;
semilogy(w, Hwrayleigh(2,:),'r',w,Hwmaterial(2,:),'b','linewidth', 1);
xlabel('\omega (rad/s)', 'fontsize',12)
ylabel('|H(\omega)|','fontsize',12)
axis([0 10 10^-5 100])
```

```
 set(gca, 'fontsize', 11)
legend('Rayleig damping', 'Hysteretic damping')
      matl=['C:\Users\Hako\Dropbox\Skole\10.
semester\Matlab\PLot\Damping\Rayandmat'];
      word=['C:\Users\Hako\Dropbox\Skole\10.
semester\Oppgave\PLot\Damping\Rayandmat'];
      saveas(h, matl,'m')
      set(gcf,'units','pixels','PaperPosition',[0 0 25,10])
       print(h,'-djpeg','-r800', word)
%% Plot material and material with aerodynamic damping
h=figure;
semilogy(w, Hwmaterial(2,:),'r',w,Hwcae(2,:),'b','linewidth', 1);
xlabel('\omega (rad/s)', 'fontsize',12)
ylabel('|H(\omega)|','fontsize',12)
axis([0.1 1 10^-3 10])
 set(gca, 'fontsize', 11)
legend('Hysteretic damping', 'Hysteretic and Aerodynamic damping')
      matl=['C:\Users\Hako\Dropbox\Skole\10.
semester\Matlab\PLot\Damping\matandcae'];
      word=['C:\Users\Hako\Dropbox\Skole\10.
semester\Oppgave\PLot\Damping\matandcae'];
      saveas(h, matl,'m')
      set(gcf,'units','pixels','PaperPosition',[0 0 25,10])
       print(h,'-djpeg','-r800', word)
```

## F.3 Aerodynamic Damping

Routine that creates the aerodynamic damping matrix. Used DOF list from SAP2000 and a list of bridge deck nodes( created manually) to find the DOFs that the aerodynamic damping term should be assign to. Function named "cae.mat"

```
function [Caedamp]=Cae(n)
%% Aerodynamic damping - Cae
% Calculates the aerodynamic damping matix

% 1. Assum that aerodynmic damping only occurs fr the bridge deck
% 2. Find nodes correnspondig to bridge deck
% 3. Find the relevant DOF; displacement in y and z direction and rotation
% about x-axes
% 4, Apply the relevant aerodynamic damping to the DOF
%% Created by Håko Olav Skogmo

V=10;
B=12.9;
D=2.5;
CD=0.7;
CDm=0;
CL=-0.25;
CLm=2.4;
CM=0.01;
CMm=0.74;
ro=1.25;

%% Load tabel with nodes and DOF
 fid=fopen('C:\Users\Hako\Dropbox\Skole\10. semester\Modell\Modell fra
scratch 3\Modell fra scratch 3.txe');
        c = textscan(fid,'%f%f%f%f%f%f\r\n%f', 'HeaderLines',
1,'collectoutput',1 );
```

```
    fclose(fid);
    DOFlist=sortrows(c{1},1);
%%Load nodes in the bridge deck girders
    fid=fopen('C:\Users\Hako\Dropbox\Skole\10. semester\Matlab\Noder
brodekke.txt');
        c = textscan(fid,'%f', 'HeaderLines', 2,'collectoutput',1 );
    fclose(fid);
    BDGnodes=sort(c{1});
%%Picks DOF in joints in bridge deck
     BDGDOFtemp =zeros(length(BDGnodes),7);
        for j=1:length(BDGnodes)
            a= DOFlist(:,1)==BDGnodes(j);
            BDGDOFtemp(j,:)=DOFlist(a,:);
        end
%% Load second part of DOF list - In the file .txe constrained equation is
shown with '-'
% berfore a number, this number is a constrain number and the the actual
DOF equation number can be found in the
%.txc file. In the end of the .txe list there a list of nodes with
constraints with all the equation of the node.
    fid=fopen('C:\Users\Hako\Dropbox\Skole\10. semester\Modell\Modell fra
scratch 3\Modell fra scratch 3.txe');
        c = textscan(fid,'%s%f%f%f%f%f\r\n%f', 'HeaderLines',
2171,'collectoutput',1 );
    fclose(fid);

    Constraints=c{2};

        for j=1:length(BDGnodes)
            a=find(Constraints(:,2)==BDGDOFtemp(j,3));
            BDGDOF(j,:)=Constraints(a,:);
        end
    CaeDOF = BDGDOF(:,[2,3,4]);
    Caedamp=zeros(n,n);
    for j=1:length(CaeDOF)
        Caedamp(CaeDOF(j,1),CaeDOF(j,1))=ro*V*D*CD;
        Caedamp(CaeDOF(j,1),CaeDOF(j,2))=ro*V*B/2*(D/B*CDm-CL);
        Caedamp(CaeDOF(j,2),CaeDOF(j,1))=ro*V*B*CL;
        Caedamp(CaeDOF(j,2),CaeDOF(j,2))=ro*V*B/2*(CLm+D/B*CD);
        Caedamp(CaeDOF(j,3),CaeDOF(j,1))=ro*V*B^2*CM;
        Caedamp(CaeDOF(j,3),CaeDOF(j,2))=ro*V*B^2/2*CMm;
    end
  Caedamp=Caedamp*30./1000;  %Må gange med lengde på elementer siden test
to see if the mass and stiffness martix is divided by 1000

end
```

## F.4 Damping

Creates the damping matrixes for Rayleigh and hysteretic damping. To create the damping matrix for Rayleigh damping the sub matrixes for stiffness and mass matrix found in the script Import are used. Function named “damping”.

```
function [crayleigh, cmaterial,A]=damping(T, k,m, msteel,
mconcrete,mjoint,ksteel, kconcrete, kjoint);
%% Creates damping matic for Rayleigh and hysteretic damping(material)
% Created by Håkon Olav Skogmo
```

```
 % Damping values
    chisteel=[0.02;0.02];
    chiconcrete=[0.05;0.05];
    chijoint=[0.035;0.035];

%%Rayleigh damping
% Frequencies used to define Rayleig constants
    wi=1;    % Eigenperiods to be damped
    wj=100; %Was 100 when the analysis where conducted
    Tsort=sort(T(:,2), 'descend');
    wn=2*pi./Tsort;
    A=[1/wn(wi) wn(wi); 1/wn(wj) wn(wj)];
 % Creates Rayleigh constants
    as=2*inv(A)*chisteel;
    ac=2*inv(A)*chiconcrete;
    aj=2*inv(A)*chijoint;
% Calculates sub-damping matrixes
    csteel= as(1)*msteel+as(2)*ksteel;
    cconcrete=ac(1)*mconcrete+ac(2)*kconcrete;
    cjoint=aj(1)*mjoint+aj(2)*kjoint;
% Direct aasembly of the sub matrixes for steel concrete and common
    crayleigh=csteel+cconcrete+cjoint;
%% Material damping
    cmaterial=
2*chisteel(1)*ksteel+2*chiconcrete(1)*kconcrete+2*chijoint(1)*kjoint;
  end
```

## F.5 Frequencies

This routine creates a frequency vector for a chosen number of eigenfrequencies, and makes a fine mesh around the eigenfrequency and a course mesh between the eigenfrequencies

```
function [w,p]=Freq(wn)
%% Makes a frequency vector to use in the calculation.
% Number of eigen frequencies are decied and number of element per eigen
% frequeny are set (d)
% The function dived makes a finer frequency mesh areound the the natural
% frequencies and coured at the intermediate frequencies. It also reduce
% number of elements per eienfrequency if the eigenfrequences are closly
% spaced
% Created by Håkon Olav Skogmo

start=1; %Set start frequency
d=20; %Number of element the area around each element should be divided in
      %Must be be diviabel by four
NumbEig=1200;  %Number of eigenfrequencies tha should be calculated
               %1200 was used under the analyses
               % 300 when reunnind the damping analyses
w=zeros(30,NumbEig);
   for j=1:NumbEig
    p=j+start-1;
    if j==1
        w(1/4*d+1:3*d/4,j)=linspace(wn(p)-((wn(p+1)-
wn(p))/10),wn(p)+(wn(p+1)-wn(p))/10,d/2);
        w(1:d/4,j)= linspace(wn(p)-0.05,w(d/4+1,j),d/4);
    elseif abs((wn(p)-wn(p-1)))>=0.04
```

```
        s=w(:,j-1);
        FirstNZ=length(s(s~=0));
        w(1/4*d+1:3*d/4,j)=linspace(wn(p)-((wn(p+1)-
wn(p))/10),wn(p)+(wn(p+1)-wn(p))/10,d/2);
        w(1:d/4,j)= linspace(w(FirstNZ,j-1),w(d/4+1,j) ,d/4);
    elseif abs((wn(p)-wn(p-1)))<0.04 && abs((wn(p)-wn(p-1)))>=0.02
        s=w(:,j-1);
        FirstNZ=length(s(s~=0));
        w(1:3*d/4,j)=linspace(w(FirstNZ,j-1),wn(p)+(wn(p+1)-
wn(p))/10,3*d/4);
    elseif abs((wn(p)-wn(p-1)))<0.02
        s=w(:,j-1);
        FirstNZ=length(s(s~=0));
        w(1:2*d/4,j)=linspace(w(FirstNZ,j-1),wn(p)+(wn(p+1)-
wn(p))/10,2*d/4)
    end
   end
w(w==0)=[];
w=unique(w);
w=[w wn(1:NumbEig)']
sort(w,'descend');
w=unique(w);
length(w);
end
```

## F.6 Unit force vector

Creates vectors of unity for DOFs corresponding to each direction. I.e all DOFs corenspong to transverse direction x is set to unity, all other to zero. Ans this is done for all 6 displacements and rotations

```
function [IUx,IUy,IUz,IRx,IRy,IRz]=Iforce(n)
%% Makes a unity matirx for DOFs in each direction, i.e all elements
%correnspondingDOFs in x direction get unity assig but the rest of the
%DOFs are zero. an the same for the rest of the directions
% Created by Håkon Olav Skogmo


%% Load tabel with nodes and DOF
 fid=fopen('C:\Users\Hako\Dropbox\Skole\10. semester\Modell\Modell fra
scratch 3\modell fra scratch 3.txe');
        c = textscan(fid,'%f%f%f%f%f%f\r\n%f', 'HeaderLines',
1,'collectoutput',1 );
    fclose(fid);

    DOFlist=sortrows(c{1},1);
%%LOad lower part of DOF list, the constraint part
    fid=fopen('C:\Users\Hako\Dropbox\Skole\10. semester\Modell\Modell fra
scratch 3\modell fra scratch 3.txe');
        c = textscan(fid,'%s%f%f%f%f%f\r\n%f', 'HeaderLines',
2171,'collectoutput',1 );
    fclose(fid);
    Constraints=c{2};
 %% MAkes a list of DOF where the constraints equatiin are replaced with
the real DOF
   DOFwithCon=zeros(length(DOFlist),7);
 for j=1:length(DOFlist)
     if DOFlist(j,2)<0
        a=find(Constraints(:,2)==DOFlist(j,3));
```

```
        DOFwithCon(j,1)=DOFlist(j,1);
        DOFwithCon(j,2:7)=Constraints(a,:);
    elseif DOFlist(j,2)>0
        DOFwithCon(j,:)=DOFlist(j,1:7);
    else
        DOFwithCon(j,:)=DOFlist(j,:);
    end
 end
 %% Make the force matrix for each of the direction wiht a 1 in the degree
with corensponding DOF
 IUx=zeros(n,1);
 IUy=zeros(n,1);
 IUz=zeros(n,1);
 IRx=zeros(n,1);
 IRy=zeros(n,1);
 IRz=zeros(n,1);
 for j =1:n
    [a,b]=find(DOFwithCon(:,2:7)==j);
    if b==1
       IUx(j)=1;
    elseif b==2
        IUy(j)=1;
    elseif b==3
        IUz(j)=1;
    elseif b==4
        IRx(j)=1;
    elseif b==5
        IRy(j)=1;
    elseif b==6
       IRz(j)=1;
    else
     flag
    end

 end
end
```

## F.7 Response

This routine calculates variances, spectral moments and spectral densities for the system. Is follows the routine describe in the theory in the section Multiple support excitations.

Functions used: Import, Damping, cae, DOFinvest, Freq, PSD, Sa

```
%%Response
%Calculates: Variance, spectral moments and spectral density
%Used the formulation defined in chapter theory
% Function uses
%   *Import
%   *Damping
%   *cae
%   *DOFinvest
%   *Freq
%   *PSD
%   *Sa
%Created by Håkon Olav Skogmo
```

```
close all
clear all
update=0;
[~,~,T,m,k,mconcrete,msteel, mjoint, kconcrete, ksteel,kjoint,
~]=Import(update);
[~, cmaterial,~]=damping(T, k,m, msteel, mconcrete,mjoint,ksteel,
kconcrete, kjoint);
n=length(m);
[Caedamp]=Cae(n);
Tsorted=sort(T(:,2),'descend');
wn=2*pi./Tsorted;
%%%%%%%%%%%%%%%%%%%%%%%%%%%%%%%%%%%%%%%%%%%%%%
 %% Load tabel with nodes and DOF
    fid=fopen('C:\Users\Hako\Dropbox\Skole\10. semester\Modell\Modell fra
scratch 3\Modell fra scratch 3.txe');
        c = textscan(fid,'%f%f%f%f%f%f\r\n%f', 'HeaderLines',
1,'collectoutput',1 );
    fclose(fid);

    DOFlist=sortrows(c{1},1);


% Find the supports DOF
    c=importdata('C:\Users\Hako\Dropbox\Skole\10. semester\Matlab\TXT
filer\Support nodes.txt');
   supportnodes=c.data;

       SupportDOF =zeros(length(supportnodes),7);
        for j=1:length(supportnodes)
            a=find(DOFlist(:,1)==supportnodes(j));
            SupportDOF(j,:)=DOFlist(a,:);
        end

 %%Make transfer matrix
 E=zeros(36,5);
 telle=0;
 for j=1:length(SupportDOF)
     %%Set number in accordance with support
     if 1<=j && j<=2
        a=2;
        telle=telle+6;
    elseif 3<=j && j<=4
        a=3;
        telle=telle+3;
    elseif 5<=j && j<=6
        a=4;
        telle=telle+3;
    elseif 7<=j && j<=8
        a=5;
        telle=telle+6;
    end

     if a>=3 && a<=4
        E(telle-2,1)=SupportDOF(j,2);
        E(telle-1,1)=SupportDOF(j,3);
        E(telle,1)=SupportDOF(j,4);
        E(telle-2,a)=1;
        E(telle-1,a)=1;
        E(telle,a)=1;
     else
```

```
        E(telle-5,1)=SupportDOF(j,2);
        E(telle-4,1)=SupportDOF(j,3);
        E(telle-3,1)=SupportDOF(j,4);
        E(telle-2,1)=SupportDOF(j,5);
        E(telle-1,1)=SupportDOF(j,6);
        E(telle,1)=SupportDOF(j,7);
        E(telle-5,a)=1;
        E(telle-4,a)=1;
        E(telle-3,a)=1;
    end
end
Em=sortrows(E,1);
Em(:,1)=[];

SupportDOF=reshape(SupportDOF(:,2:7)',numel(SupportDOF(:,2:7)),1);
SupportDOF(SupportDOF==0)=[];
SortedSupportDOF=sort(SupportDOF);
%%%%%Obs%%%%
% The Support DOF are sorted

%Find structure DOF
ks=k;
ms=m;
caes= Caedamp;
cs=cmaterial;
ks(SortedSupportDOF,:)=[];
ks(:,SortedSupportDOF)=[];
ms(SortedSupportDOF,:)=[];
ms(:,SortedSupportDOF)=[];
 cs(:,SortedSupportDOF)=[];
caes(:,SortedSupportDOF)=[];
  cs(SortedSupportDOF,:)=[];
caes(SortedSupportDOF,:)=[];

%Find base DOF
 kb=zeros(length(SortedSupportDOF),length(SortedSupportDOF));
 mb=zeros(length(SortedSupportDOF),length(SortedSupportDOF));
 cb=zeros(length(SortedSupportDOF),length(SortedSupportDOF));
 caeb=zeros(length(SortedSupportDOF),length(SortedSupportDOF));
kb=k(SortedSupportDOF,SortedSupportDOF);
 mb=m(SortedSupportDOF,SortedSupportDOF);
 cb=cmaterial(SortedSupportDOF,SortedSupportDOF);
 caeb=Caedamp(SortedSupportDOF,SortedSupportDOF);

%Find conncected DOF
 ksb=k;
 msb=m;
 caesb= Caedamp;
 csb= cmaterial;
 ksb(SortedSupportDOF,:)=[];
 msb(SortedSupportDOF,:)=[];
 csb(SortedSupportDOF,:)=[];
 ksb=ksb(:,SortedSupportDOF);
 msb=msb(:,SortedSupportDOF);
 csb=csb(:,SortedSupportDOF);
 caesb=caesb(:,SortedSupportDOF);

 %% Modes that should be investigated
[D]=DOFinvest();
%%Remove vaiable that are no need more
```

```
clearvars DOFlist E SupportDOF T Tsorted supportnodes ksteel mconcrete
mjoint msteel kjoint kconcrete fid msb m k n csb cmaterial caesb
%%%%%%%%%%%%%%%%%
[w]=Freq(wn);
[Sx]=Sa(w);
e=-ks\ksb;
B=-ms*e*Em;
Rs=(e*Em);
SUX=zeros(length(ms),length(ms));%spectal density for chosen points wave
                                    %traveling along bridge
SUY=zeros(length(ms),length(ms));%spectal density for chosen points wave
                                    %traveling perdicular to bridge
SUWave=zeros(length(ms),length(ms)); %spectal density for chosen points
wave
                                    %traveling along bridge, only
                                    %wave passage effects
VarX=zeros(length(ms),length(ms));%Complete variace
VarY=zeros(length(ms),length(ms));%Complete variace
VarWave=zeros(length(ms),length(ms));%Complete variace
VarMX=0;
VarMWave=0;
VarMY=0;
%% Calculates response spectra, variances and spectral moments
for j=1:length(w)-1
   tic;
   [Sxx,Syy,Swave]=PSD(Sx(j),w(j))
   Rr=(-w(j)^2*ms+ks+1i*cs+1i*w(j)*caes)\B;

   Sux=(Rr+Rs./(w(j)^2))*Sxx*(Rr+Rs./(w(j)^2))';
   Suy=(Rr+Rs./(w(j)^2))*Syy*(Rr+Rs./(w(j)^2))';
   Suwave=(Rr+Rs./(w(j)^2))*Swave*(Rr+Rs./(w(j)^2))';


    VarX=VarX+Sux.*(w(j+1)-w(j));
    VarY=VarY+Suy.*(w(j+1)-w(j));
    VarWave=VarWave+Suwave.*(w(j+1)-w(j));


    VarMX=VarMX+w(j).*Sux.*(w(j+1)-w(j));
    VarMY=VarMY+w(j).*Suy.*(w(j+1)-w(j));
    VarMWave=VarMWave+w(j).*Suwave.*(w(j+1)-w(j));


   for k=1:length(D)
       SUX(k,j)=Sux(D(k),D(k));
       SUY(k,j)=Suy(D(k),D(k));
       SUWave(k,j)=Suwave(D(k),D(k));
   end
toc
end
```

## F.8 Power Spectral Density of Acceleration

This routine calculates the Kanai-Tajimi spectrum adapted the expected magnitude of the earthquake. The calculation is done in the manner described in the theory

```
function [Sx]=Sa(w)
%% Calculates the kanai-Tajimi spectrum
% Uses process descibed in the theory
%Created by Håkon Olav Skogmo

%%Kanai spectrum
plote=1;

%%Input
S0=1; %Amplitude Gaussian noise process
w1=15;            %7
chi1=0.6;        %0.9
chi2=0.6;        %0.9
w2=1.5;          %0.2
PGA=3;
GF=2.73;

Hw2=((w./w2).^2)./((1-(w./w2).^2)+2*1i*chi2*(w./w2));
Hw1=(1+2*1i*chi1.*(w./w1))./((1-(w./w1).^2)+2*1i*chi1*(w./w1));
S=(abs(Hw1).^2).*(abs(Hw2).^2).*S0;
Var=0;
for j=1:length(w)-1
    Var=Var+S(j)*(w(j+1)-w(j));
end
%sigxx=integral(Hw1,0,inf);
S1=PGA/GF;
I=S1^2/Var;
Sx=(abs(Hw1).^2).*(abs(Hw2).^2)*I;
 h=figure
 plot(w,Sx,'linewidth' , 1)
 title('Kanai-Tajimi spectra','fontsize' ,12)
 ylabel('Acceleration PSD S_a (m^2/s^4 s/rad)', 'fontsize', 12);
 xlabel('\omega (rad/s)')
 set(gca, 'fontsize', 11)
      matl=['C:\Users\Hako\Dropbox\Skole\10. semester\Matlab\PLot\Kanai-
Tadjimi'];
      word=['C:\Users\Hako\Dropbox\Skole\10. semester\Oppgave\PLot\Kanai-
Tadjimi'];
      saveas(h, matl,'m')
      set(gcf,'units','pixels','PaperPosition',[0 0 25,10])
       print(h,'-djpeg','-r800', word)

%%Export specter for use in SAP2000
f=w./(2*pi);
fid=fopen('C:\Users\Hako\Dropbox\Skole\10. semester\Matlab\SAP\Sa.txt',
'w');
            fprintf(fid,'%4.6f\n', Sx);
fclose(fid);
 fid=fopen('C:\Users\Hako\Dropbox\Skole\10. semester\Matlab\SAP\omega.txt',
'w');
            fprintf(fid,'%4.6f\n', f );
fclose(fid);
    Varu=0;
    Var1=0;
    for j=1:length(w)-1
```

```
        Varu=Varu+(1/w(j+1)^4)*Sx(j)*(w(j+1)-w(j));
        Var1=Var1+Sx(j)*(w(j+1)-w(j));
    end
end
```

## F.9 Power Spectral Density of Spatially Varying Ground Accelerations

This routine calculates the power spectral density of spatially varying ground motion for the tree analyses conducted.

```
function [Sxx,Syy,Swave]=PSD(Sx,w)
%% Calculates the power spectral density for spartially varying ground
motions
%The Haruchandran -Vanmarck model coherence model
% Created by Håkon Olav Skogmo

%%Coherence - Harichandran -Vanmarcke model
v=3000; % Soil condition A
A=0.736;
alpha=0.147;
K=5210;
w0=6.85;
b=2.78;
dxx=[0  625 4325 4950;
     -625 0 3700 4325;
     -4325 -3700 0 625
     -4900 -4326 625 0];

dyy=zeros(4);

roxx=zeros(length(dxx));
royy=zeros(length(dyy));
rowave=zeros(length(dxx));
omega=K*(1+(1i*w/w0)^b)^-0.5;
%Wave traveling along bridge
roxx=A*exp(-((2*abs(dxx))./(alpha*omega))*(1-A+alpha*A))+...
(1-A)*exp(-((2*abs(dxx))./(alpha*omega))*(1-A+alpha*A)).*exp(1i*w*dxx./v);
%Wave traveling perdikular to bridge
royy=A*exp(-((2*abs(dyy))./(alpha*omega))*(1-A+alpha*A))+...
(1-A)*exp(-((2*abs(dyy))./(alpha*omega))*(1-A+alpha*A)).*exp(1i*w*dyy./v);
%Wave travelng along bridge, bu no incoherence effects
rowave=ones(4).*exp(1i*w*dxx./v);

Sxx=Sx.*roxx;
Syy=Sx.*royy;
Swave=Sx.*rowave;
end
```

## F.10 Plotting of Auto-PSD response calculations

This routine is used to plot the response for the cable, girder and pylons. To do this the DOF in the system without supports DOF coupled with the DOFs in the original system(with supports DOF).

Function used; deckandgirdernodes

```
%Plots the responses of the system obtaine from the script response
%Created By Håkon Olav Skogmo

clear all
close all
clc
%%%%%%%%%%!!!!!!!!!!!!!!!!!!!!!!!%%%%%%%%%%%%%%%%%
%%%%%%%%%%Husk å endre alle mapper når endre input fila
Var=importdata('C:\Users\Hako\Dropbox\Skole\10.
semester\Matlab\Datafiler\Kjoring 3\VARX.mat');
VarY=importdata('C:\Users\Hako\Dropbox\Skole\10.
semester\Matlab\Datafiler\Kjoring 3\VARY.mat');
VarWave=importdata('C:\Users\Hako\Dropbox\Skole\10.
semester\Matlab\Datafiler\Kjoring 3\VARWave.mat');
V=zeros(length(Var),2);
V(:,1)=linspace(1,length(Var),length(Var));
V(:,2)= abs(diag(Var));
V=sortrows(V,2);
%% Load tabel with nodes and DOF
fid=fopen('C:\Users\Hako\Dropbox\Skole\10. semester\Modell\Modell fra
scratch 3\Modell fra scratch 3.txe');
        c = textscan(fid,'%f%f%f%f%f%f\r\n%f', 'HeaderLines',
1,'collectoutput',1 );
fclose(fid);
    DOFlist=sortrows(c{1},1);

% Find the supports DOF
    c=importdata('C:\Users\Hako\Dropbox\Skole\10. semester\Matlab\TXT
filer\Support nodes.txt');
   supportnodes=c.data;
       SupportDOF =zeros(length(supportnodes),7);
        for j=1:length(supportnodes)
            b=find(DOFlist(:,1)==supportnodes(j));
            SupportDOF(j,:)=DOFlist(b,:);
        end
 SupportDOF=reshape(SupportDOF(:,2:7)',numel(SupportDOF(:,2:7)),1);
 SupportDOF(SupportDOF==0)=[];
 SortedSupportDOF=sort(SupportDOF);
 %% Make list of corrensponding DOF in reducesystem(without
 %Supports) and full system
 DOF=zeros(3564,2);
  DOF(:,1)=linspace(1,3564,3564);
  for j=1:length(SupportDOF)
    b=find(DOF==SupportDOF(j));
    DOF(b,:)=[];
  end
  DOF(:,2)=linspace(1,length(DOF),length(DOF));
  [BDGDOFSSorted,CableDOFs,TowerDOFs1,TowerDOFs2 ]=deckandgirdernodes();
  %% Make plot of standard deviation for the bridge girder and cable
  for k=2:7
    for j=1:length(BDGDOFSSorted)
        a=find(DOF(:,1)==BDGDOFSSorted(j,k));
        VARGirder(j,k)=Var(a,a);
        VARGirderY(j,k)=VarY(a,a);
        VARGirderWave(j,k)=VarWave(a,a);
    end
  end
  xgirder=linspace(50,3650, 121);
  Title={'(a)','(b)','(c)','(d)','(e)','(f)'};
```

```
 % direction={'UX' 'UY' 'UZ' 'RX' 'RY' 'RZ'};
  direction=[1 2 3 4 5 6];
  SDGirder=sqrt(real(VARGirder(:,2:7)));
  SDGirderY=sqrt(real(VARGirderY(:,2:7)));
  SDGirderWave=sqrt(real(VARGirderWave(:,2:7)));
  for k=2:7
    for j=1:length(CableDOFs)
        a=find(DOF(:,1)==CableDOFs(j,k));
        VARCable(j,k)=Var(a,a);
    end
  end

  xcable=zeros(length(VARCable),1);
  xcable(1)=0;
  xcable(length(xcable))=3700;
  xcable(2:(length(xcable)-1))=linspace(50,3650, 121);
  Title={'(a)','(b)','(c)','(d)','(e)','(f)'};
  direction=[1 2 3 4 5 6];
  SDCable=sqrt(real(VARCable(:,2:7)));
for j=1:3
       h=figure(j);
      set(h,'position',[100,100,1000,200]);
      plot(xcable,SDCable(:,j),'b',xgirder,SDGirder(:,j),'r', 'LineWidth',
1.5);

plot(xgirder,SDGirder(:,j),'g',xgirder,SDGirderWave(:,j),'b',xgirder,SDGird
erY(:,j),'r')
      xlabel('Length Bridge (m)', 'fontsize', 12)
      ylabel('\sigma (m)', 'fontsize', 12)
      legend('Analysis 1', 'Analysis 2', 'Analysis 3')
      set(gca, 'fontsize', 12)
      xlim([0 3700])
      set(gca,'ytick',[0 0.2 0.4 0.6 0.8 1])
      if j==1
        set(gca,'ytick',[0 0.05 0.1 0.15 0.2 0.25])
      end
      title(Title(j));
      grid on
      matl=['C:\Users\Hako\Dropbox\Skole\10.
semester\Matlab\PLot\SD\SDX\allgirder', num2str(direction(j))];
      word=['C:\Users\Hako\Dropbox\Skole\10.
semester\Oppgave\PLot\SDX\allgirder', num2str(direction(j))];
      saveas(h, matl,'m')
      set(gcf,'units','pixels','PaperPosition',[0 0 25 5])
      print(h,'-djpeg','-r800', word)
end
%% Make plot of pylons
 %load nodes in one of the towers in one of thepylons  only rotation
VARTower1=zeros(length(TowerDOFs1),4);
VARTower1(:,1)=TowerDOFs1(:,1);
for k=2:7
    for j=1:length(TowerDOFs1)
        a=find(DOF(:,1)==TowerDOFs1(j,k));
        VARTower1(j,k)=Var(a,a);
    end
end
for k=2:7
    for j=1:length(TowerDOFs2)
        a=find(DOF(:,1)==TowerDOFs2(j,k));
        VARTower2(j,k)=Var(a,a);
    end
```

```
end
SDTower1=sqrt(real(VARTower1(:,2:7)));
SDTower2=sqrt(real(VARTower2(:,2:7)));
y=TowerDOFs1(:,1)';
for j=1:3
       h=figure(j+3);
      set(h,'position',[100,100,200,1000]);
      plot(SDTower1(:,j),y,'b',SDTower2(:,j),y,'r', 'LineWidth', 1.5);
      ylabel('Height Pylon (m)', 'fontsize', 12)
      xlabel('\sigma (m)', 'fontsize', 12)
      set(gca, 'fontsize', 12)
      title(Title(j));
      axis([0 0.6 25, 470])
      set(gca,'xtick',[0 0.25 0.5])
      grid on
      matl=['C:\Users\Hako\Dropbox\Skole\10.
semester\Matlab\PLot\SD\SDX\SDYTower', num2str(direction(j))];
      word=['C:\Users\Hako\Dropbox\Skole\10.
semester\Oppgave\PLot\SDX\SDYTower', num2str(direction(j))];
      saveas(h, matl,'m')
      set(gcf,'units','pixels','PaperPosition',[0 0 4 13])
      print(h,'-djpeg','-r800', word)
end
```

## F.11 Pylon, Bridge Deck and Cable DOFS (deckandgirdernodes)

This is the function used in the plotting the response. The routine imports list of cable, pylon and tower nodes and finds their corresponding DOFs .

```
function [BDGDOFSSorted,CableDOFs,TowerDOFs1,
TowerDOFs2]=deckandgirdernodes()
%% FInd the DOFs in Bridge deck, Cable and both the twoers
% Created by Håko Olav Skogmo


%% Load tabel with nodes and DOF
 fid=fopen('C:\Users\Hako\Dropbox\Skole\10. semester\Modell\Modell fra
scratch 3\Modell fra scratch 3.txe');
        c = textscan(fid,'%f%f%f%f%f%f\r\n%f', 'HeaderLines',
1,'collectoutput',1 );
    fclose(fid);

    DOFlist=sortrows(c{1},1);

%%LOad lower part of DOF list, the constraint part
    fid=fopen('C:\Users\Hako\Dropbox\Skole\10. semester\Modell\Modell fra
scratch 3\Modell fra scratch 3.txe');
        c = textscan(fid,'%s%f%f%f%f%f\r\n%f', 'HeaderLines',
2171,'collectoutput',1 );
    fclose(fid);

    Constraints=c{2};

 %%Load nodes for one of the bridge deck girders
    fid=fopen('C:\Users\Hako\Dropbox\Skole\10. semester\Matlab\Noder
brodekke.txt');

b=textscan(fid,'%*s%*s%*s%*s%*s%f','HeaderLines',1,'collectoutput',1 );
```

```
    fclose(fid);

   fid=fopen('C:\Users\Hako\Dropbox\Skole\10. semester\Matlab\Noder
brodekke.txt');
        c = textscan(fid,'%f', 'HeaderLines', 2,'collectoutput',1 );
    fclose(fid);
    BDGnodes=c{1}(1:b{1}(1));

%%Loads coordinates for nodes
c=importdata('C:\Users\Hako\Dropbox\Skole\10. semester\Matlab\TXT
filer\Cable nodes.txt');
Cablenodes=sortrows(c.data(:,[1 2]),2); % Transfer nodes and x-coordinates
to array

%%Load nodes and coordinates for on of the columbs in the pylon
c=importdata('C:\Users\Hako\Dropbox\Skole\10. semester\Matlab\TXT
filer\Tower nodes.txt');
Towernodes=c.data;
Towernodes(1,:)=[]; %Remove support nodes
 %% MAkes a list of DOF where the constraints equatiin are replaced with
the real DOF
   DOFwithCon=zeros(length(DOFlist),7);
 for j=1:length(DOFlist)
     if DOFlist(j,2)<0
        a= Constraints(:,2)==DOFlist(j,3);
        DOFwithCon(j,1)=DOFlist(j,1);
        DOFwithCon(j,2:7)=Constraints(a,:);
     elseif DOFlist(j,2)>0
         DOFwithCon(j,:)=DOFlist(j,1:7);
     else
         DOFwithCon(j,:)=DOFlist(j,:);
     end
 end
BDGDOFS=zeros(length(BDGnodes),7);
%% Makes list of bridge deck girder DOF
for j=1:length(BDGnodes)
    a= DOFwithCon(:,1)==BDGnodes(j);
    BDGDOFS(j,:)=DOFwithCon(a,:);
end
%%Makes list over cables DOF
for j=1:length(Cablenodes)
    a= DOFwithCon(:,1)==Cablenodes(j);
    CableDOFs(j,:)=DOFwithCon(a,:);
end
%% Make list over Tower DOF
Pylon 1
TowerDOFs1=zeros(length(Towernodes),4);
TowerDOFs1(:,1)=Towernodes(:,2);
for j=1:length(Towernodes)
    a= DOFwithCon(:,1)==Towernodes(j,1);
    TowerDOFs1(j,2:7)=DOFwithCon(a,2:7);
end
%Pylon 2
TowerDOFs2=zeros(length(Towernodes),4);
TowerDOFs2(:,1)=Towernodes(:,4);
for j=1:length(Towernodes)
    a= DOFwithCon(:,1)==Towernodes(j,3);
    TowerDOFs2(j,2:7)=DOFwithCon(a,2:7);
end
%%Loads coordinates for nodes
```

```
c=importdata('C:\Users\Hako\Dropbox\Skole\10. semester\Matlab\TXT
filer\Koordinater.txt');
BDGnodesCOR=c.data(:,[1 2]); % Transfer nodes and x-coordinates to array
%Sort the Bridge deck DOFS after coordinat in x direction
for j=1:length(BDGnodesCOR)
    a= BDGDOFS(:,1)==BDGnodesCOR(j,1);
    BDGDOFSSorted(j,:)=BDGDOFS(a,:);
end
end
```

## F.12 Non-Stationary Response

Plots the spectral density and simplified non-stationary response for a given DOF.

```
%%Non-stationary response
%%Plots spectral density of the response and the simplified non-stationary
%%solution
%Created by Håkon Olav Skogmo
close all
clear all
%% LOAD vaiances, spectral densities and omega fro the result of analysis
Var=importdata('C:\Users\Hako\Dropbox\Skole\10.
semester\Matlab\Datafiler\Kjoring 3\VARY.mat');
PSDX=importdata('C:\Users\Hako\Dropbox\Skole\10.
semester\Matlab\Datafiler\Kjoring 3\SUY.mat');
w=importdata('C:\Users\Hako\Dropbox\Skole\10.
semester\Matlab\Datafiler\Kjøring 2.0\Omega.mat');

%Node number in D that is to be investigated '
%1-6 mid-span
%7-12 quarter point
%13-18 Top pylons
DOF=14;%REMNBER TO CHANGE FILE NAME
%% Plot spectral densities

    h=figure
    semilogx(w(1:length(w)-1),real(PSDX(DOF,:)),'linewidth', 1.5)
    xlabel('\omega (rad/s)','fontsize', 12)
    ylabel('Displacement   PSD   S_u (m^2 s/rad)', 'fontsize', 12)
    set(gca, 'fontsize', 12)
    title('(a)','fontsize',14);
     word=['C:\Users\Hako\Dropbox\Skole\10. semester\Oppgave\PLot\Su\top'];
    set(gcf,'units','pixels','PaperPosition',[0 0 11 9])
    print(h,'-djpeg','-r200', word)

%% Make plot of the simplified non.stationary response.
% if there are several maximas
more=1
    [values, indexs]=sort(real(PSDX(DOF,:)),'descend');
[value,index]=max(real(PSDX(DOF,:)));

w0=w(index);
%w0=0.42
Damp=0.05;

hor=[0 10];
```

```
%Load DOF number for the DOF where the spectral density are saved.
[D]=DOFinvest();
wn=w0*sqrt(1-Damp^2);
t=linspace(0,50,1000);
t=unique([t,10]);
Vartime=real(Var(D(DOF),D(DOF))).*(1-exp(-
Damp.*w0.*t).*(1+2*((Damp*w0/wn)^2)...
    .*(sin(wn.*t)).^2+Damp*w0/wn.*sin(2*wn.*t)));
a=find(t==10)
ver=real(Vartime(a))
h=figure
hold on
plot(t,real(Vartime),'b','linewidth', 1.5)
plot([10 10],[0,ver],'r','linewidth', 1.5)
plot([0 10],[ver, ver],'r','linewidth', 1.5)
ylim([0, real(Var(D(DOF),D(DOF)))]);
xlabel('Time (s)', 'fontsize',12)
ylabel('Variance  \sigma^2 (m)','fontsize',12)
set(gca, 'fontsize', 12)
 title('(b)','fontsize',14);
 box on
 word=['C:\Users\Hako\Dropbox\Skole\10. semester\Oppgave\PLot\Non-
sta\top'];
set(gcf,'units','pixels','PaperPosition',[0 0 11 9])
print(h,'-djpeg','-r200', word)
```

## F.13 Extreme values

This routine calculates the extreme values for a node at the mid-span, quarter point and top of the pylon.

Function used: DOFinvest

```
%%Extrem value
%% Calculate the peak factor and the extreme values
%%Created by Håkon Olav Skogmo
clear all
close all
clc

%%Extreme values
PSDX=importdata('C:\Users\Hako\Dropbox\Skole\10.
semester\Matlab\Datafiler\Kjoring 3\SUY.mat');
w=importdata('C:\Users\Hako\Dropbox\Skole\10.
semester\Matlab\Datafiler\Kjoring 3\Omega.mat');
VarX=importdata('C:\Users\Hako\Dropbox\Skole\10.
semester\Matlab\Datafiler\Kjoring 3\VARY.mat');

Var=zeros(18,1);
VarM=zeros(18,1);

%Node number in D that is to be investigated '
%1-6 mid-span
%7-12 quarter point
%13-18 Top pylons
Ts=10;
[D]=DOFinvest();
for k=1:18
```

```
    for j=1:length(w)-1
        Var(k)=Var(k)+real(PSDX(k,j)*(w(j+1)-w(j)));
        VarM(k)=VarM(k)+w(j)^2.*real(PSDX(k,j)*(w(j+1)-w(j)));
    end
    v(k)=sqrt(VarM(k)/Var(k))/pi;
    E(k)=sqrt(2*log(v(k)*Ts))+0.5772/sqrt(2*log(v(k)*Ts));
    Ext(k)=E(k)*sqrt(real(VarX(D(k),D(k))));
end
E(16:18)=[];
E(10:12)=[];
E(4:6)=[];

Ext(16:18)=[];
Ext(10:12)=[];
Ext(4:6)=[];
```